Analysis of auditory brainstem neurons in the grassfrog

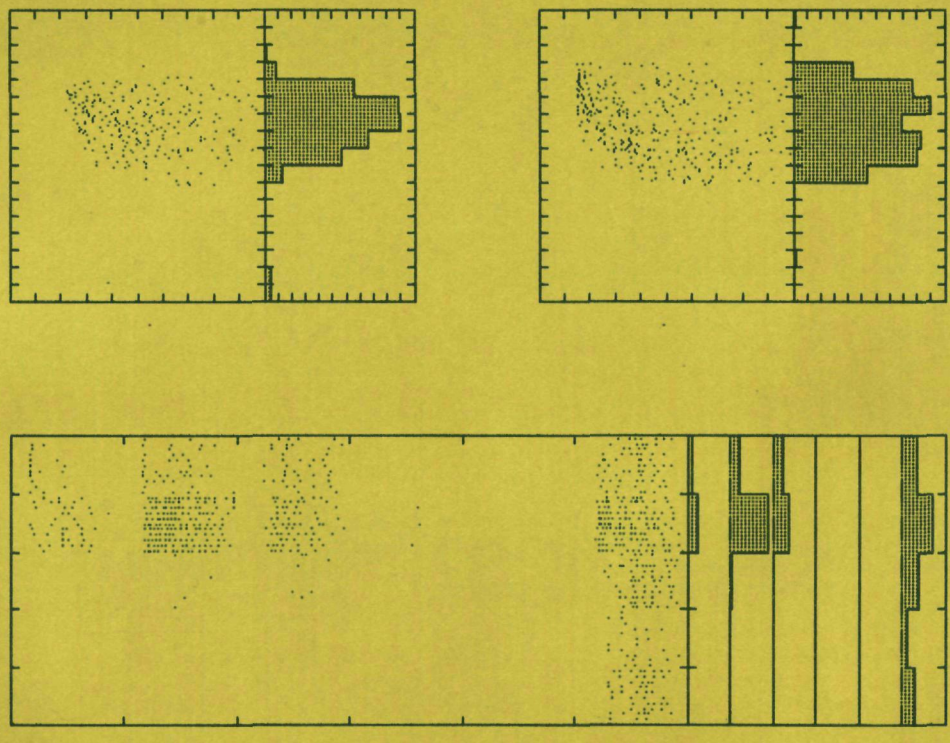

Ivo van Stokkum

Front cover, first page and back cover illustrate three aspects of the analysis of auditory brainstem neurons. The front cover shows the response of an auditory midbrain neuron to different kinds of amplitude-modulated sound. Each dot represents the occurrence of an action potential plotted on the horizontal time-axis. The amplitude-modulation frequency of the sound stimuli varies vertically. The histograms represent the rate response as a function of amplitude-modulation frequency. The first page shows a flow diagram of the model for the auditory brain stem, which is presented in this thesis. The response of a model neuron to the same amplitude-modulated sounds is shown on the back cover, and can be compared directly with the front cover.

Analysis of auditory brainstem neurons in the grassfrog

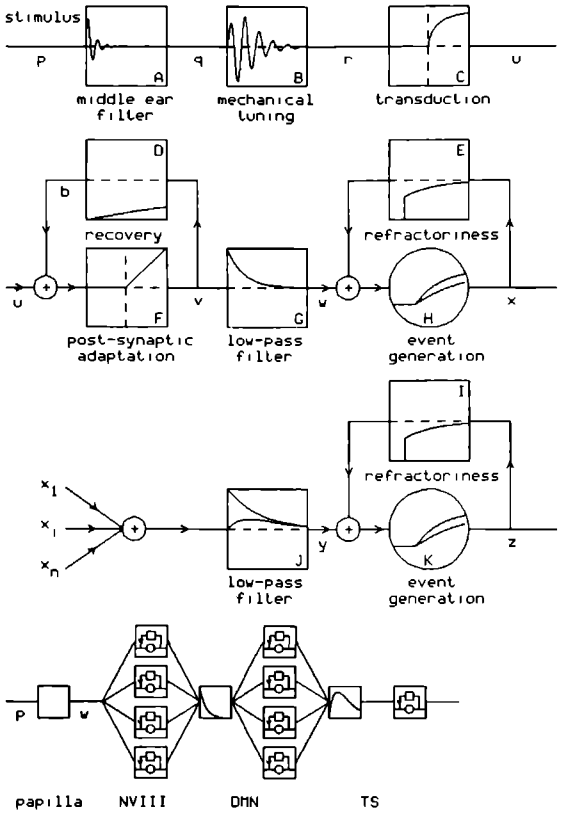

CIP-gegevens Koninklijke Bibliotheek, Den Haag

Stokkum, Ivo Henricus Marie van

Analysis of auditory brainstem neurons in the grassfrog
Ivo Henricus Marie van Stokkum. - [S.l. : s.n.]. - ill.
Thesis Nijmegen. - With ref.
ISBN 90-9002912-5
SISO 606.1 UDC 612.8:612.85(043.3)
Subject headings: auditory neurophysiology, neural modelling.

Analysis of auditory brainstem neurons in the grassfrog

een wetenschappelijke proeve op het gebied van
de natuurwetenschappen

Proefschrift

ter verkrijging van de graad van doctor
aan de Katholieke Universiteit te Nijmegen,
volgens besluit van college van decanen
in het openbaar te verdedigen op woensdag 13 september 1989,
des namiddags te 3.30 uur

door

Ivo Henricus Marie van Stokkum

geboren op 11 februari 1962 te Boxmeer

Promotor: Prof. Dr. C.C.A.M. Gielen

Co-referent: Dr. W.J.M. Epping

This investigation was supported by the Foundation for Biophysics, which is subsidized by the Netherlands Organization for Scientific Research (NWO).

für Eva-Maria

Abbreviations

AM	amplitude modulated
AMF	amplitude modulation frequency
AP	whole nerve action potential
BF	best frequency
BP	band-pass
CCH	crosscoincidence histogram
CF	characteristic frequency
CoSTID	coherent spectro-temporal intensity density
DMN	dorsal medullary nucleus
EDR	electrodermal reflex
EOD	electric organ discharge
EPSP	excitatory postsynaptic potential
F_c	centre frequency
FRH	first-order recurrence-time histogram
LP	low-pass
NVIII	eighth nerve
PESE	pre-event stimulus ensemble
PRR	pulse repetition rate
SNR	signal-to-noise ratio
SON	superior olivary nucleus
SPL	sound pressure level
TS	torus semicircularis

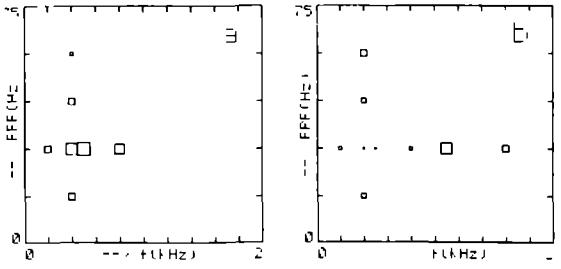

Fig. 2. Magnitude (indicated by size of squares) of vocal (a) and EDR (b) response as function of carrier frequency and PRR of synthetic calls. The stimuli were presented in a free field situation at intensities of 66-95 (a) and 85 (b) dB peak SPL. This last intensity corresponds to a calling male at a distance of 20 cm. Fig. 2 was adopted from Walkowiak and Brzoska (1982) and Brzoska (1984).

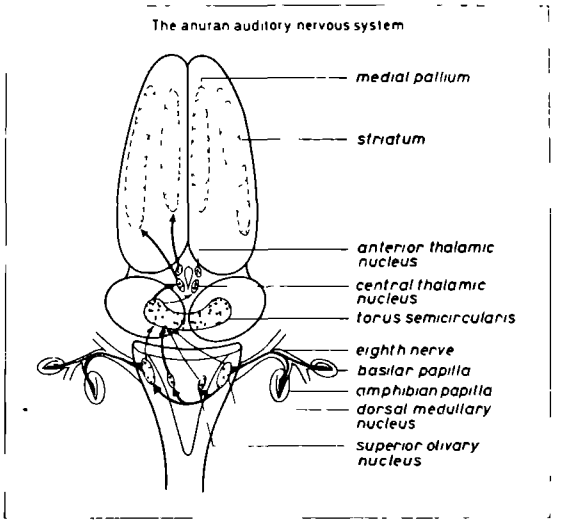

Fig. 3. Schematic overview of the organization of the anuran auditory nervous system. For convenience only ascending neural pathways entering and leaving the left TS are indicated. Fig. 3 with kind permission of W. Epping (1985).

One would expect that stimuli which resemble the mating call give rise to evoked calling, and not to an EDR response. During the mating season synthetic mating calls with varying carrier frequency and PRR were presented to isolated male grassfrogs in a free field situation. In Fig. 2 the responses are summarized. The increase in mating call activity (Fig. 2a) was maximal with a PRR of 30 Hz, and a carrier frequency of 0.4 or 0.5 kHz. These values correspond to the natural mating call. Note that as shown in Fig. 2a a carrier frequency of 1.1 kHz did hardly evoke any calling. Synthetic calls resembling the natural call were ineffective in eliciting the EDR (Fig. 2b). Here the variation with the 1.1 kHz carrier was the most effective.

Another response they reported is male phonotaxis. Presentation of a long territorial call, which consists of twice the number of pulses of the mating call, at an intensity of 85 dB SPL caused turning and swimming of the male towards the loudspeaker.

Walkowiak and Brzoska conclude that PRR and carrier frequency are important cues for the recognition of conspecific calls.

2 Anatomy

The most relevant structures involved in the processing of sound are shown in Fig. 3. In the auditory receptor organs, the amphibian and basilar papilla, sound energy is transformed into neural activity. The properties of the papillae and of the haircells inside them give rise to filtering of the incoming sound stimuli. Eighth nerve (NVIII) fibres innervating the papillae are tuned to frequencies of 0.1-1.0 kHz (amphibian papilla) and 1.0-1.5 kHz (basilar papilla) (Feng et al., 1975). In the dorsal medullary nucleus (DMN) the populations of fibres innervating both papillae arrive separately (Fuzessery and Feng, 1981). Thus the DMN is tonotopically organized. The DMN has ascending connections with the superior olivary nucleus (SON) and, to a lesser extent, with the torus semicircularis (TS). The SON, in its turn, is the main ascending input to the TS. In the SON a tonotopic organization has been found (Schneider-Lowitz, 1983) but in the TS no clear tonotopic organization has been demonstrated (but see Feng, 1983). For convenience only ascending neural pathways entering and leaving the left TS are indicated in Fig. 3. Not shown is the recently discovered superficial reticular nucleus (Rose and Wilczynski, 1984) which receives input from the SON and the DMN and which projects to the TS (Wilczynski, 1988). Neurons responding to auditory stimuli have been recorded up to the level of the thalamus. In forebrain areas so far only auditory evoked potentials have been obtained.

In this study recordings have been made in two brainstem nuclei: the DMN and the TS, which is also called auditory midbrain. The DMN is a homogeneous nucleus containing one morphological cell type (Opdam et al., 1975). By contrast the TS contains a variety of morphological cell types and

Contents

I	Introduction	8
II	Representation of time-dependent correlation and recurrence-time functions. A new method to analyse non-stationary point processes. Co-authors P.I.M. Johannesma and J.J. Eggermont Biological Cybernetics 55, 17-24 (1986).	16
III	Sensitivity of neurons in the dorsal medullary nucleus of the grassfrog to spectral and temporal characteristics of sound. Hearing Research 29, 223-235 (1987).	24
IV	Responses of auditory brainstem neurons in the grassfrog to clicks. Co-author W.J.M. Epping Acta Biologica Hungarica (in press).	36
V	A model for the peripheral auditory nervous system of the grassfrog. Co-author C.C.A.M. Gielen Hearing Research (in press).	44
VI	A model for the auditory midbrain of the grassfrog for monaural stimuli. Hearing Research (submitted).	58
VII	Summary	74
	References	79
	Samenvatting	84
	Curriculum vitae	86
	Dankwoord	87

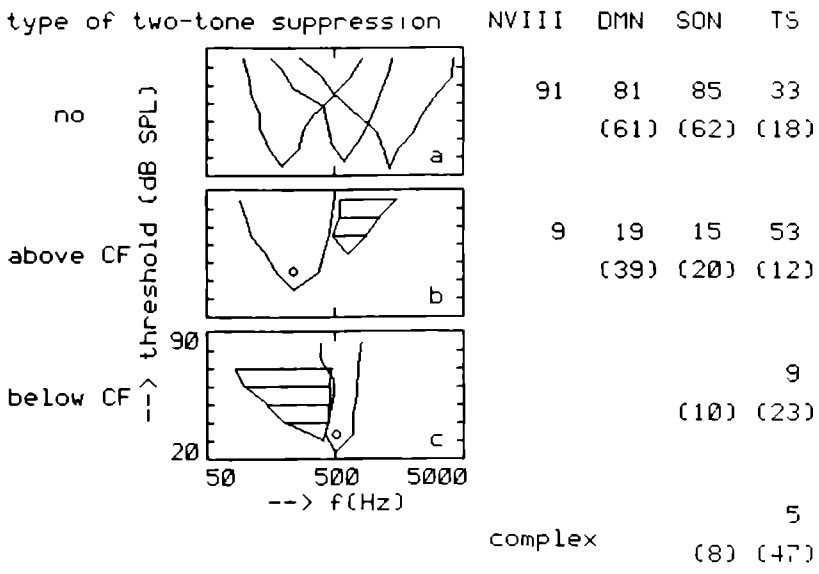

Fig. 4. Distribution of different types of spectral selectivity. Tuning curves and suppresion curves (striped) are shown in a-c. The circle indicates a tone at CF at 10 dB above threshold, to which the response was suppressed by tones inside the suppression curve. (a) no two-tone suppression. (b) two-tone suppression by tones above CF. (c) two-tone suppression by tones below CF. A fourth class of neurons with more complex characteristics is not illustrated.
Figs. 4a and 4b are taken from Schneider-Lowitz (1983), Fig. 4c is taken from Walkowiak (1980). The distribution of response types in the grassfrog is adopted from these papers. In parentheses the distribution found by Fuzessery and Feng (1982, 1983) in the leopard frog is indicated. Further explanation in text.

has several subdivisions (e.g. Feng, 1983; Potter, 1965a). The DMN is the first nucleus in the auditory brain stem where neuronal information processing takes place. The DMN has been scarcely studied because the animal preparation is difficult. The TS is a favourite object of study, since it is easily accessible, and contains a variety of complex but reproducible neuronal responses.

3 Neurophysiology

Electrophysiology is an important method to investigate the properties of the auditory neurons and to unravel their role in the processing of sound. Most studies concentrate on the exploration of single-unit characteristics. In these studies parameters of a sound stimulus are varied, and the action potentials of a neuron are recorded extracellularly. A selective response of a neuron to a certain range of parameters is then supposed to reflect the function of this neuron in the processing of sound.

From Fig. 1 it is clear that important communication signals possess a relatively simple spectral structure but a complicated temporal structure. In the following the selectivities of neurons for spectral and temporal characteristics of sound are discussed.

3.1 Spectral selectivity

A simple model for the spectral selectivity of a neuron consists of a linear band-pass filter followed by an action-potential generating mechanism with a threshold. Thus sounds possessing enough energy in the pass-band of the filter produce a generator potential which exceeds the threshold and generates action potentials.

The spectral selectivity is usually displayed in terms of frequency threshold curves, commonly called tuning curves. A tuning curve represents the threshold intensity a neuron needs to produce extra action potentials when tones with a particular carrier frequency are presented. The carrier frequency with the lowest threshold is called the characteristic frequency (CF). In Fig. 4a tuning curves are shown for three NVIII fibres with CF's of 0.2, 0.6 and 1.3 kHz. The proportion of auditory neurons whose spectral selectivity can be characterized with only a tuning curve declines between NVIII and TS.

In NVIII fibres with CF's below 0.5 kHz most often two-tone suppression can be observed. Two-tone suppression is a nonlinear phenomenon, in which addition of a second tone outside of the pass-band of the filter suppresses the generator potential and thus reduces the number of action potentials. The simple model of a band-pass filter

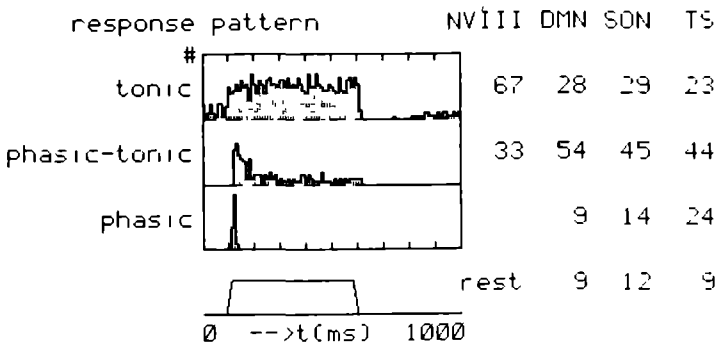

Fig. 5. Distribution of main response patterns. The PSTH's were obtained with a CF tone at 20 dB above threshold. The envelope of the tone is indicated below. The PSTH's are taken from Schneider-Lowitz (1983), the distribution was adopted from this paper and Walkowiak (1980).

followed by an event generator breaks down for these neurons. A way to investigate the spectral selectivity of these neurons is to present two-tone stimuli, and to try to deduce the regions of activation and suppression in the frequency-intensity plane. The circle in Fig. 4b indicates a CF tone with an intensity 10 dB above threshold. The response evoked by this tone can be suppressed by frequency-intensity combinations inside of the striped suppression curve. This two-tone suppression is thought to be of mechanical origin (Capranica and Moffat, 1980). The proportion of units showing suppression by tones above CF increases between NVIII and TS, presumably as a result of inhibitory neural interactions.

Suppression of response by tones below CF has been found in the TS of the grassfrog. This cannot be of mechanical origin because it is not found in the NVIII. Thus inhibitory neural interactions in the spectral domain become more important ascending from DMN to TS.

An extensive study of responses to two-tone combinations by Fuzessery and Feng (1982, 1983) in the leopard frog showed a different distribution of response types, which is indicated in parentheses in Fig. 4. In the TS of the leopard frog they found more complex responses, 28% of the neurons showed suppression by tones below and above CF, and 19% of the neurons could be excited by combinations of two tones. Many units of this last type responded to combinations of two tones with nearby carrier frequencies. A combination of tones of 1200 Hz and 1300 Hz at equal intensity is identical to an amplitude modulated tone of 1250 Hz. Thus another way to interpret the selectivity for two-tone combinations is that these neurons respond selectively to amplitude modulated tones. Selective responses to AM sound have been investigated by Epping and Eggermont (1986b) and Rose and Capranica (1985).

Summarizing: the simple model of spectral selectivity breaks down for a large fraction of the neurons in the auditory brainstem. Regarding the importance of carrier frequency in call recognition (Fig. 2) there is sufficient spectral selectivity available in neuronal responses.

3.2 Response patterns

3.2.1 PSTH

Usually the distribution of action potentials in response to sound stimuli is studied by means of peri-stimulus time histograms (PSTH's). The PSTH's in Fig. 5 result from summing the response to repeated presentations of a 500 ms duration tone at CF with an intensity of 20 dB above threshold, whose envelope is indicated in the lower part of Fig. 5. The main response patterns are: tonic, phasic-tonic and phasic. In a tonic response pattern the number of action potentials generated per unit of time during the presentation of the stimulus is approximately constant. A phasic-tonic pattern results when the response gradually declines to a lower level, and a phasic pattern means that the neuron responds only to the stimulus onset. One third of the NVIII neurons shows a phasic-tonic response pattern, which is known to be caused by short-term synaptic adaptation. To evoke more action potentials in a neuron exhibiting short-term adaptation one has to resort to amplitude modulated stimuli.

3.2.2 Cable properties of neurons

Several mechanisms are responsible for the diversity of neuronal response patterns. Short-term adaptation has been mentioned above. Another mechanism is the spatiotemporal integration of inputs. A neuron consists of a soma, dendrites and an axon. Action potentials are generated at the

transition of soma and axon and are conducted actively to other neurons. Inputs from other neurons arrive on the dendrites and on the soma, where they change the transmembrane resistance. The effect of incoming action potentials can be either excitatory or inhibitory, and the resulting passive change of the transmembrane potential V is called an excitatory or inhibitory post-synaptic potential. The passive propagation of these post-synaptic potentials to the site of spike initiation is determined by the cable properties of neurons. The following is adopted from Rall (1964, 1977).

The propagation of a voltage disturbance along a cylindrical membrane is described by the so-called cable equation:

$$\frac{\partial V}{\partial T} + V = \frac{\partial^2 V}{\partial X^2} \qquad (1)$$

Here $T = \frac{t}{\tau}$ with membrane time constant $\tau = R_m C_m$, the product of transmembrane resistance R_m and membrane capacitance C_m. Further $X = \frac{x}{\lambda}$ with characteristic length $\lambda = \sqrt{\frac{R_m d}{4R_i}}$, with R_i the specific resistance of the intracellular medium and d the diameter of the cylinder. The left-hand part of Eq. 1 corresponds to the dynamics of a leaky integrator, whereas the right-hand part reflects a diffusion term. The solution of the cable equation in response to a point charge input $\delta(X,T)$ is given by:

$$V(X,T) = \frac{e^{-T-\frac{X^2}{4T}}}{\sqrt{T}} \qquad (2)$$

Rall applied these fundamentals of cable theory to neuronal structures. In Fig. 6 the somatic potential is displayed in response to excitatory inputs on proximal (Fig. 6a) and distal (Fig. 6b) parts of the dendrites. Note that the peak in Fig. 6a is five times as high as the peak in Fig. 6b. From these examples it is clear that the spatiotemporal pattern of inputs can produce a range of different time courses of the generator potential.

3.2.3 Time course of generator potential

After the presentation of experimental data in Fig. 5 the analysis of temporal response patterns is formalized. Let w be the generator potential of a NVIII fibre, which results after filtering of the sound stimulus, mechano-electrical transduction and adaptation in the haircell-neuron synapse (see Chapter V). The generation of action potentials, which is viewed as a stochastic point process, is described with a generator function $g(w)$

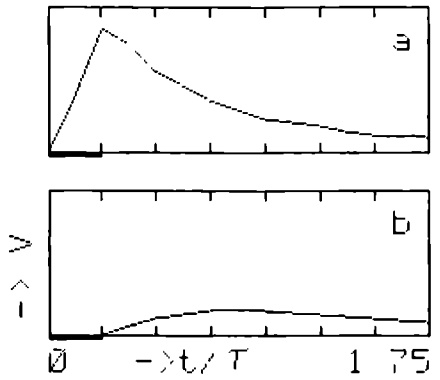

Fig. 6. Model calculations of effect of location of excitatory inputs upon the time course of the soma membrane depolarization. On the abscissa time in units of the membrane time constant τ. During the first 0.25 τ (indicated by the black bar) the inputs of (a) and (b) arrived on, respectively, proximal and distal parts of dendrites. Fig. 6 was adopted from Rall (1964).

(Johannesma and Van den Boogaard, 1985). In point process literature $g(w)$ is known as the intensity function (e.g. Cox and Isham, 1980).

$$P[N(t+dt)-N(t)=1] = g(w(t),\ N(s),\ s<t)\ dt \qquad (3)$$

Here $N(t) = \int_0^t ds\ x_i(s)$ forms the counting process and $x_i(t) = \sum_{j=1}^{N_i} \delta(t-t_{i,j})$ forms the generated point process, with $t_{i,j}$ the times of occurrences of action potentials. The probability per unit of time to generate an action potential, $g(w)$, depends upon the past. After generation of an action potential refractory mechanisms prohibit the generation of a new action potential for a few ms. Thus during the absolute refractory period, τ_{abs}, $g(w) = 0$. Thereafter during a relative refractory period the generator potential w gradually rises to the value it would have had without event generation.

Bibikov (1974, 1975, 1977, 1983) experimentally determined the time course of $g(w)$ circumventing these refractory mechanisms. He presented CF tonepip stimuli with a duration of 100-300 ms and a rise and fall time of 10 ms, at an intensity of 5 dB above threshold. He analysed the first spikes after stimulus onset. These events are not influenced by refractory mechanisms, when there have been no events during a period preceding the stimulus onset. Under the stimulus conditions the distribution of first spike latencies was stochastic, and enabled him to estimate $g(w)$ in the following way.

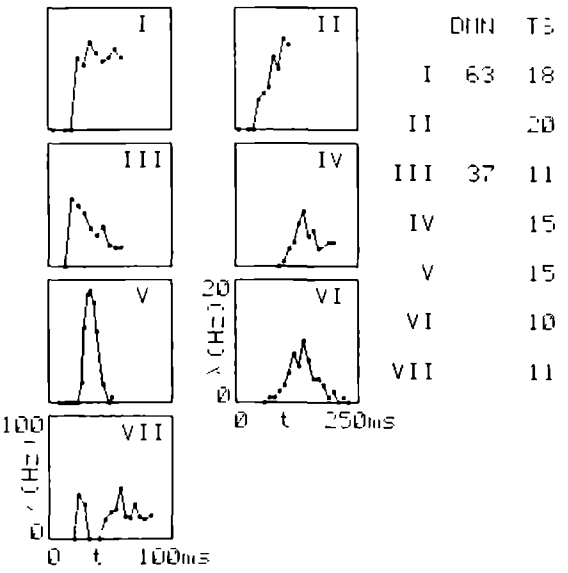

Fig. 7. Distribution of response types to tonepips at an intensity of 5 dB above the neuron's threshold. The probability density of action potential generation (λ) as a function of the time after stimulus onset is plotted for seven typical TS neurons in *Rana ridibunda* Note the different scalings between left and right column. Fig. 7 was adopted from Bibikov (1977) and Bibikov and Kalinkina (1983).

Divide the time after stimulus onset in bins of width Δt. The probability that the first spike falls in bin k is:

$$P[N(k)=1,N(k-1)=0] = P[N(k)=1|N(k-1)=0] \cdot P[N(k-1)=0] \quad (4)$$

In Chapter V it is shown that $P[N(k)=1|N(k-1)=0]$, the desired probability where refractory effects are excluded, is equal to $1-e^{-g(w(k))\Delta t}$. Let $q(j)$ be the number of first spikes falling in bin j, and let M be the total number of stimulus presentations. Combining these experimental variables with Eq. 4:

$$1-e^{-g(w(k))\Delta t} = P[N(k)=1|N(k-1)=0] = \frac{P[N(k)=1,N(k-1)=0]}{P[N(k-1)=0]} = \frac{q(k)}{M-\sum_{j=1}^{k-1} q(j)} \quad (5)$$

Thus from the distribution of first spike latencies $q(k)$ the time course of $g(w(k))$ can be recovered. In Fig. 7 the function $g(w(k))$ ($= \lambda$ in Fig. 7) is shown for seven TS neurons. Bibikov (1977) classified the responses of TS neurons into seven classes, of which these neurons are examples. These seven classes can be interpreted as follows. A response probability that rises relatively fast to a maximum (classes I,III,V,VII) indicates that the neuron possesses a short integration time, typically less than 10 ms. Probably such a neuron receives its inputs near the soma, comparable to the model calculation of Fig. 6a. By contrast a slowly growing response probability (classes II,IV,VI) indicates that the neuron integrates stimulus energy. This is presumably due to inputs arriving on the distal parts of dendrites, cf. Fig. 6b.

A second criterion to distinguish the classes is the time course of the response probability after the maximum has been reached. The responses of classes I,III,V and of classes II,IV,VI show a progressively more peaked character. This can be caused by progressively more short-term adaptation of the input supplying units. One can also propose that inhibition plays a role in generating the different types of responses, especially for class VII.

DMN neurons belong to classes I and III, they possess short integration times, and show signs of adaptation in 37% of the cases (class III). Here again we see much more diversity and complexity in the responses of TS neurons as compared to DMN neurons.

3.3 Temporal selectivity

Inspired by the distinct temporal structure of the mating call Bibikov (1980) investigated the rate response of TS neurons to temporally structured stimuli. The rate response of a neuron is the number of action potentials generated in response to a stimulus. He discovered that in the grassfrog neurons preferred a PRR of 27 Hz. At this PRR a pulse duration of 6-12 ms was most effective.

Schneider-Lowitz (1983) and Walkowiak (1984) investigated the rate responses to pulse trains in NVIII, DMN, SON and TS. Their stimulus is shown schematically in the left-hand part of Fig. 8. The basic element is a pulse of 10 ms duration with a rise and fall time of 2.5 ms. The carrier frequency of the pulse was equal to the CF of the investigated neuron. This pulse resembles the basic element of the natural call (Fig. 1a). Trains of 500 ms duration are composed of these pulses, with PRR varying between 1 and 100 Hz. The stimuli were presented through a loudspeaker in front of the animal, at an intensity of 70 dB peak SPL at the position of the animal. In this way binaural interaction possibly contributed to the

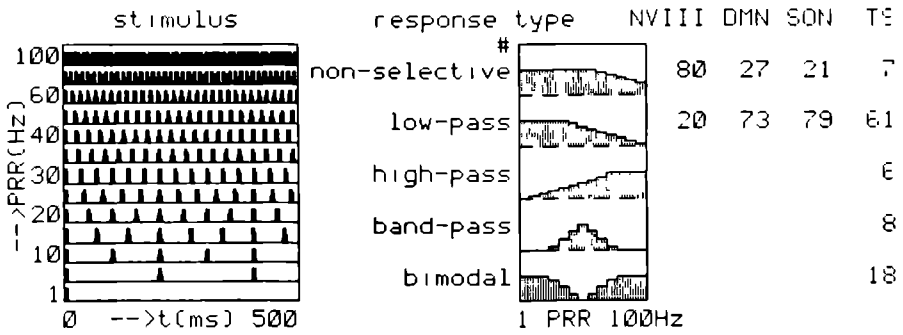

Fig. 8. Distribution of response types to pulse trains in different nuclei. The responses are classified on the basis of the number of spikes per stimulus pulse (#). The stimulus consisted of trains of pulses with a duration of 10 ms. Fig. 8 was adopted from Schneider-Lowitz (1983) and Walkowiak (1984). Further explanation in text.

results (Melssen and Van Stokkum, 1988).

A diversity of response types is found with the PRR stimulus. Different from the methods used by Walkowiak and Schneider-Lowitz I have recalculated the rate responses to the pulse trains, by dividing the rate response through the number of stimulus pulses. When a neuron responds with one event to each pulse irrespective of PRR the response is called non-selective. Due to short-term adaptation the response per pulse usually declines with increasing PRR. The criterion to classify a response as selective is that the response declines by at least 50% relative to the maximum response. A PRR where the response is 50% of the maximum is called a cut-off PRR. The percentage of selective responses increases ascending from NVIII to TS, and three new response types appear in the TS. An important observation of Walkowiak and Schneider-Lowitz was that the cut-off PRR's of temporally selective neurons encompassed the natural range of PRR's. Recall that the evoked calling response in Fig. 2a showed a band-pass character with respect to PRR, whereas the EDR response showed a bimodal character. Thus the temporally selective neurons, which are abundant in the TS, might be involved in call recognition.

4 Scope of this thesis

In the previous section several neuronal characteristics were described: frequency selectivity (3.1), response pattern (3.2) and temporal selectivity (3.3). But how are these neuronal characteristics related to each other? In the past the concept of spectro-temporal receptive field, which combines the aspects of frequency selectivity and response pattern, has been introduced (Aertsen, 1981; Hermes, 1982). It appeared that in TS neurons which receive input from several frequency channels these two aspects cannot be studied separately (Epping and Eggermont, 1985a). Furthermore new kinds of selectivities were revealed with amplitude modulated sounds and clicks as stimuli (Epping and Eggermont, 1986a,b). The central question in this thesis is how the neuronal selectivities found with different stimuli can be combined into a functional description of the neuron. To attack this question experimentally a broad ensemble of spectrally and temporally structured stimuli was presented to DMN and TS neurons (Chapters III-VI). In analysing the neuronal responses to these stimuli special attention was paid to possible underlying mechanisms (Section 3). Comparison of the response characteristics on the levels of DMN and TS provided further information about the development of neuronal selectivities. Based upon the analysis of the neuronal responses in DMN and TS and upon various data from the literature a monaural model for the auditory nervous system of the grassfrog is presented in Chapters V and VI. The model reproduces most of the different kinds of selectivities found in NVIII, DMN and TS, as described in Section 3 and Chapters III-VI. With one parameterset the model reproduces the selectivities of one neuron to the set of stimuli. Variation of parameters reproduces the different kinds of selectivities that are found in the different nuclei.

A problem with the analysis of neuronal responses is that usually stationarity is assumed, which is a prerequisite for time averaging. A method for the analysis of non-stationary point processes is presented in Chapter II. The introduced time-dependent correlation diagram forms the precursor of the well known crosscoincidence histogram (e.g. Aertsen et al., 1979). This

method is applied to electric organ discharges of elephant nose fish, to responses from TS neurons recorded by Epping and Eggermont, and to responses to a random click stimulus in Chapters III and IV.

In Chapter III an overview is given of the selectivities of DMN neurons in response to spectrally and temporally structured stimuli. Most of these stimuli have been used before by Epping and Eggermont (1986a,b; 1986) to investigate the properties of TS neurons. A qualitative model is proposed to explain the complex of selectivities found in a representative DMN neuron which was analysed in depth.

In Chapter IV the responses of DMN and TS neurons to click stimuli are confronted. In accordance with Section 3.3 part of the TS neurons showed response properties resembling those of DMN neurons The rest of the TS neurons exhibited more complex responses.

In Chapter V a monaural model is presented for the peripheral auditory system which reproduces the properties of NVIII and DMN neurons. The qualitative model of Chapter III is worked out quantitatively. The model is based upon systems theory, signal analysis and the properties of neurons. Properties of neurons used are: spatiotemporal integration (Section 3.2.2), action potential generation and absolute and relative refractory period (Section 3.2.3) Through a combination of these properties a DMN neuron functions as a coincidence detector. A coincidence detector is a neuron whose spatiotemporal integrative properties cause a peaked generator potential when excitatory inputs arrive simultaneously. Asynchronously arriving inputs cause a flattened generator potential, which remains subthreshold. This class of DMN neurons is suited to detect the pulses of natural calls, which synchronize NVIII inputs.

In Chapter VI the model of Chapter V is extended to reproduce the responses of neurons in the TS. The main difference between the properties of DMN and TS neurons was the large temporal integration found in 45% of the TS neurons (Fig. 7, Section 3.2.3). The model uses this temporal integration to reproduce the temporal selectivities which are found for the first time in the TS (Fig. 8, Section 3.3). In particular it is shown that temporal integration reproduces the high-pass character of rate responses to pulse or click trains. Adjustment of the amount of coincidence detection on the DMN level and of the amount of temporal integration on the TS level reproduces band-pass rate responses with respect to PRR and amplitude-modulation frequency. Thus it is shown that variation of only a few of the model parameters reproduces the response characteristics of qualitatively different TS neurons.

In Chapter VII the results of this thesis are summarized. The model is discussed in relation to the concepts of spectro-temporal receptive field and sensory interpretation of neural activity (Johannesma, 1981). Finally the neuroethological implications of the results are discussed.

Chapter II

Representation of time-dependent correlation and recurrence time functions

A new method to analyse non-stationary point processes

Ivo van Stokkum, Peter Johannesma and Jos Eggermont

Abstract

Correlation functions based on time averaging are not suited to study non-stationary point processes (e g the electric organ discharge activity of weakly-electric pulse fish) To overcome this problem, we present here a time-dependent correlation method, which can also be applied to study complicated correlations of moderately non-stationary point processes (e g neuronal spike trains) Indication of recurrence time aspects of the point processes provides a more complete representation of the correlation functions In addition higher order correlations between two point processes are represented

1 Introduction

A process consisting of a sequence of identical events, the duration of an event being shorter than the minimum interval between events, can be modelled as a point process Examples are the electric organ discharges of weakly-electric pulse fish, and the action potentials of neurons To study point processes correlation methods are used Autocorrelation functions can be useful for modelling the underlying event generating mechanism Crosscorrelation functions can help in determining a functional connection between two simultaneous point processes With the assumption that the point processes are stationary, the correlation functions are averaged over time, resulting in the well known auto- and cross-coincidence histograms

In neurophysiology these histograms are a widely used tool According to Perkel et al (1967) moderate non-stationarities of irregularly discharging nerve cells have little effect on the detection of interactions between cells In this paper the limitations of time averaged correlation functions with non-stationary point processes are demonstrated

There can be several reasons for the non-stationarity of a point process Firstly the event generating mechanism can be non-stationary, as with the weakly-electric elephant-nose fish Secondly non-stationarities may be induced by a stimulus, or a stimulus ensemble Time-dependent correlation between two neurons, induced by a repeatedly administered stimulus, has been studied extensively by Gerstein and Perkel (1972) and Schneider et al (1983) A stationary stimulus ensemble can cause a non-stationary response, due to habituation and adaptation With a non-stationary stimulus ensemble one also has to be on the alert for possible stimulus dependent correlations (Eggermont et al , 1983a)

The time-dependent correlation diagrams presented here are the precursors of the coincidence histograms They can be used to establish the sense of time averaging Furthermore, recurrence time aspects of points processes can easily be incorporated, enabling the representation of higher order correlations

2 Methods

Methods developed in this paper were applied to pulse trains recorded from two different preparations

1) Two elephant-nose fish, *Gnathonemus petersii*, were allowed to swim freely in two different compartments of an aquarium The compartments were separated by a perforated, dark plastic plate, so that the fish could sense each others electrical activity, but could not approach nor see each other The electric organ discharges (EOD's) of the fish were recorded with stainless steel electrodes in the corners of their compartments

2) Recordings of neuronal activity were made from

the auditory midbrain of the immobilized grassfrog, *Rana temporaria*, using two tungsten microelectrodes. Single-unit spike trains were obtained from the electrode signal by a spike-sorting procedure. Details can be found in Epping and Eggermont (1987).

For off-line analysis EOD's and spikes were stored as events in a PDP 11/34 computer, with a resolution of, respectively, 10 and 60 μs

2.1 Crosscorrelation functions

The starting point for our analysis is formed by a realization of the two point processes A and B, emanating from an experiment of duration T:

$$A(t) = \sum_{i=1}^{N_A} \delta(t - a_i) \ , \ B(t) = \sum_{j=1}^{N_B} \delta(t - b_j) \qquad (1)$$

where a_i and b_j are the times of occurrence of the events, and $0 < t < T$ Now we define the time-dependent crosscorrelation function

$$\begin{aligned} CC_{AB}(t,\tau) &= A(t)B(t+\tau) \\ &= \sum_i \delta(t - a_i) \sum_j \delta(t + \tau - b_j) \\ &= \sum_i \delta(t - a_i) \sum_j \delta(\tau - (b_j - a_i)) \end{aligned} \qquad (2)$$

$CC_{AB}(t,\tau)$ equals zero unless the arguments of both delta functions are equal to zero Thus $t = a_i$ is substituted into the argument of the second delta function This definition needs some justification Strictly speaking the time-dependent crosscorrelation function is equal to the expectation value $E[A(t)B(t+\tau)]$ In our case no homogeneous ensemble is available, so we estimate the time-dependent crosscorrelation function from a single realization of the two point processes.

Recurrence time aspects can be introduced by attaching additional labels to the b-events: $b_{j,i,k}$ is the j-th event from the b-train, with respect to the i-th event from the a-train it has serial order k. By definition every b_j event corresponds to an N_A-tupel of $b_{j,i,k}$ events, one for every i. The time-dependent recurrence time function of order k is then defined as.

$$CC_{AB,k}(t,\tau) = \sum_i \delta(t - a_i) \sum_j \delta(\tau - (b_{j,i,k} - a_i)) \qquad (3)$$

In this paper the difference between forward and backward recurrence times (Perkel et al , 1967) is contained in the positive respectively negative sign of the relative time τ. We remark that·

$$CC_{AB}(t,\tau) = \sum_{k=1}^{N_B} CC_{AB,k}(t,\tau) \qquad (4)$$

Under the assumption that the point processes are stationary, one can replace the expectation value by a time-average. In this way a single realization leads to the crosscoincidence histogram, which is an estimate of the crosscorrelation function $CC_{AB}(\tau)$ Averaging $CC_{AB}(\tau)$ or $CC_{AB\,k}(\tau)$ over time t, and dividing time τ in bins of width Δ, results in the crosscoincidence histogram $CCH_{AB}(n)$ or the recurrence time histogram $CCH_{AB,k}(n)$

$$\begin{aligned} CCH_{AB}(n) &= \frac{1}{T\Delta} \int_0^T dt \int_{(n-\frac{1}{2})\Delta}^{(n+\frac{1}{2})\Delta} d\tau A(t)B(t+\tau) \\ &= \frac{1}{T\Delta} \sum_{i,j} \int_{(n-\frac{1}{2})\Delta}^{(n+\frac{1}{2})\Delta} d\tau \delta(\tau - (b_j - a_i)) \end{aligned} \qquad (5)$$

$$CCH_{AB,k}(n) = \frac{1}{T\Delta} \sum_{i,j} \int_{(n-\frac{1}{2})\Delta}^{(n+\frac{1}{2})\Delta} d\tau \delta(\tau - (b_{j,i,k} - a_i)) \qquad (6)$$

The crosscoincidence histogram is symmetric with respect to n under simultaneous exchange of A and B·

$$CCH_{AB}(n) = CCH_{BA}(-n) \qquad (7)$$

The other three functions, (2), (3) and (6), are obviously not symmetric under exchange of A and B

Coincidence histogram plots are well known, but also time-dependent correlation and recurrence time functions can be visualized For the (t,τ) window of interest symbols are plotted where the arguments of both delta functions equal zero See Fig 3 for an example of a time-dependent crosscorrelation diagram, where dots are used as symbols

2.2 Autocorrelation functions

Autocorrelation can be considered as a special case of crosscorrelation, substituting A for B in the formulas of 2 1. For instance, using (2), the time-dependent autocorrelation function $AC_A(t,\tau)$ is

$$\begin{aligned} AC_A(t,\tau) &= A(t)A(t+\tau) \\ &= \sum_i \delta(t - a_i) \sum_j \delta(\tau - (a_j - a_i)) \end{aligned} \qquad (8)$$

An example of a time-dependent autocorrelation diagram is shown in Fig 2 In this figure vertical bars, squares and crosses are used to label the first, second and third order recurrence times To overcome the disadvantages of symbols, i e the different and rather large size, one can use coloured dots (De Valk et al , 1985) to encode the recurrence time order. This facilitates the perception of the figures

2.3 Interchange of the two point processes in the time-dependent crosscorrelation function

The time-dependent crosscorrelation function is not symmetric under interchange of A and B

$$CC_{AB}(t,\tau) = \sum_i \delta(t-a_i) \sum_j \delta(\tau-(b_j-a_i)) \quad (2a)$$

$$CC_{BA}(s,\sigma) = \sum_j \delta(s-b_j) \sum_i \delta(\sigma-(a_i-b_j)) \quad (2b)$$

Crosscorrelation functions always contain autocorrelation aspects of the two point processes (Perkel, 1970) This is nicely visible in formulas (2a) and (2b) In the diagram representing (2a) adjacent events b_j are plotted around a trigger moment $t = a_i$, within a τ-window This means that $CC_{AB}(t,\tau)$ contains autocorrelation aspects of B in the τ-direction, which can be visualized when the b_j are labeled according to their serial number k Autocorrelation aspects of A, which are contained in the t-direction, cannot easily be observed in $CC_{AB}(t,\tau)$ In the opposite case, $CC_{BA}(s,\sigma)$ contains autocorrelation aspects of A and B in, respectively, the σ- and s-direction The difference between using the a_i or the b_j as trigger moments is illustrated in the time-dependent crosscorrelation diagrams of Fig 4 A higher order correlation, two subsequent events from B, triggered by an event from A, can be seen directly in Fig 4a, but not in Fig 4b

3 Examples

The first two examples are from the electrical activity of the elephant-nose fish In Fig 1 an eventdisplay of 40 s of electric organ discharge (EOD) activity of a solitary fish is shown While recording the EOD-activity the motor behaviour of the fish was observed The fish was suspended in the water all the time, and movements of its chin appendage were accompanied by bursts of EOD's In each line the EOD's during 5 s are represented by dots The first five lines are characterized by pairs of events, separated by somewhat larger intervals We call this the quiet mode In the sixth and eighth line bursts of EOD's are visible So the EOD-activity of the elephant-nose fish is clearly non-stationary

In Fig 2 the accessory time-dependent autocorrelation diagram, with recurrence times up to third order labeled, is presented In the midline an eventdisplay of 40 s is shown, each EOD represented by a dot Horizontally the events within plus and minus 500 ms from a trigger event are displayed The first, second and third event before or after a trigger event at $\tau = 0$ are marked with vertical bars, squares and crosses Higher order recurrence times are represented by dots At the bottom the first, second and third order recurrence time histograms are shown, completed with the autocoincidence histogram All histograms are scaled to the maximum, excluding the central bin, of the autocoincidence histogram This time-dependent autocorrelation diagram enables a more thorough investigation of the quiet mode The pairs of EOD's are now visible as vertical bars at about 80 ms The bars scattered around 200 ms represent the intervals between the pairs of EOD's The second order recurrence times, marked by squares, are grouped around 280 ms, and appear to be slowly modulated The third order recurrence times, the sum of the first and second order recurrence times, are marked by crosses and are scattered around 360 and 480 ms A possible model for the quiet mode consists of commands initiating a pair of EOD's, with an interval of 80 ms The commands are delivered at an interval of about 280 ms, which is slowly modulated This model is corroborated by other examples of the quiet mode, from ten different elephant-nose fish The burst mode is visible as a gradual shortening and lengthening of the first order recurrence times from 80 ms to about 15 ms For a detailed analysis of the burst mode a smaller (t,τ) window is necessary From this example it is clear that time-averaging of a non-stationary point process leads to uninterpretable histograms

In Fig 3 the time-dependent crosscorrelation diagram of the EOD-activity of two elephant-nose fish is shown Because the fish were allowed to swim freely in their compartments, there was no control of the amplitudes of their reciprocal stimulation Vertically time is running from 0 to 50 s, horizontally EOD's of fish B within plus or minus 100 ms relative to an EOD of fish A are represented by dots From $t = 5$ to 20 s there is apparently a preferred latency of 10-12 ms, well known as the echoresponse (Russell et al , 1974) Looking backward, there is a weak echoresponse in the negative direction, between $t = 3$ and 16 s In this and the following figures the first, second and third order recurrence time histogram are drawn under the diagram, all scaled to the maximum of the crosscoincidence histogram at the bottom The echoresponse around $\tau = 11$ ms is clearly visible in the first order recurrence time histogram, and in the crosscoincidence histogram But time averaging obscures the weak echoresponse around $\tau = -11$ ms Again the non-stationary character of the point processes becomes clear in the diagram Horizontal bands appear

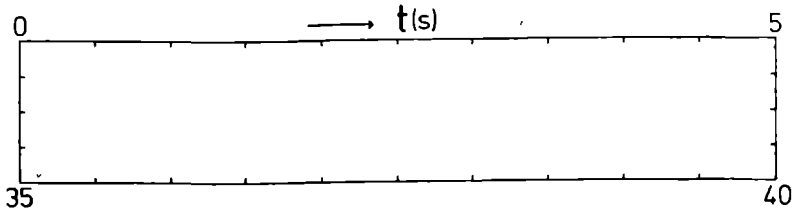

Fig. 1. Eventdisplay of EOD's of an elephant-nose fish. There were 414 events in 40 s. Time is divided into 8 segments of 5 s, each event is represented by a dot.

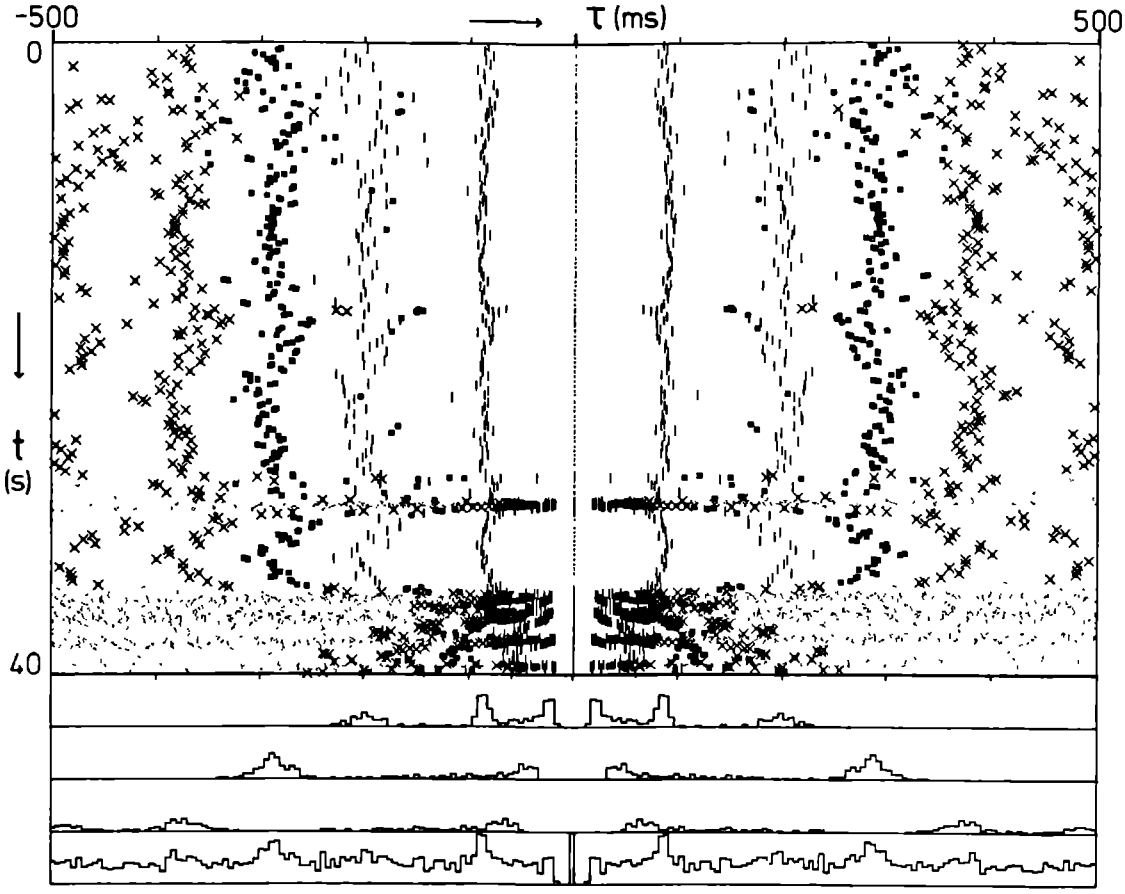

Fig. 2. Time-dependent autocorrelation diagram of the events shown in Fig. 1. Horizontally relative time τ, vertically absolute time t. First, second and third event after or before $\tau = 0$ are marked with |, □ and × respectively. At the bottom the accessory recurrence time histograms of order 1, 2 and 3, and the autocoincidence histogram.

due to bursting activity of the fish.

The next two examples are taken from the auditory midbrain of the grassfrog. In auditory research forward as well as reverse correlation methods are used (Eggermont et al., 1983b). In the forward approach a stimulus, e.g. a tonepip or a click, is presented repeatedly, and the response of a neuron to the stimulus is analysed. In the reverse approach, an action potential of a neuron is taken as a sign that the stimulus ensemble contained some important feature. The stimuli before the spikes constitute the pre-event stimulus ensemble, which is analysed further.

A click stimulus ensemble was presented to a neuron with a spontaneous activity of 2/s which responded with a 12 ms latency to tonepips with a carrier frequency below 300 Hz. The stimulus ensemble, consisting of clicks with a duration of 0.7 ms is considered as a realization of a point process. The interclick intervals are homogeneously Poisson distributed, with an average rate of 16/s and a minimum interval of

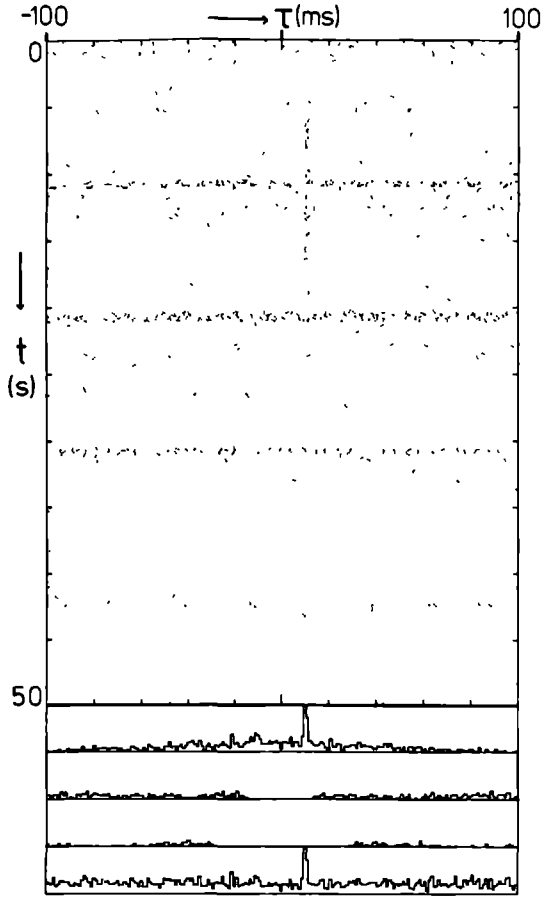

Fig. 3. Time-dependent crosscorrelation diagram of EOD's from two elephant nose fish. EOD's of fish *A* (731 events) are used as triggers. Triggered EOD's of fish *B* (914 events) are plotted horizontally as dots. At the bottom the accessory recurrence time histograms of order 1, 2 and 3 and the crosscoincidence histogram.

1 ms.

Time-dependent crosscorrelation diagrams of the spike train and the click ensemble are shown in Fig. 4. The unit's response is non-stationary. The unit is suppressed by sound first, but this suppression gradually declines. In the reverse correlation diagram, Fig. 4a, the clicks surrounding the spikes are plotted horizontally, and marked according to their serial number as in Fig. 2 In the right hand part of Fig 4a a random picture is visible, as is to be expected for the clicks that follow the spikes. At the left side of the diagram a clear structure is visible. The stimuli of the pre-event stimulus ensemble consist mostly of two clicks separated by an interval of 20 ms, and situated at 30 and 10 ms before the trigger spike. Sometimes a third click, marked by a cross, is visible at 30 ms before the spike. This appears in combination with a click within 10 ms before the spike or an interclick interval of a few milliseconds. The very selective response of the unit to these click combinations is perhaps related to its low frequency sensitivity. The interpretation of the accessory histograms shown in the lower part of Fig. 4a is not so clear cut, because the relations between the recurrence times of different order are lost. In Fig. 4b the forward correlation is presented. Only vertical bars are visible, indicating that the unit responds with only one spike within an interval of 50 ms, preferably at 10 or 30 ms. Combining the evidence from these two representations it can be concluded that this neuron responded selectively to a pair of clicks having a separation of 20 ms with a single spike at a latency of 10 ms. The time-dependent analysis presented in Fig. 4 can be compared with the time-averaged first and second order kernel-analysis in Fig. 8h of Epping and Eggermont (1986a).

The last example is from a double unit recording. The single unit spectral sensitivities, as determined with 46 ms tonepips at a sound pressure level of 89 dB are presented in Figs 5a and 5b, as event displays. The ordinate of a dot, that represents a spike, corresponds to the logarithm of the carrier frequency of the tonepip. The abscissa corresponds to the time after the stimulus presentation. Unit *A* has a spontaneous activity of 2.4/s, which is suppressed by tonepips with a carrier frequency below 1.6 kHz. Unit *B* has a spontaneous activity of 0.3/s. It responds to tonepips with a carrier frequency below 800 Hz with a latency of 65 ms.

A stimulus ensemble consisting of variations on the natural mating call, masked by a stepwise increasing noise background (Eggermont and Epping, 1986) was presented to the double-unit. Both units are excited by the noise, unit *A* responding with about four times as much spikes as unit *B*. Fig. 6 contains four time-dependent crosscorrelation diagrams with recurrence times indicated. The upper two are derived from two simultaneously recorded spike trains. The lower two, Figs. 6e and 6f, are derived from the same spike train of unit *A* and another spike train of unit *B* recorded during a subsequent presentation of the same stimulus ensemble. These nonsimultaneous crosscorrelation diagrams, comparable with the shift predictor of Perkel et al. (1967), are an estimator for the influence of stimulus coupling of the events. The simultaneous crosscorrelation diagrams, Figs. 6a and 6b contain also the possible influence of neural interaction. A difference between a simultaneous and a nonsimultaneous diagram thus indicates the presence of neural

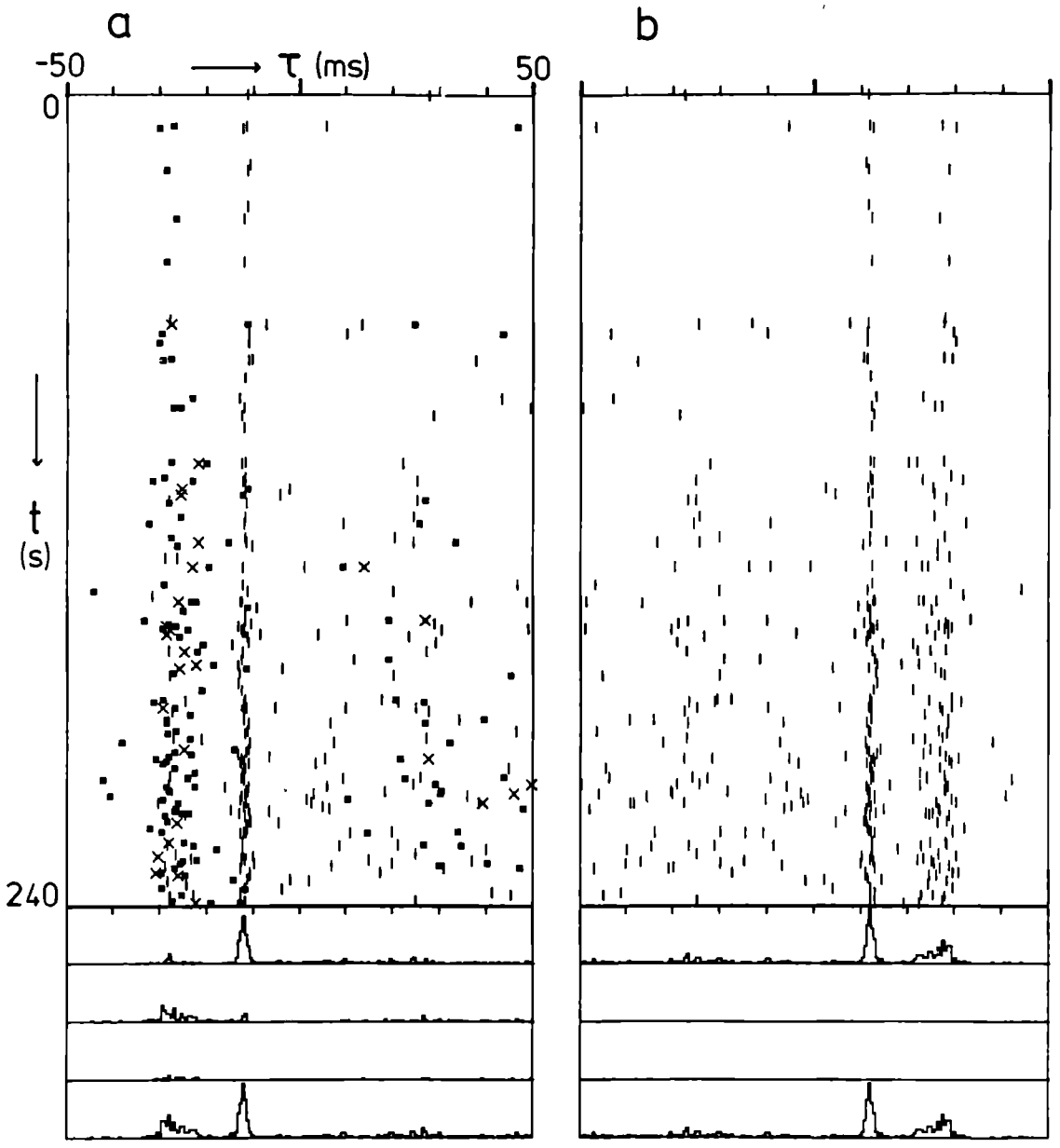

Fig. 4. Time-dependent crosscorrelation diagrams of spike train of unit 268,0,5 with Poisson distributed click stimulus ensemble. First, second and third order recurrence times are marked with |, □ and × respectively. (a) reverse correlation, spikes (140 events) are used as trigger moments for the clicks. (b) forward correlation, clicks (3754 events) are used as trigger moments for the spikes. Under the diagrams the accessory recurrence time histograms of order 1, 2 and 3 and the crosscoincidence histogram.

interaction. At the top of Figs. 6a and 6b, a condensation of symbols in the vertical direction is visible. This slight non-stationarity is caused by habituation of the single unit responses to the noise.

In the left and right diagrams, spikes from unit A, respectively unit B, are used as triggers. The right diagrams contain more squares and crosses than the left, because unit A fires more often than unit B does.

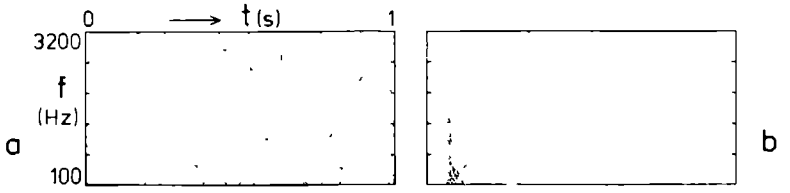

Fig. 5. (a) spectral sensitivity of unit 264,1,0 (*A*), as determined with 46 ms tonepips. (b) spectral sensitivity of unit 264,0,1 (*B*).

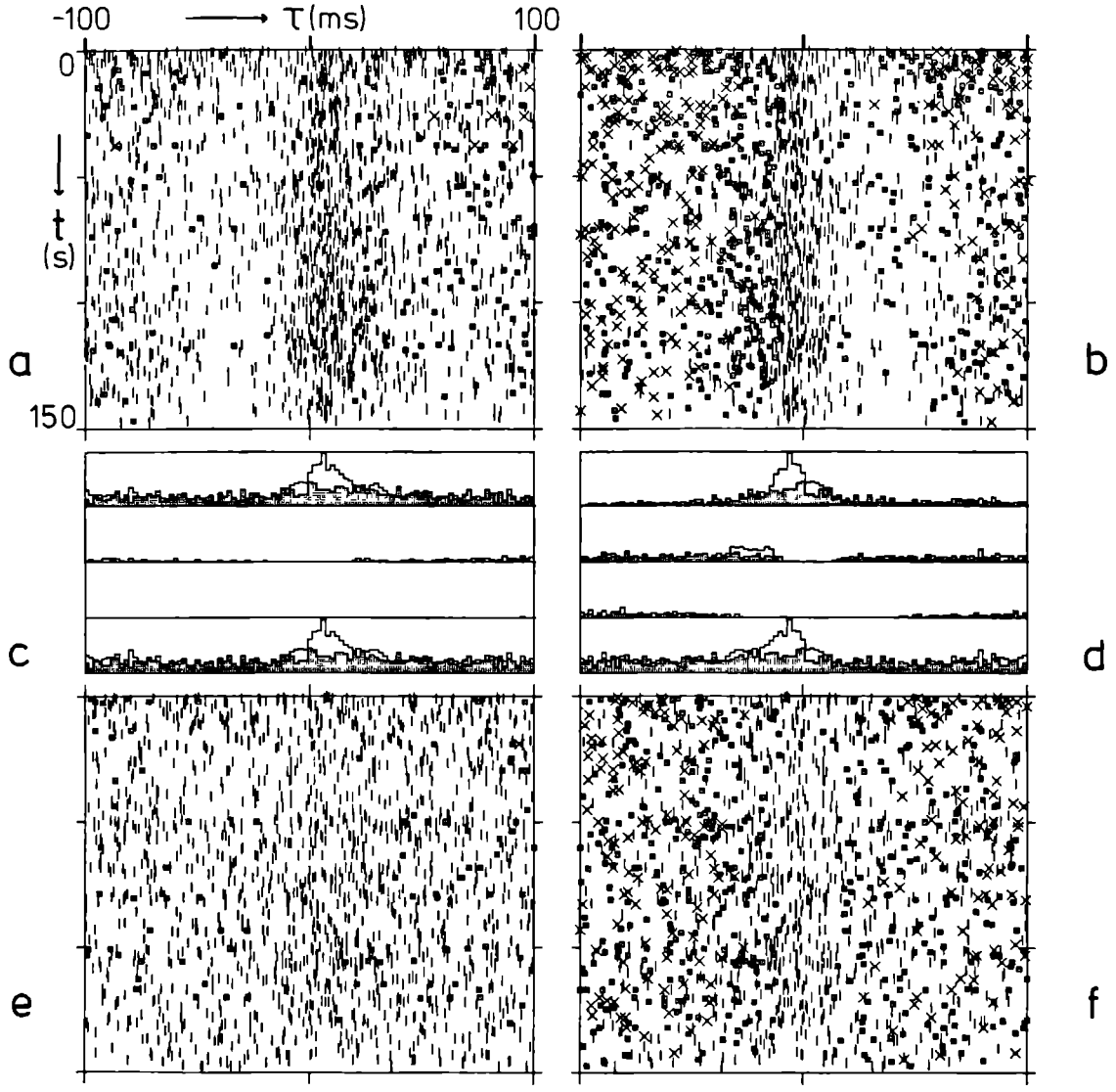

Fig. 6. Time-dependent crosscorrelation diagrams of spike trains from unit 264,1,0 (*A*) and unit 264,0,1 (*B*). (a) simultaneous time-dependent crosscorrelation diagram, spikes from unit *A* (2188 events) are used as triggers. (b) as (a) but now with spikes from unit *B* (528 events) as triggers. (c) simultaneous and nonsimultaneous (shaded) recurrence time histograms of order 1, 2 and 3 and crosscoincidence histogram, derived from Figs. 6a and 6e respectively. (d) as (c) but now derived from Figs. 6b and 6f. (e) nonsimultaneous time-dependent crosscorrelation diagram, spikes from unit *A* (2188 events) are used as triggers. (f) as (e), but now with spikes from unit *B* (473 events) as triggers.

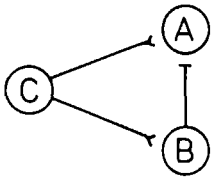

Fig 7 Model which can explain the results of Fig 6
C is a common input source

For independent spike trains forward and backward recurrence times are distributed equally So the first observation is that the two spike trains are not independent, because the negative and positive τ-parts of the diagrams of Figs 6a and 6b differ When comparing the simultaneous and nonsimultaneous crosscorrelation diagrams, two differences appear In the simultaneous diagrams there is a condensation of symbols near the midline Next to this condensation a rarefaction is visible, to the left in Fig 6a and to the right in Fig 6b Looking more carefully at Fig 6b, it can be seen that a trigger spike from unit *B* is generally preceded by one, two or sometimes three spikes from unit *A* within 100 ms, the last one at approximately 6 ms But after a trigger spike from unit *B*, unit *A* is fairly silent for about 50 ms

A model which can explain this crosscorrelation is sketched in Fig 7 Talking in terms of the crosscoincidence histogram of Fig 6d, the peak around -6 ms, which straddles the origin, is caused by a common input The trough at the right of it is caused by an inhibitory influence from unit *B* on unit *A* This reduced probability of spikes from unit *A* after a trigger spike from unit *B*, is seen most clearly in the lower third part of Fig 6b, corresponding with the highest noise level of the stimulus An inhibitory influence of unit *B* on unit *A* can contribute to the complementary spectral sensitivities of the units, as shown in Fig 5

4 Conclusions

Time-dependent correlation functions form in principle a complete representation, and thus are a proper tool to analyse non-stationary point processes

When second or third order recurrence times are expected within the relative time window, indication of recurrence times in the time-dependent crosscorrelation diagram is recommendable The effect of interchange of the two point processes was shown in Figs 4 and 6 Contrary to recurrence time histograms, relations between different order recurrence times are conserved in the diagram It was shown in Fig 4a that this enables the detection of higher order correlations between two point processes Time-dependent correlation methods are necessary with non-stationary point processes, such as the electric organ discharge activity of the elephant-nose fish With moderately non-stationary point processes, such as the action potentials of neurons, there is need for time-dependent methods to unravel complicated histograms Aside from the neuronal coupling, the correlated events, which might be a vehicle for the coding of information in the central nervous system, can be visualized in the time-dependent correlation diagram

Acknowledgements
This investigation was supported by the Netherlands Organisation for the Advancement of Pure Research (ZWO) The authors are grateful to Ad Aertsen, Willem Epping, Willem Melssen and Peter van Mier for critical reading of the text, to the software group for their computational support, and to Astrid van Alst who prepared the original manuscript

Chapter III

Sensitivity of neurons in the dorsal medullary nucleus of the grassfrog to spectral and temporal characteristics of sound

Ivo van Stokkum

Abstract

The responses of 58 dorsal medullary nucleus units to a set of spectrally and temporally structured stimuli were investigated Responses to tonepips and noise indicated monomodal spectral sensitivities, with diverse response patterns Phase-locking was strong for frequencies from 0 1 to 0 2 kHz, and in one unit extended up to 0 6 kHz To clicks, amplitude modulated tone bursts and natural and artificial versions of the mating call various responses were found Most low frequency units fired tonically They showed a non-selective or low-pass rate response to increasing modulation frequency, and a low-pass synchronization behaviour to the envelope A group of mid frequency units fired phasically and exhibited a band-pass rate characteristic to AM tone bursts Frequently this was combined with a low-pass rate characteristic to click trains These units hardly responded to the time-reversed mating call, but fired in a time-locked fashion to the pulses of the original mating call, up to a signal to noise ratio of 0 dB This suggests that aspects of pulse envelope and interpulse interval are coded in the DMN

1 Introduction

The dorsal medullary nucleus is the first auditory relay nucleus High frequency fibres from the basilar papilla terminate in the dorsomedial part of the DMN, whereas mid and low frequency fibres from the amphibian papilla terminate ventrolaterally (Lewis et al , 1980, Fuzessery and Feng, 1981) According to Frishkopf and Capranica (1966), Feng and Capranica (1976), Bibikov and Kalinkina (1982) and Fuzessery and Feng (1983) all DMN units show monomodal tuning curves Feng and Capranica (1976) found that half of the DMN units received input from both ears Only low frequency units show two-tone suppression (Fuzessery and Feng, 1983) Synchronization to sinusoidal waveforms was found by Bibikov and Kalinkina (1982) Nearly all fibres exhibited good phase-locking from 0 1 to 0 2 kHz In addition some units showed phase-locking up to 0 8-1 0 kHz

The natural calls of the grassfrog (*Rana temporaria* L) have a relatively simple spectral and a distinctive temporal structure An example of its mating call is shown in Fig 1 It consists of a train of practically identical pulses with a slowly changing interpulse interval and a more rapidly changing pulse amplitude In the past, studies of the single-unit representation of temporal characteristics of sound have concentrated on the torus semicircularis, the largest auditory midbrain nucleus Thus, most studies conducted in the grassfrog and other anurans focused on rate coding Bibikov (1980) found that the optimal pulse duration at a constant pulse repetition rate of 27/s was 6-12 ms Varying the amplitude modulation frequency of tones or noise Bibikov and Gorodetskaya (1981), Rose and Capranica (1985) and Epping and Eggermont (1986b) reported a diversity of responses, which they classified as low-pass, band-pass, high-pass, bimodal or band-suppression and non-selective Using pulse or click trains with different pulse repetition rates Walkowiak (1984) and Epping and Eggermont (1986a) reported a similar diversity There are a few accounts of temporal selectivity in the medulla Fuzessery and Feng (1983) found temporal low-pass units in both the dorsal medullary nucleus and superior olivary nucleus These units responded consecutively to pulse trains up to PRR's of 280 Hz In the same nuclei Schneider-Lowitz, cited in Walkowiak (1984), found weakly band-pass units as well Using continuous amplitude

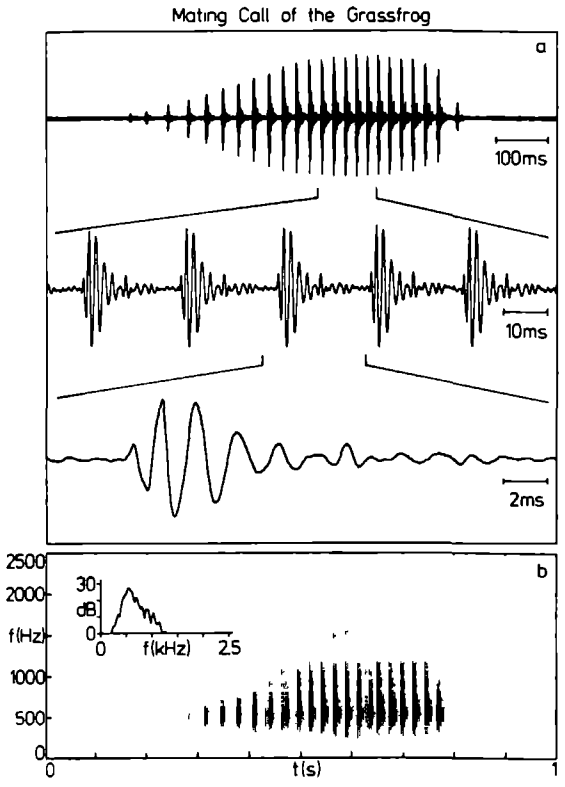

Fig. 1. Example of grassfrog mating call. (a) Oscillogram showing the pulsatile structure on different time scales. (b) Sonogram representing a spectro-temporal image of the mating call, on the same time scale as the upper oscillogram. The inset shows the spectral content of the call averaged over time. From Eggermont and Epping (1986).

modulated tones Gorodetskaya and Bibikov (1985) observed an enhancement of small amplitude changes in the SON for modulation frequencies of 70 to 150 Hz. Finally in the auditory nerve Rose and Capranica (1985) found that the firing rate of eighth nerve fibres was largely independent of the rate of amplitude modulation. Strong synchronization to the envelope of pulses and of AM-sound is reported in the eighth nerve (Frishkopf and Goldstein, 1963; Rose and Capranica, 1985) and in the medulla (Fuzessery and Feng, 1983). In the midbrain the synchronization to the envelope has declined appreciably, although a small number of units shows the same synchronization capability as in the medulla and auditory nerve (Rose and Capranica, 1985; Epping and Eggermont, 1986b). Generally speaking synchronization to the envelope is declining with higher pulse repetition rates or amplitude modulation frequencies. Ascending from auditory nerve to midbrain synchronization capability decreases, whereas rate coding becomes more prominent.

In this report the first results are presented of an investigation into the coding of spectral and temporal features of sound in the DMN. A broad set of stimuli, which has also been used by Epping and Eggermont (1985a, 1986a,b) and Eggermont and Epping (1986), is presented. From their studies in the TS it appeared that a simple characterization with a few stimuli usually was impossible. Spectral sensitivities as determined with tonepips and noise are presented. Responses of DMN units with similar spectral sensitivity to temporally structured stimuli are compared. As an illustration the response of one unit to all stimuli is presented in detail.

2 Materials and methods

2.1 Animal preparation and recording procedure

Adult grassfrogs (*Rana temporaria* L.) from Ireland were anaesthetized with a 0.05% solution of MS-222. After a hole was drilled into the parietal and exoccipital bones above the brain stem, the animal was allowed to recover overnight. The next day it was immobilized with an intralymphatic injection of Buscopan (0.12 mg per gram bodyweight). A local anaesthetic, Xylocaine 4%, was applied to the wound margins. The cartilage over the medulla was removed, thereby exposing the choroid plexus. This dense network of blood vessels covers the dorsomedial side of the alar plates and the fourth ventricle. The animal was placed in a sound attenuated room (IAC type 1202A) onto a damped vibration-isolated frame. Temperature was maintained around 15°C and the skin was kept moist to aid cutaneous respiration. The animal's condition was monitored with help of ECG recording (Epping and Eggermont, 1985a) and by examination of the blood flow in the choroid plexus. A successful preparation was usually kept intact for two days.

The position of the dorsal medullary nucleus was determined from anatomical studies of Opdam et al. (1976). Ultrafine or tapered tungsten microelectrodes (Micro Probe Inc.), coated with Parylene-c, having a 5-25 μm exposed tip and a 1 kHz impedance of 1-5 MΩ were used for extracellular recording. Using hydraulic microdrives one or two electrodes were lowered just medial to the

large blood vessel (vena spinalis posterior) overlying the alar plate longitudinally. Great tissue lag was noticed due to indention of the choroid plexus. After piercing the choroid plexus and penetrating the dorsomedial part of the alar plate abundant auditory activity was usually found, from which sometimes single units could be isolated. Occasionally separable few-unit recordings from one electrode were obtained, with help of a spike separation procedure (Eggermont et al., 1983a). Waveform features and spike epochs were stored on a PDP 11/34 with a resolution of 40 μs, and analysed off-line with a PDP 11/44.

2.2 Acoustic stimulus presentation

The acoustic stimuli were generated by a programmable stimulus generator, as described by Epping and Eggermont (1985a). The stimuli were presented to the animal by two electrodynamic microphones (Sennheiser MD211N) coupled to the tympanic membrane using a closed sound system. The sound pressure level was measured in situ with a half inch condenser microphone (Brüel and Kjær 4143) connected to the coupler (Hermes et al., 1981). The frequency response of the system was flat within 5 dB for frequencies between 100 and 3000 Hz, a sufficient range for studying the auditory system of the grassfrog (Brzoska et al., 1977). The amplitude characteristics of the left and right coupler were equal within 2 dB for the range of interest. The stimuli were usually presented ipsilaterally with respect to the recording site, at sound pressure levels of 70 to 100 dB peak. These sound pressure levels are sufficient to evoke behavioural responses (Walkowiak and Brzoska, 1982; Brzoska, 1984). The following stimulus ensembles have been used:

(1) *Tonepips.* To study spectral sensitivity tonepips of 46 ms, modulated with a gamma envelope, were presented once per second. The carrier frequency was chosen pseudorandomly from 45 logarithmically equidistant values between 0.1 and 5 kHz. The envelope had a rise and fall time of, respectively, 9 ms (20%) and 37 ms (80%). Examples of two gammatones are shown in Fig. 2. For a more extensive description of this stimulus see Epping and Eggermont (1985a). To study two-tone suppression a second tonepip at BF, attenuated 0, 10 or 20 dB with respect to the tonepip stimulus, was presented simultaneously.

(2) *Noise.* Pseudorandom Gaussian white noise with a cut-off frequency of 5 kHz generated by a Hewlett Packard HOI3722A noise generator was used to study spectral sensitivity and phase-locking (Epping and Eggermont, 1985a). A -3 dB per octave low-pass filter with a cut-off frequency of 100 Hz converted this white noise to pink noise.

(3) *Periodic click trains.* Trains of 10 equidistantly spaced clicks, with onset intervals of 3 s. The intervals between clicks were varied pseudorandomly between 128 and 4 ms, corresponding with logarithmically equidistant PRR's of 7.8 to 250/s. The duration of the condensation click was 0.7 ms, and its amplitude spectrum was flat within 5 dB for the range of interest (Epping and Eggermont, 1986a).

(4) *Sinusoidally amplitude modulated tone bursts.* Tone bursts of 500 ms duration with 100 ms rise and fall times were presented every 3 s. BF was chosen as carrier. The modulation depth was 16 dB, corresponding with 84%. The AMF's were the same as the PRR's of the periodic clicks trains. In addition an unmodulated tone burst was presented (Epping and Eggermont, 1986b).

(5) *Random clicks.* Stimulus ensemble consisting of 0.7 ms clicks with an average rate of 16/s. The interclick intervals are drawn independently from a negative exponential distribution with a minimum interval of 1 ms. The interval distribution corresponds to a Poisson process with a deadtime of 1 ms (Epping and Eggermont, 1986a).

(6) *Variations on the mating call.* The mating call of Fig. 1, which was recorded at 16°C, was taken as starting point for spectral and temporal variations. The basic sequence consisted of 10 s silence, followed by three original mating calls. After this the envelope of the original mating call served as amplitude modulator for carrier frequencies of 201, 557, 1067 and 1542 Hz. Then the interpulse intervals of the original mating call were multiplied by 0.5, 1, 2 and 4, corresponding with PRR's of 72, 36, 18 and 9 Hz. Finally the original mating call was presented again followed by its time-reversed version. Intervals between the calls were about 2.5 s. To this sequence of mating calls and variations thereupon an increasing noise background was added. The noise was either white or pink, see stimulus 2. The peak ratios between vocalizations and noise were consecutively ∞, 6, 0 and -6 dB. After the sequence with the highest noise level a 50 s silence was added (Eggermont and Epping, 1986).

(7) *Pulse waveform variations.* To study the effect of pulse waveform a sequence consisting of a click, a pulse from the mating call, tonepips, gammatones, and if appropriate also their time-

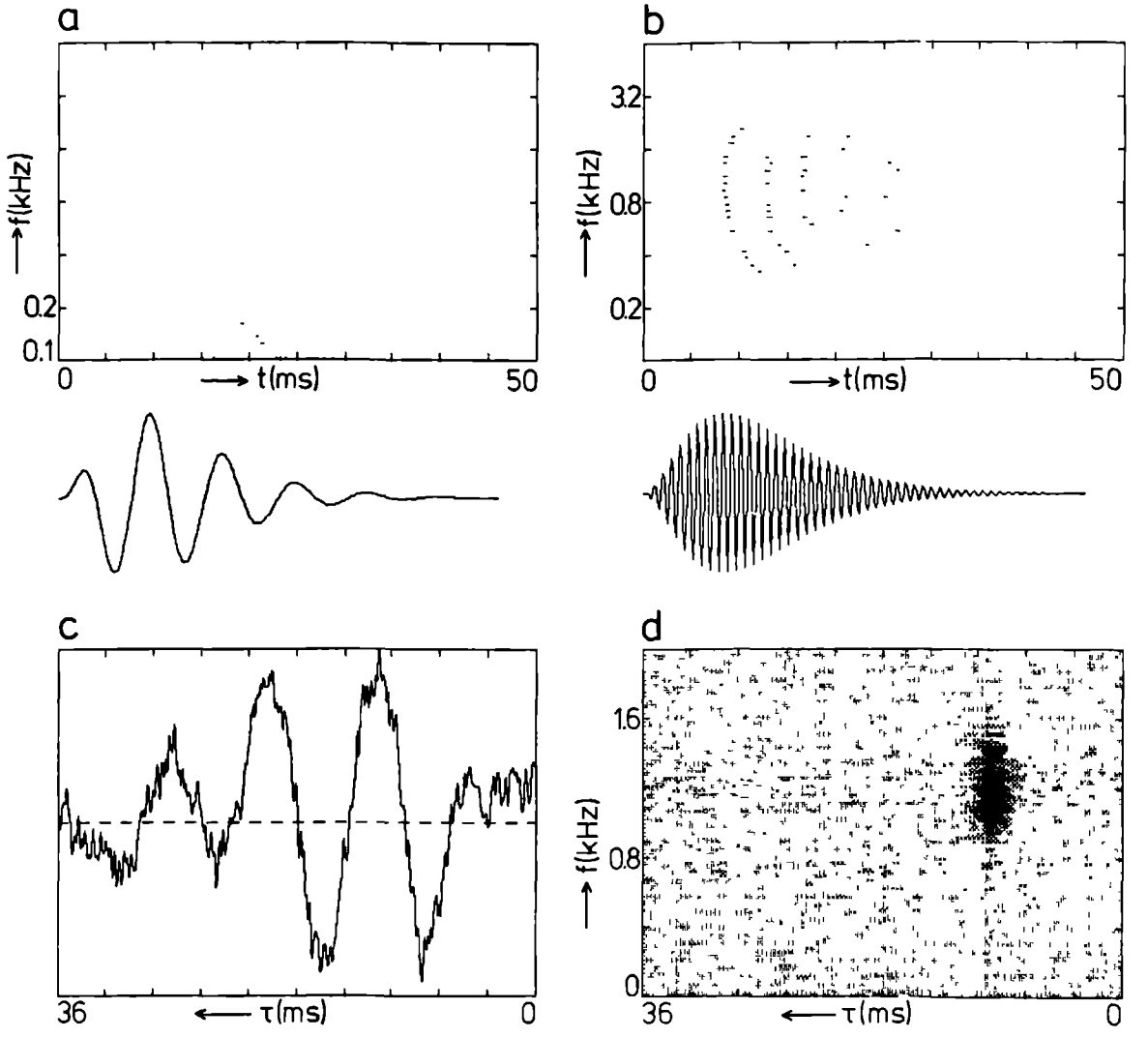

Fig 2. Spectral sensitivities of units 297,0,1 (a,c) and 284,0,2 (b,d) as determined with gammatones and noise. (a) Unit 297,0,1. Reordered eventdisplay of response to tonepip stimulus, 34 events. Underneath gammatone with carrier frequency of 131 Hz on the above time scale. (b) Unit 284,0,2. Reordered eventdisplay of response to tonepip stimulus, 507 events. Underneath gammatone with carrier frequency of 1111 Hz. (c) Unit 297,0,1. Reverse correlation function of 129 events during 335 s of pink noise stimulus. (d) Unit 284,0,2. Average PESE-CoSTID of 1570 events during 84 s of white noise stimulus. All stimuli were presented ipsilaterally at intensities of 90 dB peak SPL.

reversed versions, was used. The tonepips had 1 ms rise and fall times and durations of 5, 10, 20 and 50 ms. The gammatones had rise and fall times of, respectively, 20% and 80% of 10, 20 and 50 ms. BF was chosen as carrier for the tonepips and gammatones. Onset interval was 1 s.

(8) *Search stimulus.* Consisting of variations on the mating call, tonepips and 500 ms pink noise bursts.

For adequate datacollection all stimuli were repeated, respectively, 4, 32, 10, 10, 3, 5 and 20 times immediately after each other. The responses are presented as reordered eventdisplays (Epping and Eggermont, 1985b, 1986a,b; Eggermont and Epping, 1986), except for stimuli 2 and 5. Thereby the actual response is reordered systematically according to a stimulus parameter. Period histograms were made of the responses to the pulse trains and AM tone bursts. From these the synchronization index, defined as the vector strength

(Goldberg and Brown, 1969), was derived. Responses to the noise stimulus were analysed by crosscorrelating the response with a functional of the stimulus. First order crosscorrelation resulted in the averaged pre-event stimulus, or Revcor function (De Boer and Kuyper, 1968). A second order functional, the coherent spectro temporal intensity density (CoSTID), represents the energy distribution of a signal in the time-frequency plane (Johannesma et al., 1981). A CoSTID of the Revcor function, and an average CoSTID of the pre-event stimulus ensemble were calculated, and normalized for the frequency spectrum of the noise (Hermes et al., 1981).

3 Results

Experiments were performed throughout the year, except for the winter, on 16 male and female grassfrogs. From 79 recordings in 12 frogs 58 were designated as single unit on the ground of spikewaveform constancy. These 58 single units were analysed further. The units could be recorded from from 3 minutes to 3 hours. In the other frogs either only synchronized multi-unit activity or no activity at all was found. At the end of some electrode tracks the fading auditory activity was replaced by spontaneous activity, most probably from ventral medullary nucleus units. Twenty-six of the 58 units were spontaneously active, five of them had a spontaneous activity of more than 2/s.

3.1 Tonepips

Forty-eight units were tested with the tonepip ensemble. Of the five that did not respond, four responded only to clicks. In Figs. 2a and 2b responses of two units are shown. The responses to the four presentations of each tonepip are superimposed. Both units responded tonically, the unit in Fig. 2b showing a chopping response pattern. In Fig. 5e a phasic response is visible. From the reordered eventdisplay a best excitatory frequency was estimated, respectively, 130, 1100 and 630 Hz in Figs. 2a, 2b and 5e. In case of phasic responses the frequency corresponding with the shortest latency was chosen as BF. Twelve units responded phasically to the tonepips, and 10 of the 31 tonically responding units showed a chopping response pattern. The latencies were between 6 and 15 ms for 36 of the 43 units. Three of the longer latency units were excited contralaterally. One of these three had a BF of 0.7 kHz for ipsilateral and a

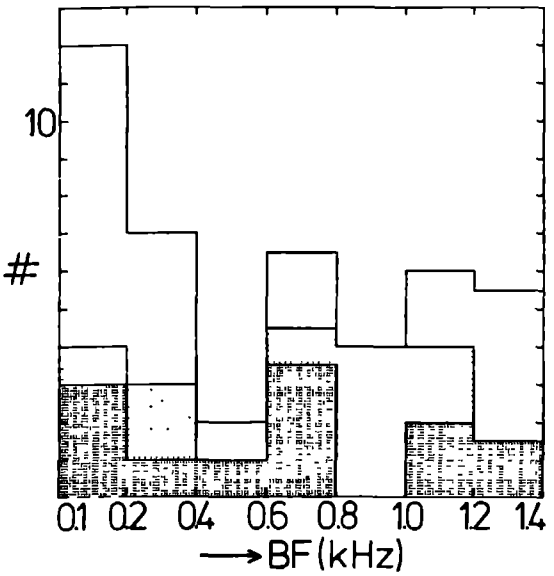

Fig. 3. Histogram of best frequencies of 43 units as determined with tonepip stimulus. Units with chopper characteristic are indicated by the light grey-tone, phasically responding units by the dark grey-tone. Intensity of tonepips 90 dB peak SPL, except for 3 units. All units, except for 3, stimulated ipsilaterally.

BF of 1.2 kHz for contralateral stimulation. A histogram of the response properties of 43 units is shown in Fig. 3. In the remainder of this article units with a BF below 0.4 kHz are called low frequency units. Mid frequency units have BF's between 0.4 kHz and 1.0 kHz, and units with BF greater than 1.0 kHz are designated high frequency units. All seven of the low frequency units tested with a two-tone stimulus showed two-tone suppression by mid frequency tones to various extents. None of the four mid and high frequency units tested showed two-tone suppression.

3.2 Noise

The noise stimulus was presented to 21 units, mostly at 90 dB peak SPL. In addition, 25 units were exposed to noise in combination with other sounds. Of these 46 units nine did not respond to noise at all, of which only one was low-frequency-sensitive. Twenty of the 21 units showed existence of a stimulus-response relation with the noise, as determined with help of a crosscoincidence histogram (Aertsen et al., 1979). Nine of the 12 low frequency units showed a reverse crosscorrelation function, an example is shown in Fig. 2c. The CoSTID of this Revcor function showed a peak from 100 to 200 Hz. The only Revcor function

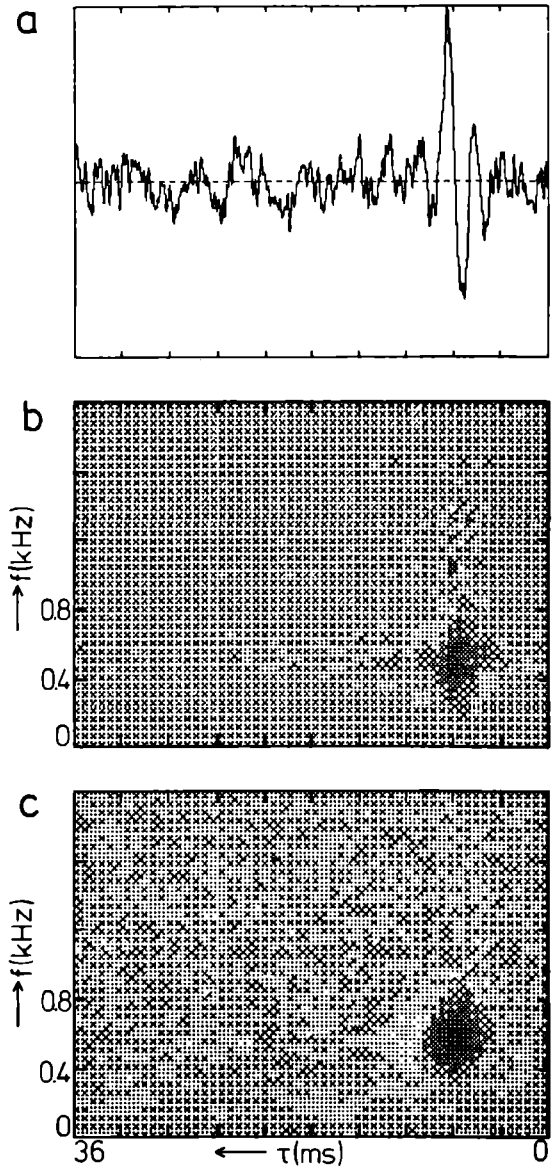

Fig. 4. Spectral sensitivity of unit 307,0,2 as determined with pink noise at an intensity of 50 dB peak SPL. (a) Average PESE, or Revcor function, 1642 events in 116 s. (b) CoSTID of average PESE, scaled to one-tenth of the extrema of (c). (c) Average CoSTID of PESE.

of a mid frequency unit is shown in Fig. 4a. The CoSTID of this Revcor function, Fig. 4b, showed a peak from 360 to 660 Hz. These 10 units thus exhibited phase-locking to parts of the noise, in one unit extending up to 660 Hz. The CoSTID of the Revcor function qualitatively agreed with the average PESE-CoSTID shown in Fig. 4c. Quantitatively however they disagreed, Fig. 4b has been scaled to one-tenth of the extrema of Fig. 4c. The 10 units without a Revcor function all showed a PESE-CoSTID, an example is shown in Fig. 2d. A broad maximum at 10 ms before a spike from 0.9 to 1.6 kHz indicates the high frequency sensitivity of the unit. All spectral sensitivities determined with noise were monomodal. Four units with spontaneous activities from 1 to 14/s showed post-activation suppression with tonepips as well as with noise.

3.3 Unit 297,0,6

An example of the response of a mid frequency unit to the stimulus set is shown in Fig. 5. The unit is practically not spontaneously active. It responds with one spike to tonepips with carrier frequencies between 500 and 800 Hz, see Fig. 5e. At an intensity of 80 dB peak SPL the latency is 10 ms. The latency as determined with the periodic click trains (Fig. 5a) at 100 dB peak SPL is 7 ms. In Fig. 5a one spike to each click is seen for PRR's up to 50 Hz. For higher PRR's its response to the later clicks disappears, ending with one spike after the onset of click trains with a PRR of 250 Hz. The iso-intensity rate histogram at the right of the reordered eventdisplay shows a temporal LP response with a cut-off PRR of 79 Hz. The cut-off PRR is defined as the PRR were the response is half the maximum. The synchronization index histogram at the right also shows a temporal LP characteristic, with a cut-off PRR greater than 200 Hz. For a PRR of 250 Hz the synchronization index is not properly defined because the unit responds only with a single spike at the stimulus onset. The response to AM tone bursts with a carrier frequency of 630 Hz is shown in Fig. 5b. The first spike appears at 57 ms after onset, the last spike at 104 ms. Thus all spikes are elicited during the rise time of the AM tone bursts. Moreover the unit is only sensitive to AMF's between 50 and 125 Hz, with a maximum at 79 Hz. The synchronization index is nearly one. The random clicks with an average rate of 16/s evoke a non-stationary response. This is visible in the time-dependent crosscorrelation diagram (Van Stokkum et al., 1986) in Fig. 5c. Vertically at $\tau = 0$ ms, an eventdisplay of the stimulus may be envisioned. Each stimulus event functions as trigger for the spikes, and all spikes within 50 ms are plotted horizontally. The cross-coincidence histogram that results after integration over time t is shown underneath. The unit's response declines within 10 s to a level of 1 spike/s. Then the response slowly grows again, ending with

8 spikes/s The latency changes in the diagram from 10 to 9 ms A suppression is seen after the activation around 10 ms There are no spikes from 12 to 20 ms after a click, regardless of the clicks in between

After these rather artificial stimuli the response to variations on the mating call is presented in Fig 5d In the upper part (∞), where no noise is added, the unit responds with a time-locked spike to nearly every pulse of the original mating call (x), the mid frequency carrier variation and the 1, 2, 4 times interpulse interval variations The responses to the 1067 Hz carrier variation and to the 5 times interpulse interval variation are about half as much There is hardly any response to the time-reversed mating call (r) The noise evokes no spikes, which is visible in the first 10 s of the 6, 0 and -6 parts The first noise presentation, which is represented in the first lines of the 6, 0 and -6 parts, shows a greatly decreased response to the mating call, the mid frequency carrier variation and the 1, 2 and 4 times interpulse interval variations The other four stimulus presentations, as can be seen in the next four lines, show a greater response The noise masks the responses to the 1067 Hz carrier variation and the 5 times interpulse interval variation The persisting responses are 60% and 15% at a signal to noise ratio of, respectively, 6 and 0 dB

Finally in Fig 5f the response to pulse waveform variations is shown The carrier frequency is 630 Hz, the click is at 100 dB peak SPL, the other pulses are at 80 dB peak SPL The unit responds with one spike to the click (c), the pulse from the mating call (x), the tonepips and the 10 and 20 ms gammatones A smaller response is seen to the 50 ms gammatone, to the 10 ms time-reversed gammatone, and to the time-reversed mating call pulse (first r) At a 10 dB higher intensity the unit only failed to respond to the 20 and 50 ms time-reversed gammatones These responses of unit 297,0,6 will be interpreted in the discussion

Fig 5 Response of unit 297,0,6 to the stimulus set From left to right in Figs (a) and (b) a reordered eventdisplay, the accessory iso-intensity rate histogram, and the synchronization index histogram are shown

(a) Periodic click trains 1154 events, 1600 clicks

(b) AM tone bursts, 630 Hz carrier frequency, 70 events

(c) Random clicks Time-dependent crosscorrelation diagram of clicks with spikes, underneath the accessory crosscoincidence histogram 3251 events, 11755 clicks

(d) Variations on the mating call Eventdisplay reordered according to noise level x indicates the mating call shown in Fig 1, l m, i and h are variations of carrier frequency 201, 557, 1067 and 1542 Hz, 5, 1, 2 and 4 are variations of interpulse interval, r is the time-reversed mating call A pink noise was added, signal to noise ratios are shown at the left 1504 events

(e) Spectral sensitivity as determined with 46 ms gammatones, reordered eventdisplay, 13 events

(f) Pulse waveform variations From left to right click (c), pulse from mating call (x), time-reversed pulse from mating call (r), tonepips of 5, 10, 20 and 50 ms, gammatones (Γ) of 10, 20 and 50 ms, alternated by time-reversed gammatones (r) Underneath the accessory histogram Carrier frequency 630 Hz, 196 events, 260 pulses

All stimuli were presented ipsilaterally, at intensities of 80 (e,f), 90 (b,d) and 100 (a,c) dB peak SPL

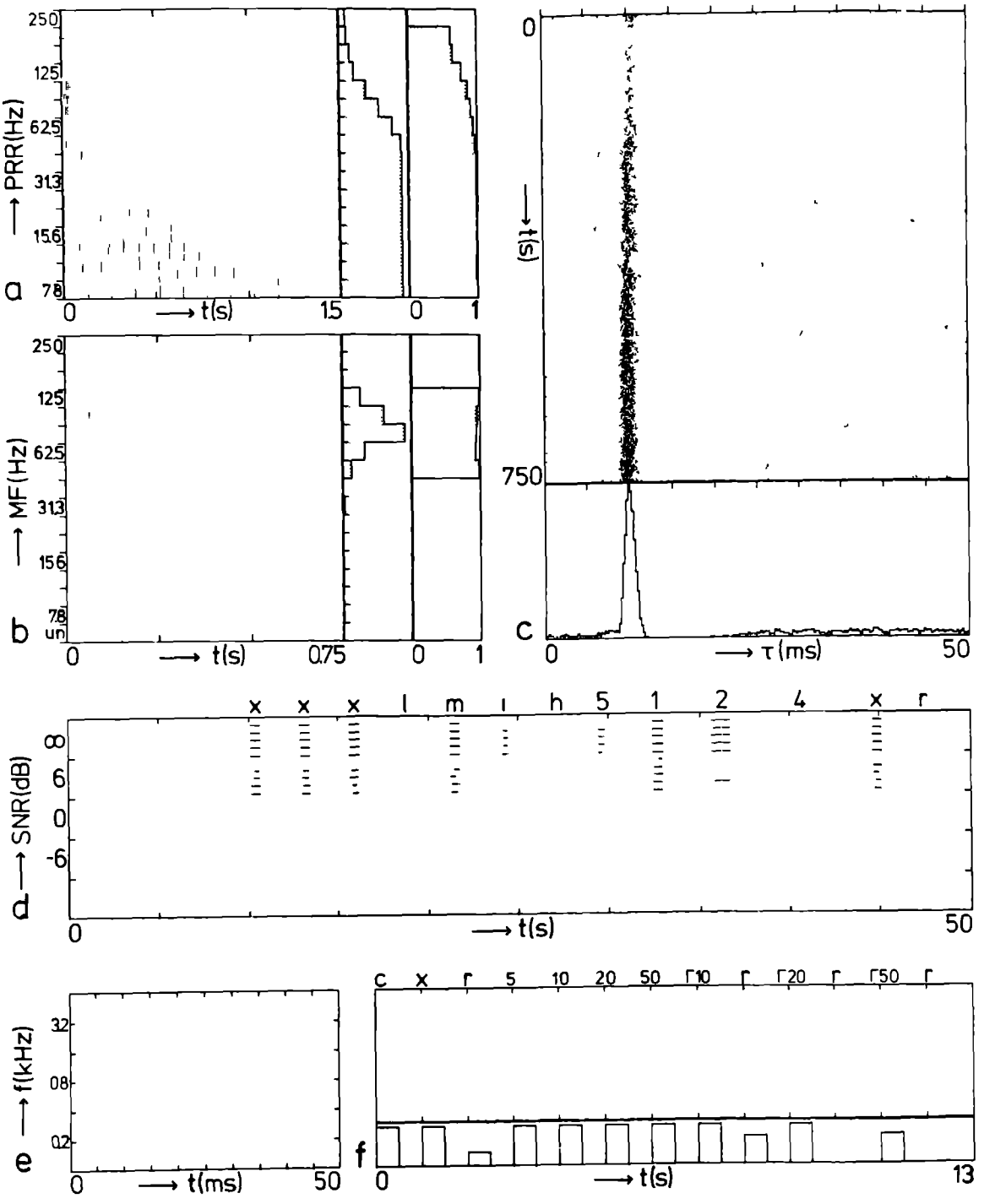
a
PRR(Hz)
250
125
625
313
156
78
0
t(s)
15
0
1
b
MF(Hz)
250
125
625
313
156
78
us
0
t(s)
0.75
0
1
c
0
t(s)
750
0
τ(ms)
50
d
SNR(dB)
8
6
0
-6
x x x l m i h 5 1 2 4 x r
0
t(s)
50
e
f(kHz)
3.2
0.8
0.2
0
t(ms)
50
f
c x r 5 10 20 50 r10 r r20 r r50 r
0
t(s)
13

Table I Summary of responses to temporally structured stimuli

Dotted lines indicate correlations Further explanation in text Special abbreviations act activation, act-sup activation followed by suppression, tuning preference for interclick interval corresponding to BF Rate response types NS non-selective, HP high-pass, BPa weakly band-pass, BPb pronounced band-pass $r \approx x$ response to normal and time-reversed waveform approximately equal, $r \ll x$ response to time-reversed waveform much smaller, r, x not no response to normal or time-reversed waveform P phasic, T tonic

Spectral sensitivity	Random clicks	Click trains	AM tone bursts	Mating call variations	Pulse variations
Low	3 tuning	2 tuning	5 NS	4 $r \approx x$	8 T, $r \approx x$
	1 act	2 LP	2 LP	3 r, x not	
		1 NS	2 BPa		
			1 complex		
(400 Hz)					
Mid	4 act-sup	4 LP	4 BPb	7 $r \ll x$	2 P, $r \ll x$
	1 act	2 NS	1 LP	3 $r \approx x$	2 T, $r \approx x$
		1 HP	1 NS		
		1 BPa	1 BPa		
(1000 Hz)					
High	2 act	3 LP	2 BPa	4 r, x not	3 T, $r \approx x$
	1 act-sup	1 BPb	1 BPb	2 $r \approx x$	1 P, $r \ll x$
		1 NS	1 NS		1 P, $r \approx x$
No	3 act-sup	2 LP		3 r, x not	
Units	15	20	21	26	17

3.4 Temporal sensitivity

The responses of 39 units to the temporally structured stimuli are summarized in Table I With the random clicks three main response patterns are found A preference for interclick intervals corresponding to BF, called tuning, is found in three low frequency units Four units show only activation, whereas eight units show activation followed by suppression, e g Fig 5c The range of suppression lasts from 6 to 60 ms This activation-suppression response is combined with a LP rate response to click trains, e g Fig 5a Latencies to clicks are all between 5 and 12 ms Time-locking to the clicks is usually strong, resulting in non-selective or LP synchronization characteristics

In Fig 6a the response of a low frequency unit (BF 160 Hz) to AM tone bursts with a carrier frequency of 200 Hz is shown The firing rate is highest for the unmodulated tone burst, and practically independent of AMF This is termed a non-selective rate response The synchronization index histogram shows a LP characteristic, with a cut-off AMF of 62 5 Hz The peak at an AMF of 200 Hz results from phase-locking to the 200 Hz carrier, producing a modulation depth of 100% Five of the 10 low frequency units showed a non-selective rate response A pronounced band-pass rate response is shown by four of the seven mid frequency units, e g Figs 5b and 6b The response of the unit in Fig 6b to AM tone bursts with a carrier frequency of 800 Hz is again best for the rising parts In contrast to Fig 5b the response persists, albeit weaker This unit responds best to AMF's from 79 to 156 Hz The synchronization to the modulator is weak, as is seen in the synchronization index histogram at the right, probably due to the later part of the response Seven of the 10 mid frequency units respond in a time-locked fashion to the pulses of the original mating call, and show hardly any response to the time-reversed mating call Three of these seven also show a smaller response to the 5 times interpulse interval variation, and all seven units respond to the calls against a noise background up to at least 0 dB, e g Fig 5d One mid frequency unit responds to the normal and to the time-reversed mating call at an intensity of 90 dB peak SPL, but much stronger to the normal mating call at 70 dB peak SPL The low (4) and high (2) frequency units which respond to the mating call also respond to its time-reversed version With the pulse waveform variations the tonically responding units respond to time-reversed and normal waveforms, whereas three of the four phasically responding

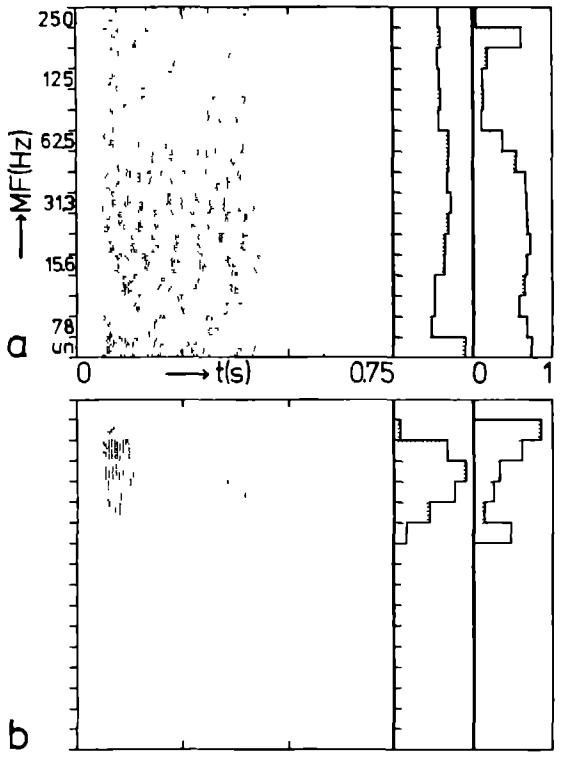

Fig. 6. Responses to AM tone bursts, see legend Fig. 5 (a) Unit 297,1,0, carrier frequency 200 Hz, 2397 events, 80 dB peak SPL. (b) Unit 281,1,0, carrier frequency 800 Hz, 442 events, 90 dB peak SPL.

units do not respond to the time-reversed pulse waveforms, e.g Fig. 5f.

4 Discussion

4.1 Recordings

The preparation was moderately successful. In the preparations where no single units could be isolated the vena spinalis posterior was nearer to the middle. This probably hindered the penetration of the DMN. In one preparation the alar plates and the fourth ventricle could be seen through the choroid plexus. The entrances of electrode-tracks where auditory activity was found were in accordance with the topological maps of Opdam et al. (1976).

The general results are in agreement with the literature. Latencies of 5 to 12 ms to clicks, and mostly of 6 to 15 ms to tonepips, monomodal spectral sensitivities, two-tone suppression of low frequency units by mid frequency tones and phasicon responses are also reported by Fuzessery and Feng (1983). The usually ipsilateral stimulus presentation introduced a sampling bias, in view of the contralateral excitatory and ipsilateral inhibitory inputs found by Feng and Capranica (1976).

4.2 Spectral sensitivity

The distribution of BF's in Fig. 3 is comparable with Fig. 7 in Epping and Eggermont (1985a) for the TS. But in the present study no units with BF higher than 1 4 kHz were encountered BF mismatches like the one found in this study were also reported by Epping and Eggermont (1985b) in the TS Care must be taken with the interpretation of the temporal response patterns to gammatones, because these tones are short and decay fast. There appear to be correlations between BF's of 0.6 to 0.8 kHz and a phasic response pattern, and between BF's of 0.8 to 1 0 kHz and a chopping response pattern

The spectral sensitivities as determined with noise agree with those determined with tonepips, e.g Fig 2. But the spectral sensitivity as determined with tonepips was always broader than the one determined with noise, e g. Figs 2b and 2d. Phase-locking as determined with noise extends up to 660 Hz, at a temperature of 13°C But the quantitative difference between the CoSTID of the average PESE, Fig 4b, and the average PESE-CoSTID, Fig. 4c, indicates that the phase-locking is only weak Epping and Eggermont (1985a) found phase-locking up to about 250 Hz in the TS They remarked that the upper frequency limit for phase-locking seems to be positively correlated with the temperature Bibikov and Kalinkina (1982) reported some DMN units showing phase-locking up to 1 kHz but unfortunately did not mention the temperature In the eighth nerve phase-locking is also found up to 1 kHz (Hillery and Narins, 1987)

4.3 Unit 297,0,6

An attempt will be made to synthesize the responses of unit 297,0,6 to the different stimuli, shown in Fig. 5. In response to clicks the unit shows a LP rate response, Fig 5a This can be explained by the post-activition suppression pattern seen in Fig. 5c. A click first activates the unit, resulting in a spike after 7 ms in Fig. 5a. But after the spike the response is suppressed for at least 8 ms. This can be due to adaptation of the input supplying units. An absolute refractory

time of 8 ms is less probable, interspike intervals as short as 2 5 ms are found in DMN units A third possibility is inhibition Adaptation might also explain the long-term non-stationarity seen in Fig 5c This is qualitatively comparable to the adaptation pattern of Fig 3c in Zelick and Narins (1985)

Unit 297,0,6 responds phasically to tonepips with carrier frequencies of 0 5 to 0 8 kHz, Fig 5e Megela and Capranica (1981) reported a group of rapidly adapting mid frequency auditory nerve fibres, exhibiting little or no spontaneous activity Perhaps such fibres provide input to the unit The latency of 10 ms to tonepips is longer than the 7 ms latency to clicks due to the lower intensity and longer rise time of the tonepip

The BP rate response during the onset of AM tone bursts, Fig 5b, is qualitatively comparable with the whole nerve action potential (AP) modulation detection function in Fig 3 of Hillery (1984) The AP reflects the synchronous activity of groups of eighth nerve fibres A rapid intensity change as provided by a click or tonepip with short rise time provides a cue for time-locking of eighth nerve fibres It thus seems that unit 297,0,6 needs synchronous inputs The LP part of the BP rate response is probably again due to adaptation, as in Fig 5a It is noteworthy that the modulator of AMF's around 79 Hz bears a great resemblance to the envelope of a pulse from the mating call, Fig 1a The lack of response to the AM tone bursts after 100 ms might again be due to adaptation The smaller response to time-reversed pulse waveforms in Fig 5f is probably due to the long rise times, as with the low AMF's in Fig 5b

Finally the response to the variations on the mating call, Fig 5d The time-locked response to each pulse of the normal mating call can be understood from the spectral sensitivity of Fig 5e together with the envelope sensitivity of Fig 5b The weak response to the 1067 Hz carrier variation was not expected from Fig 5e But at a 10 dB higher intensity the spectral sensitivity was found to extend from 380 to 1200 Hz The weaker response to the 5 times interpulse interval variation, corresponding with a 72 Hz PRR, can be understood from Fig 5a, where the response is seen to adapt for PRR's higher than 50 Hz There is no response to the noise, probably because it does not synchronize the inputs The weak responses are masked at the first noise level, whereas the responses to calls with a mid frequency carrier persist The non-stationarities of Figs 5c and 5d may be related, they both show slow recovery In spite of the 50 s silence after the highest noise level the unit's properties regarding the masking by the noise change

Summarizing, unit 297,0,6 responds with one time-locked spike to clicks and pulses with mid frequency carriers and short rise times, after that the unit's activity is suppressed for 8 ms Convergent input by fast-adapting mid frequency sensitive auditory nerve fibres might explain its sensitivity

4.4 Temporal sensitivity

A variety of responses to temporally structured stimuli is shown in Table I On the one hand this is remarkable in view of the absence of cellular subdivisions in the DMN (Opdam et al , 1976, Feng, 1986) On the other hand a variety of adaptation patterns is already found in the auditory nerve (Megela and Capranica, 1981) The main findings in the DMN are the activation followed by suppression and the discrimination between short and long rise times The first provides a temporal LP filter with cut-off PRR's as low as 40 Hz, the second selects for pulse envelopes with short rise times In contrast to the studies in the TS (Walkowiak, 1985, Epping and Eggermont, 1986a,b) no BP units with best AMF's or best PRR's under 50 Hz have been found The BP rate characteristics found in the DMN with AM tone bursts seem to be more related to the pulse envelope than to the interpulse interval, e g Figs 5b and 5d A further investigation into the coding of temporal features of sound against a noise background is in progress

4.5 Behavioural relevance

Walkowiak and Brzoska (1982) reported an evoked calling response to mating calls Male grassfrogs stimulated with mating calls at intensities of 66-95 dB peak SPL increased their calling rates with 100 to 400%, relative to the spontaneous rate of mating calls The mating call envelope with a carrier frequency of 400 Hz was equally effective An interpulse interval variation of 2 times the normal interpulse interval was not much less effective, whereas a 5 times interval variation was considerably less effective

A group of mid frequency units in the DMN reported here have similar characteristics, e g Fig 5d These units are suitable building blocks for the identification of mating calls, even against

a noise background. Inspection of the responses of 207 auditory midbrain units to the variations on the mating call stimulus (Eggermont and Epping, 1986) showed no such clear discrimination of normal and time-reversed mating call. Both calls seemed to be about equally effective, with some units responding better to one of them. In view of the hypothesized identification function of the TS it is remarkable that this discrimination is no longer present on the single unit level.

Acknowledgements
This investigation was supported by the Netherlands Organisation for the Advancement of Pure Research (ZWO). The author thanks Koos Braks for animal preparation, and Willem Melssen for help with the recordings. Willem Epping, Jos Eggermont, Peter Johannesma, Willem Melssen and Peter van Mier are thanked for helpful discussions and critical reading of the text. Marianne Nieuwenhuizen prepared the original manuscript.

Chapter IV

Responses of auditory brainstem neurons in the grassfrog to clicks

Ivo van Stokkum and Willem Epping

Abstract

Single unit recordings were made in the dorsal medullary nucleus and in the torus semicircularis of the immobilized grassfrog The natural calls have a periodic pulsatile structure To investigate the coding of pulse repetition rate periodic click trains with varying pulse repetition rate and an ensemble of clicks distributed randomly in time were used as stimuli In the dorsal medullary nucleus strong time-locking to clicks was found Most units showed an activation followed by suppression response Some units showed a preference for pulse repetition rates matching their low-frequency sensitivity In the torus semicircularis part of the units showed responses similar to dorsal medullary nucleus units Other response types were activation irrespective of pulse repetition rate, and suppression followed by activation The responses to the two stimulus ensembles were more compatible in the dorsal medullary nucleus than in the torus semicircularis

1 Introduction

The natural calls of the male grassfrog (*Rana temporaria* L) consist of pulse trains with a periodic structure (Brzoska et al , 1977, Van Gelder et al , 1977) The dominant frequency in a pulse is about 0 5 kHz A pulse has a rise time of 2 ms and a fall time of about 10 ms The pulse repetition rate ranges from 10 to 40 Hz, depending on temperature (Walkowiak and Brzoska, unpublished results)

Walkowiak (1984) has used pulse trains to investigate the coding of PRR in the torus semicircularis of the grassfrog His pulse trains with a duration of 0 5 s consisted of 10 ms pulses with 2 5 ms rise and fall times, and were presented at best frequency With respect to average rate the responses could be classified as low-pass, band-pass, high-pass, bimodal or non-selective as a function of PRR As an abstraction of the pulses click stimuli have been used by Epping and Eggermont (1986a) to investigate the coding of PRR Using trains of 10 equidistantly spaced clicks they also reported a diversity of average-rate responses The synchronization capability to individual clicks or pulses mostly was a low-pass function of PRR Thus it seems that information about PRR is conveyed mainly in the average rate of TS neurons and is not preserved well in the fine-temporal structure of spike trains

To investigate the mechanisms which underlie the observed temporal selectivities an ensemble of randomly distributed clicks has been used (Bibikov, 1981, Epping and Eggermont, 1986a) In a forward-correlation approach, by which the spikes following a click are analysed on basis of the crosscoincidence histogram, Bibikov (1981) determined the time-course of activation and suppression in the spike-generating region of a neuron In a reverse-correlation approach Epping and Eggermont (1986a) analysed the configuration of clicks preceding a spike on basis of first- and second-order system kernels Again various combinations of activation, suppression and facilitation by clicks were observed

In this report responses to click stimuli from neurons in the dorsal medullary nucleus are presented, using the same stimuli as Epping and Eggermont (1986a) used in the torus semicircularis The results in both brainstem nuclei are compared An attempt is made to relate the responses of a neuron to the two different stimulus ensembles In a forthcoming paper (Epping, in prepa ration) the possibility of predicting the responses to click trains using the responses to the random click ensemble will be evaluated

2 Material and method

2.1 Animal preparation and recording procedure

The methods are described extensively in Epping and Eggermont (1986a) and Van Stokkum (1987) A brief description will be given here Adult grassfrogs (*Rana temporaria* L) from Ireland were anaesthetized with a 0 05% solution of MS-222 A hole was drilled into the parietal and exoccipital bones, exposing the dura above the brainstem The animal was allowed to recover overnight and the next day it was immobilized with an intralymphatic injection of Buscopan (0 12 mg per gram bodyweight) A local anaesthetic, Xylocaine 4%, was applied to the wound margins The animal was placed in a sound attenuated room (IAC type 1202A) onto a damped vibration-isolated frame Temperature was maintained around 15°C and the skin was kept moist to aid cutaneous respiration The animal's condition was monitored with help of ECG recording and by examination of the blood flow in superficial vessels below the dura A successful preparation remained intact for two days The preparation of the dorsal medullary nucleus turned out to be much more difficult than that of the torus semicircularis

The position of the DMN and of the TS were determined from anatomical studies (Hermes et al , 1982 Opdam et al 1975) Parylene-c coated microelectrodes (Micro Probe Inc) with a 1 kHz impedance of 1-5 MΩ were used for extracellular recording Using hydraulic microdrives one or two microelectrodes were lowered into the brain stem This again was much more difficult for the DMN than for the TS because of the tissue lag caused by the choroid plexus Waveform features and spike epochs were stored on a PDP 11/34 with a resolution of 10 μs, and analysed off-line with a PDP 11/44

2.2 Acoustic stimulus presentation

The acoustic stimuli were generated by a programmable stimulus generator They were presented to the animal by two electrodynamic microphones (Sennheiser MD211N) coupled to the tympanic membrane using a closed sound system The sound pressure level was measured in situ with a half inch condenser microphone (Bruel and Kjær 4143) connected to the coupler Stimuli were presented ipsilaterally to the DMN and contralaterally to the TS, at a sound pressure level of 100 or 110 dB peak

The condensation click had a duration of 0 7 ms, and its amplitude spectrum was flat within 5 dB for the range of interest (Epping and Eggermont, 1986a) Two different stimulus ensembles were used

(1) *Periodic click trains* Trains of 10 equidistantly spaced clicks were presented every 3 s A sequence consisted of 16 different PRR's presented pseudorandomly The PRR's were chosen logarithmically equidistant between 7 8 and 250 Hz, which corresponds with interclick intervals between 128 and 4 ms The sequence was repeated 10 times The total duration of the stimulus was 480 s, in which 1600 clicks were presented

(2) *Random clicks* Stimulus ensemble of clicks with an average rate of 16/s The interclick intervals are drawn independently from a negative exponential distribution with a minimum interval of 1 ms The interval distribution corresponds to a Poisson distribution with a dead-time of 1 ms The total duration of the stimulus was 750 s, in which 11755 clicks were presented

The response to the periodic click trains is presented as an eventdisplay reordered according to PRR Temporal integration of the response results in an average rate histogram as function of PRR A measure for the degree of time locking of spikes to the individual clicks in the periodic trains can be determined from the period histogram and is called the synchronization index A value of 1 means that all spikes coincide in one bin of the period histogram, whereas a value of 0 indicates a flat period histogram

The response to the random clicks is presented in two ways The first usually non-stationary 30 s of the response were discarded from the stimulus-response analysis The remaining 720 s generally were reasonably stationary Averaging the forward crosscorrelation function obtained from the clicks and the spikes over time results in a cross-coincidence histogram In addition to the CCH a first-order recurrence-time histogram was calculated, representing the distribution of the first spike after a click To analyse the fine-structure of the CCH its power spectrum was calculated with a resolution of 3 9 Hz In a few cases the time-dependent crosscorrelation function (Van Stokkum et al , 1986) was determined in order to investigate the stationarity of the response

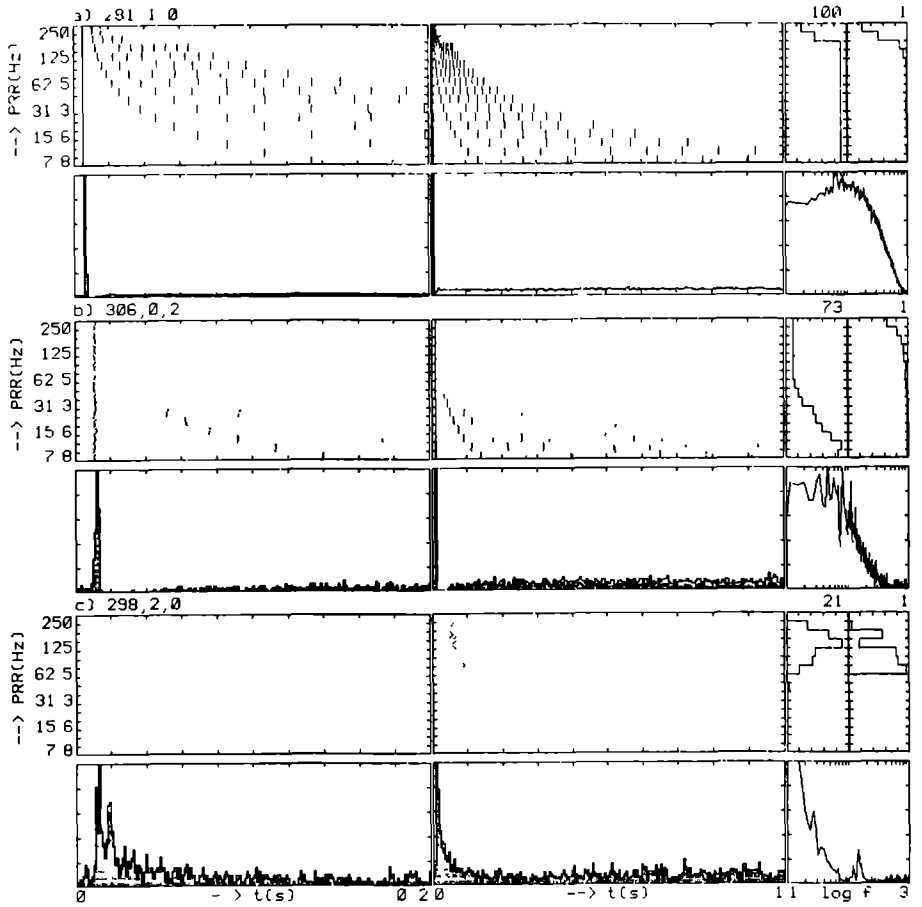

Fig. 1. Responses of three DMN units to click stimuli with an intensity of 110 dB peak SPL. Unit number is indicated at the left. In the upper row from left to right: reordered eventdisplay of response to the periodic click trains on a timebase of 0.2 and 1 s, rate histogram and synchronization-index histogram. The number above the rate histogram indicates the maximum number of events elicited with 10 click trains. The synchronization-index histogram is scaled from 0 to 1. In the lower row from left to right: CCH obtained from the randomly distributed clicks and the spikes on a timebase of 0.2 and 1 s. The shaded FRH indicates the distribution of the first spike after a click. Both histograms have been scaled to the maximum of the CCH. The power spectrum of the CCH is shown at the right, with frequency varying logarithmically from 10 to 1000 Hz.

3 Results

This paper is based on the responses of 24 DMN units and 43 TS units recorded in 26 grassfrogs. Only TS units responsive to both stimulus ensembles have been analysed.

The lowest thresholds found were 60 to 70 dB peak SPL. The stimulus intensities used were usually well above threshold.

Responses from three DMN units are presented in Fig. 1. The reordered eventdisplays of unit 281,1,0 show strong time-locking to the clicks. The unit responds with one spike to each click at a latency of 4 ms up to a PRR of 156 Hz. The rate histogram of unit 281,1,0 shows a cut-off PRR of 200 Hz. The cut-off PRR is defined as the PRR were the rate response is half the maximum. The synchronization-index histogram shows a low-pass character, with again a cut-off PRR of 200 Hz. Note that the synchronization index is practically 1, up to 125 Hz. The cross-coincidence histogram of unit 281,1,0 shows an activation followed by suppression response. The activation latency is 4 ms. The suppression duration is 5 ms. The power spectrum of the CCH is mainly low-pass. Its half maximum is reached at 400 Hz. Unit 306,0,2 responds in a similar way. It has a cut-off PRR of 25 Hz, and a suppression duration of 32 ms. A different type of response is shown by unit 298,2,0, which was sensitive for low-

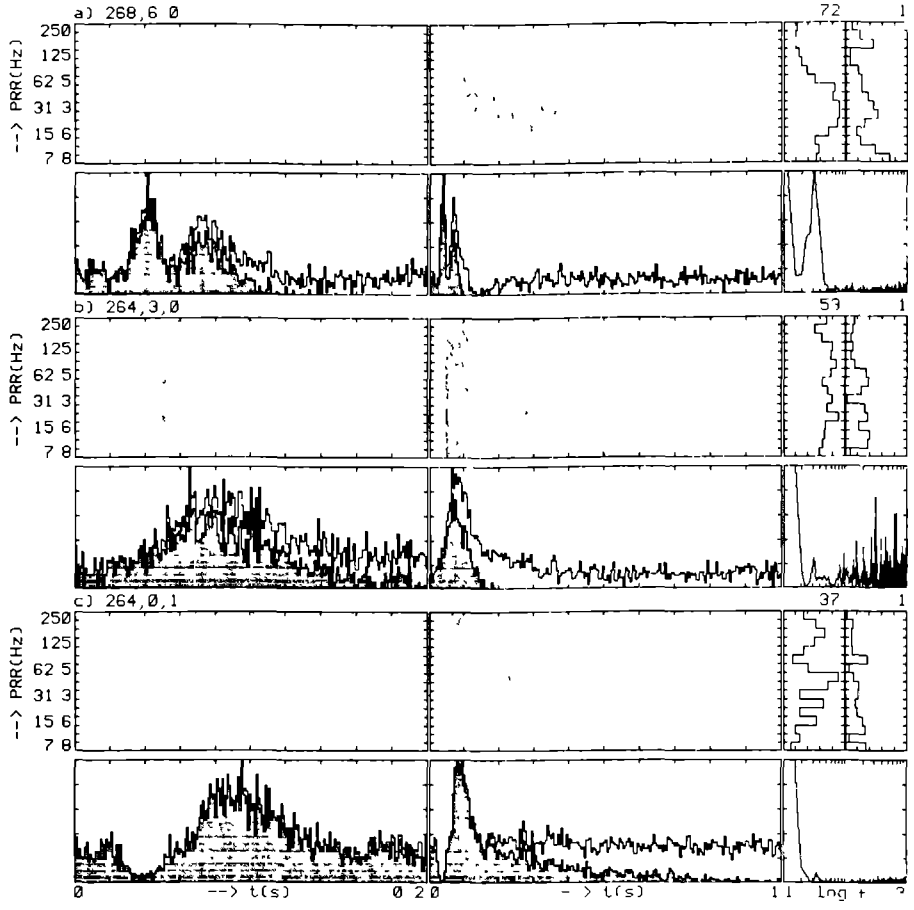

Fig. 2. Responses of three TS units to click stimuli with an intensity of 100 dB peak SPL. See legend Fig. 1.

frequency tonepips. Its rate histogram is tuned to a PRR of 62-200 Hz. The latency of 50 ms to the click trains indicates integration of multiple clicks. The CCH shows a double peak. These peaks consist of first spikes after a click, as indicated by the shaded FRH. Therefore it is plausible that each spike is a response to two or more clicks. The power spectrum of the CCH at the lower right shows a peak between 100 and 200 Hz. A response to the random clicks with multiple peaks in the CCH and a peak in its power spectrum is called tuning. In Fig. 3a the time-dependent crosscorrelation function obtained from the spikes and the clicks is plotted, together with the CCH and the FRH. In Fig. 3 the reverse correlation is shown. Vertically at $\tau = 0$ s an eventdisplay of the spikes may be envisioned. Each spike functions as trigger for the clicks, and all clicks within 0.2 s before the spike are plotted horizontally. Integration of this function over time t results in the CCH shown underneath. This CCH is the mirror image of the CCH in Fig. 1c. The FRH representing the distribution of the first clicks preceding the spikes is indicated by the shaded histogram. This is different from Fig. 1c, because the first spike after a click is not necessarily related to the first click before a spike. The facilitation by multiple clicks is visible in the clusters of clicks before $\tau = 0$ s and in the FRH which extends up to $\tau = -18$ ms. To the left thereof higher-order click recurrence-times contribute to the CCH. After $t = 200$ s it can be seen that each spike is a response to two or more clicks, confirming the suggestion derived from the FRH in Fig. 1c. Looking along the absolute-time axis a gradual decrease of response is seen. This unit thus did not exhibit a steady-state response after 30 s.

Another response type to the random clicks found in the DMN is activation. In this case there was also facilitation by multiple clicks.

In the TS part of the units shows responses similar to DMN units (Epping and Eggermont, 1986a). Three different response types of TS units are presented in Fig. 2. The response of unit 268,6,0 to

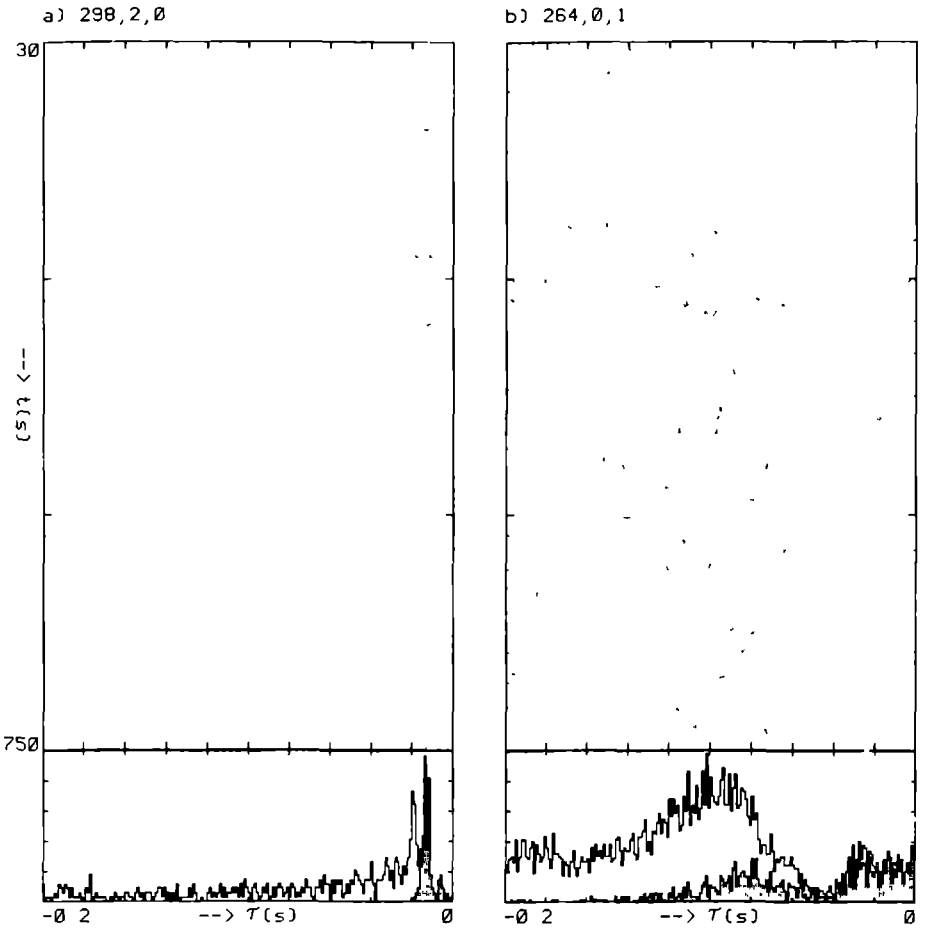

Fig. 3. Diagram of time-dependent crosscorrelation function obtained from the spikes and the clicks. Underneath CCH and shaded FRH. Further explanation in text. (a) DMN-unit 298,2,0. 115 spikes, 11262 clicks. (b) TS-unit 264,0,1. 895 spikes, 11262 clicks.

the click trains shows a preference for intermediate PRR's. The rate histogram has a weakly band-pass character. The FRH is double peaked indicating a response to multiple clicks with an appropriate temporal relation. The powerspectrum of the CCH shows a peak at 30 Hz. Unit 264,3,0 shows a practically non-selective response to PRR's. An onset spike at a latency of 50 ms is followed by tonic activation. The CCH shows a very broad activation peak. A qualitatively different response is shown by unit 264,0,1. In its CCH suppression is followed by activation. The rate response to the click trains shows a multimodal histogram with a minimum at 79 Hz. The peak in the FRH is almost equal to the peak in the CCH. Analogous to Fig. 1c spike elicitation by multiple clicks is therefore plausible

To investigate this further the time-dependent crosscorrelation function is shown in Fig. 3b The distribution of clicks before the spikes shows a high density of clicks between τ = -0.13 s and τ = -0.07 s. The large difference between the CCH and the shaded FRH indicates the contribution of higher-order click recurrence-times to the peak in the CCH.

In Figs. 4a and 4b latency histograms are shown for the DMN and for the TS. The DMN latency histogram shows a peak between 4 and 5 ms, probably reflecting the shortest transmission of activation via the papillae and the auditory nerve. In Fig. 4c the relation is shown between the suppression duration of units showing an activation followed by suppression response pattern to random clicks, and the cut-off PRR of low-pass rate responses to periodic click trains. The relation is reciprocal, except for one TS unit Fig. 4d shows the range of combined activation and suppression latencies found with TS units. The units

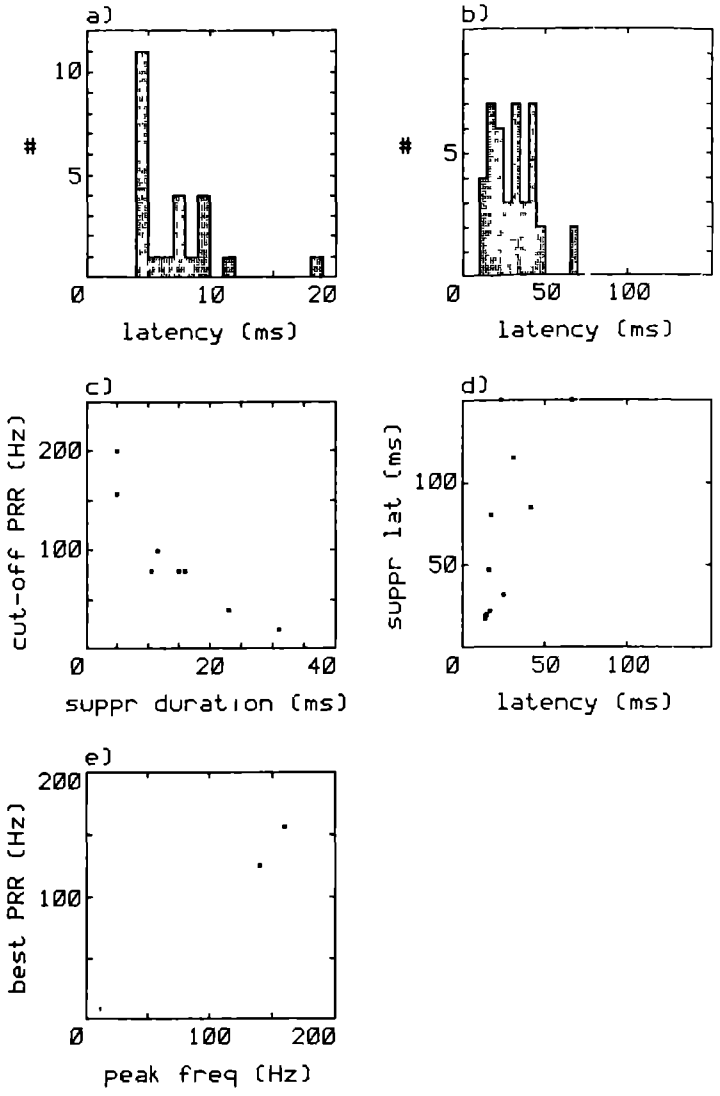

Fig 4
(a) Latency histogram of DMN units to clicks
(b) Latency histogram of TS units to clicks
(c) Scatterdiagram of duration of suppression as determined from response to random clicks and cut-off PRR as determined from rate response to periodic click trains Squares indicate DMN units, points indicate TS units
(d) Scatterdiagram of latency and suppression latency for TS units. Both latencies are determined from response to random clicks
Squares indicate units showing an activation-suppression response, points indicate a suppression-activation response.
(e) Scatterdiagram of peak frequency in power spectrum of CCH and best PRR as determined from rate histogram Squares indicate DMN units, points indicate TS units

with a suppression-activation response, indicated by points, show a weak correlation between these latencies

Finally in Fig 4e the relation between the preference for the PRR of click trains and the peak frequency of the CCH power spectrum is shown. For the two DMN units (squares) both measures show a strong correlation About half of the TS units exhibit good correlation, for the others the correlation is not so clear An overview of the responses to the random click ensemble is shown in Table I Units with a suppression or suppression-activation response are only found in the TS

Table I. Responses to the random click ensemble

	DMN	TS
activation-suppression	11	6
tuning	4	11
activation	3	9
suppression-activation		15
suppression		2
	18	43

4 Discussion

The minimum latency to clicks of 4 ms found for DMN units is compatible with minimum latencies of 2-4 ms found for auditory fibres (Hillery and Narins, 1987). DMN units show two basic response types, as revealed by the responses to the random clicks. A click that is above threshold elicits a time-locked response (see Figs. 1a and 1b). After this activation usually suppression can be observed in the CCH, with a range of durations (see Figs. 1a,b and 4c). This suppression is most probably responsible for the low-pass rate response to the periodic click trains.

When a click is subthreshold more clicks are needed with an appropriate temporal relation. In that case the power spectrum of the CCH and the rate histogram of the response to periodic click trains may show tuning (see Figs. 1c, 3a and 4e). These DMN units are also sensitive to low-frequency tonepips. At least three mechanisms can account for the activation followed by suppression response type: refractory mechanisms, adaptation of input supplying units, and inhibition. This is discussed elaborately in Van Stokkum (1987). The activation response type is probably an intermediate between the other two types.

In the DMN Schneider-Lowitz (1983) used the same pulse train stimulus as Walkowiak (1984). He found that 28% of the units showed a non-selective rate response up to PRR's of 100 Hz. The other units responded in a manner comparable with the low-pass rate responses found with the periodic click trains. It is remarkable that he did not observe such responses in the auditory nerve. He concluded that the temporal information processing starts in the DMN.

In the TS part of the units shows responses similar to DMN units. These units usually have latencies under 20 ms. Their time-locking to clicks is also strong, with synchronization indices between 0.8 and 1.

A preference for PRR's around 30 Hz as shown by unit 268,6,0 (Fig. 2a) may be useful for coding natural calls. As discussed by Epping and Eggermont (1986a) the range of best PRR's as found with clicks seems to be wider than the PRR-range of the natural calls. However Walkowiak (1984) found a better match between units showing preference for PRR and natural-call PRR. This may be due to the difference between his 10 ms pulses and our 0.7 ms clicks. Also his free field stimulation versus our monaural closed sound system may contribute to the PRR selectivity.

A large group of TS units shows a suppression followed by activation response to the random clicks (see Figs. 2c and 4d), which points at neural inhibition. According to the latencies found (Figs. 4b and 4d) this inhibition may be present within the TS. The depth of the trough in the CCH was often down to zero, suggesting that spike generation was preceded by inhibition.

In the DMN good compatibility of responses to periodic click trains and to random clicks was found (Figs. 4c and 4e). In the TS this relation often is not so clear. Epping and Eggermont (1986a) already discussed that the different adaptation levels caused by the two stimulus ensembles may be responsible for this. Another reason for the incompatibility of the responses may be the absence of response to a single click. In the DMN most units respond to a single click, whereas in the TS more often integration of several clicks is necessary to elicit a spike. The temporal sequence of suppressive and facilitatory influences necessary to elicit a spike (see Figs. 2c and 3b) is even harder to investigate.

The rate histogram to the periodic click trains and the power spectrum of the CCH in general only showed qualitative agreement. The peaks in the power spectra of Figs. 1c and 2a coincide with the peaks in the rate histograms. Quantitatively however there are differences, as can be seen in Figs. 1a and 1b. There are two possible explanations for the discrepancies. Firstly the neuron under study is too complex for a first-order analysis. Therefore Epping and Eggermont (1986a) have extended the analysis up to second order. Secondly the power spectrum of the CCH has methodological disadvantages. A histogram only has positive contributions. This leads to a large DC-term in the power spectrum, and may also lead to frequency-doubling effects. Negative contributions to the firing probability can only be seen as far as they reduce the background. The interpretation of the suppression in the CCH as a kind of dead-time in Fig. 4c was more successful to explain the low-pass rate histogram than the power spectrum. It can be concluded that the power spectrum of the CCH is useful to investigate qualitatively a multiply peaked histogram.

In this paper a time-averaged analysis of the responses to the random clicks was presented. But some units in the DMN as well as in the TS responded in a non-stationary way. Non-stationarities found were adaptation, partially or totally, and disinhibition. A proper way to analyse

these responses is the time-dependent correlation function (Van Stokkum et al., 1986). In Fig. 3 of this paper and in Fig. 4 of Van Stokkum et al. (1986) and Fig. 5c of Van Stokkum (1987) examples of this analysis are shown. In most cases it appeared that the combination of the CCH with the FRH preserved the main response characteristics. A time-dependent analysis as shown in Fig. 3 is useful for a detailed analysis of the clicks preceding a spike and of non-stationarities in the response.

The relevance of click stimuli for investigation of the auditory system of the grassfrog seems to be mainly methodological. As Bibikov (1981) already pointed out, the time course of activation and suppression in the spike-generating region of a neuron may be revealed with the random click ensemble. The presence of inhibition is clear when there is initial suppression in the CCH (Fig. 2c). This underlines the importance of analysis of the temporal structure of responses. The difference between the results of Walkowiak (1984) using 10 ms pulses, and our results with clicks points at another mechanism for PRR selectivity. The pulse shape and the on-off time ratio may also contribute to selectivity for natural calls: Bibikov (1980) found that the optimal pulse duration at a PRR of 27 Hz was 6-12 ms.

Acknowledgements

This investigation was supported by the Netherlands Organization for the Advancement of Pure Research (ZWO). The authors thank Koos Braks for animal preparation and Willem Melssen for help with the recordings. Peter Johannesma and Willem Melssen are thanked for helpful discussions and critical reading of the text.

Chapter V

A model for the peripheral auditory nervous system of the grassfrog

Ivo van Stokkum and Stan Gielen

Abstract

A model is presented which incorporates several data from the literature on isolated parts of the peripheral auditory nervous system into a coherent model The usefulness of the model lies in the fact that it describes the functional properties of eighth nerve fibres and dorsal medullary nucleus neurons in response to monaural stimuli

The components are a middle ear filter, transduction and tuning of the haircell, short-term adaptation, event generation with refractory properties, and coincidence detection In a foregoing paper (Van Stokkum (1987), Hear Res 29, 223-235) a class of dorsal medullary nucleus neurons was described, which preferred fast intensity changes Using a coincidence detection mechanism the proposed model reproduces the same preference Variation of the parameters of the model successfully reproduces the range of response patterns which have been obtained from eighth nerve fibres and dorsal medullary nucleus neurons With one set of parameters the output of the model in response to a set of spectrally and temporally structured stimuli qualitatively resembles the response of a single neuron In this way the responses to the different stimuli are synthesized into a framework, which functionally describes the neuron

1 Introduction

For almost three decades the anuran auditory system has been studied with electrophysiological methods (for reviews see Fritzsch et al , 1988) Thereby much work has been devoted to the exploration of single-unit characteristics In these studies parameters of a sound stimulus were varied, and the response of a neuron was recorded extracellularly A selective response of a neuron to a certain range of parameters is then supposed to be related to the function of this neuron in the processing of sound Large quantities of single-unit data have been gathered and interpreted However, this interpretation has not yet led to a mathematical description in terms of a coherent model, which explains the response characteristics of neurons to a wide class of stimuli In this paper we present a quantitative model, which simulates the responses of eighth nerve fibres and dorsal medullary nucleus neurons DMN neurons are innervated chiefly by fibres from the ipsilateral NVIII and the contralateral DMN (Feng, 1986)

The natural calls of the grassfrog and of several other anurans consist of trains of pulses For the identification of these calls several cues are available, such as spectral content, pulse shape, pulse repetition rate, and slow pulse amplitude modulation Many authors (e g Gerhardt and Doherty, 1988) have shown that these and other cues are actually used in female mate choice In contrast, many electrophysiological studies have been limited to a single class of stimuli, exploring the selectivity for either frequency or amplitude modulation In a foregoing paper (Van Stokkum, 1987) we have investigated neurons in the DMN of the grassfrog, using an ensemble of stimuli with spectral as well as temporal parameter variation It is our belief that the use of a broad ensemble of stimuli will provide more insight into the underlying mechanisms which are responsible for the observed neural selectivities Therefore we developed a model which incorporates spectral as well as temporal aspects of signal processing Thereby our attention was focused upon neural mechanisms, whereas less attention was paid to the precise origin of the frequency selectivity, which constitutes a research area in itself Our model consists of a system-theoretical description of frequency selec-

tivity, adaptation, event generation in the NVIII, and coincidence detection in the DMN In this paper the model is restricted to monaural stimuli The results of the model simulations will be compared to experimental data described in the literature (NVIII and DMN) or obtained in our lab (DMN)

2 Methods

Single unit recordings were made in the DMN of the immobilized grassfrog The sound stimulus was presented ipsilaterally through a closed sound system The frog's mouth was kept open during the experiment, in order to decouple both ears (Vlaming et al , 1984) A detailed description of the recording and sound stimulation methods has been given before (Van Stokkum, 1987)

2.1 Components of the model

2.1.1 Middle ear

The transfer of the sound pressure stimulus from the coupler to the inner ear is described by an impulse response $h(t)$, which is shown in Fig 1A Based on measurements of the amplitude and phase of the tympanum displacement as a function of frequency (Vlaming et al , 1984) Aertsen et al (1986) have modelled the auditory periphery Departing from their model we have derived the impulse response of the middle ear

$$h(t) = 2\gamma e^{-\gamma t} \sin(\omega_1 t)\Theta(t) \qquad (1)$$

with $\Theta(t) = 1$ if $t > 0$, and $\Theta(t) = 0$ if $t \leq 0$ The parameters ω_1, the middle ear resonance frequency, and γ, the decay rate, are put equal to, respectively, 2π 0 876 kHz, and 1 297 $(\text{ms})^{-1}$ This description of the middle ear response is valid up to about 1 5 kHz (Vlaming et al , 1984)

2.1.2 Mechano-electrical transduction and tuning

Anurans possess two separate auditory receptors, the amphibian and the basilar papilla The tuning mechanism is different for each papilla (for review see Zakon and Wilczynski, 1988) The tuning of the amphibian papilla is in part due to an active process, which is metabolically vulnerable The basilar papilla is thought to be tuned only mechanically In Figs 1B-E the model is drawn in parallel for haircells of the amphibian and basilar papilla

The response of a haircell to mechanical stimulation of its stereocilia is nonlinear, showing rectification and saturation (Hudspeth, 1983) Following Crawford and Fettiplace (1981b) this is modelled with a function shown in Fig 1B

$$r(q) = \frac{q}{q + q^\circ}\Theta(q) + \frac{q}{q^\circ - \rho q}\Theta(-q) \qquad (2)$$

In the turtle Crawford and Fettiplace measured a mean half-saturation sound pressure q° of 86 dB SPL, and a mean ρ, the ratio of maximum increase and decrease, of 4 The saturation at higher sound pressure levels models well known nonlinear phenomena like two-tone suppression and difference-tone excitation (Capranica and Moffat, 1980) This way of modelling two-tone suppression has also been proposed by Crawford and Fettiplace (1981b) The cascade linear filter - nonlinearity - linear filter, in systems theory known as a sandwich system, has been used before by Johannesma (1971) to model frequency selectivity

Pitchford and Ashmore (1987) demonstrated electrical resonance in haircells of the *amphibian* papilla The membrane potential showed oscillations, the frequency of which varied in accordance with the tonotopical organization of the amphibian papilla In the rostral part of the amphibian papilla they measured resonance frequencies between 0 06 and 0 33 kHz Furthermore Whitehead et al (1986) measured otoacoustic emissions with frequencies between 0 5 and 1 0 kHz These may originate from haircell membrane oscillations in the caudal part of the amphibian papilla The frequency tuning of the haircell membrane will be described by a band-pass filter with impulse response $f_t(t)$

$$f_t(t) = 2\beta_t^{-2} t e^{-\frac{t}{\beta_t}} \sin(\omega_t t)\Theta(t) \qquad (3)$$

The time-constant β_t determines the sharpness of the filter, and ω_t is equal to 2π F_c, the centre frequency The characteristic frequencies of NVIII fibres innervating the amphibian papilla range from 0 1 to 1 0 kHz An example of an impulse response $f_t(t)$ is shown in Fig 1C Such an impulse response is called a gammatone (Aertsen and Johannesma, 1980) Van Gisbergen et al (1975) showed that the frequency selectivity of low-frequency cochlear nucleus neurons in the cat as determined with noise stimuli could be adequately described with gammatone impulse responses (see also De Boer and Kuyper, 1968)

The mechanical tuning of the *basilar* papilla is also modelled with a filter $f_t(t)$ (see Fig 1D) The

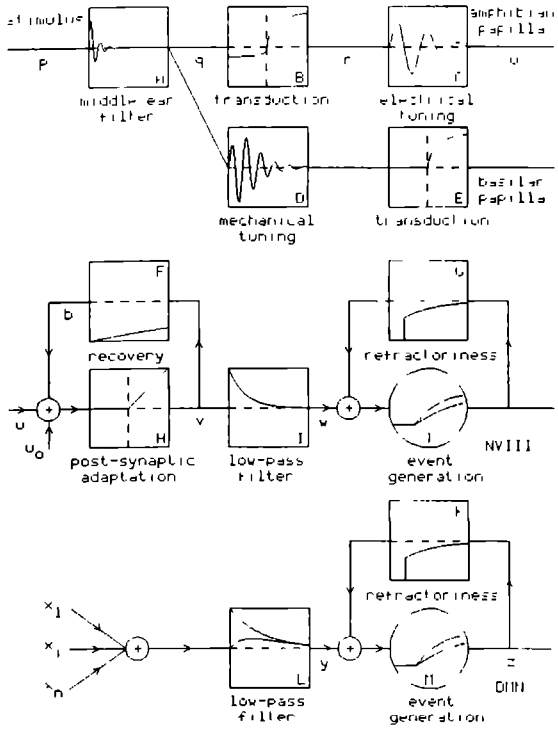

Fig. 1. Model for the processing of sound by the amphibian and basilar papilla, NVIII and DMN of the grassfrog. The stimulus waveform is band-pass filtered by the middle ear (Fig. 1A), and filtered and transduced into a haircell potential (Figs. 1B and C for the amphibian papilla, Figs. 1D and E for the basilar papilla). The synapse between the haircell and the dendrite of the NVIII fibre consists of a short-term adaptation mechanism (Figs. 1F and 1H) and a low-pass filter (Fig. 1I). From the generator potential w of the NVIII fibre action potentials are generated (Fig. 1J), which form the point process x. Absolute and relative refractory mechanisms are incorporated in the negative feedback (Fig. 1G). Several NVIII fibres converge upon a DMN neuron, where they add linearly. From the generator potential y of the DMN neuron action potentials are generated in the same way as above.
In Figs. 1A,C,D,F,G,I,K and L impulse responses are drawn on a timebase of 5 ms. Figs. 1B,E and H represent the instantaneous nonlinearities of Eqs. 2, 4 and 5. Figs. 1J,M show the probability of event generation (Eqs. 12, 13) as function of the generator potentials w, y. Further explanation in text.

characteristic frequency of NVIII fibres innervating the basilar papilla is between 1 and 1.5 kHz for the grassfrog (Schneider-Lowitz, 1983). For the basilar papilla the mechano-electrical transduction follows the mechanical filter, and a function like $r(q)$ (Eq. 2) would generate no output in its linear range, when followed by the low-pass filter of the haircell membrane. We assume that the dynamical characteristics of the transduction cause a rectification. The transduction is modelled with $u(r)$, shown in Fig. 1E:

$$u(r) = \frac{r}{r + r^0}\Theta(r) \tag{4}$$

2.1.3 Adaptation

Megela and Capranica (1981) have demonstrated a diversity of short-term adaptation patterns in the anuran auditory nerve. The basilar papilla fibres show more or less the same modest adaptation to 750 ms tone bursts. Fibres innervating the amphibian papilla showed response patterns ranging from tonic to phasic, which in some cases depended upon carrier frequency or intensity (Megela, 1984).

The short-term adaptation component is basically a half-linear high-pass filter. It is a simplified version of the model of Eggermont (1985), who ascribed adaptation to postsynaptic processes. The input is provided by a transmitter release proportional to u plus u_0, where u_0 is the spontaneous release. There is only release when $u + u_0$ is positive. The transmitter occupies postsynaptic receptors giving rise to an output v, proportional to the number of active receptors. The receptors are inactivated with rate λ. The inactivated receptors $(-b)$ recover with rate μ. Note that b is a negative quantity, which is added to u plus u_0. The adaptation component is described by the following equations:

$$v = (u + u_0 + b)\Theta(u + u_0 + b) \tag{5}$$

$$\frac{db}{dt} = -\lambda v - \mu b \tag{6}$$

The differential equation for b corresponds with a first-order low-pass filter, with time-constant μ^{-1} (see Fig. 1F). When $u_0 = 0$, multiplication of input u with α results in multiplication of the output v with α, a consequence of the halflinearity of the rectifier (Fig. 1H). Note that omission of the rectifier would leave us with a high-pass filter.

2.1.4 Phase-locking

Auditory nerve fibres show phase-locking which declines with increasing frequency. Hillery and Narins (1987) found phase-locking up to 900 Hz. A possible explanation for the decline of phase-

locking is the low-pass filtering by the haircell membrane, demonstrated in the guinea-pig by Palmer and Russell (1986) Low-pass filtering is also performed postsynaptically in the form of excitatory postsynaptic potentials Crawford and Fettiplace (1980) measured a decay time-constant of 1 ms for the EPSP's, in the turtle, at room temperature The decline of phase-lock is modelled with a first-order low-pass filter $l(t)$ (see Fig 1I)

$$l(t) = \omega_2 e^{-\omega_2 t}\Theta(t) \tag{7}$$

Parameter ω_2 determines the cut-off frequency for phase-locking, and is put equal to 1 $(\text{ms})^{-1}$

2.1.5 Event generation

The generation of action potentials (events) is a stochastic process and is modelled with help of a generator function $g(w)$, known in point process literature (e g Cox and Isham, 1980) as the intensity function The probability of event generation in an interval dt is

$$P[N(t+dt)-N(t) = 1] = g(w(t),\ N(s), s < t)\, dt \tag{8}$$

Here $N(t)$ is the counting process, which represents the number of events up to time t Thus $N(t)$ is the integral of the generated point process $x(t)$ (e g Cox and Isham, 1980) The argument of the generator function depends in two ways on the events generated in the past Firstly, after an event has been generated the probability per unit of time to generate an event, $g(w)$, is zero for an absolute refractory period τ_{abs} Secondly, to model relative refractoriness a negative feedback is supplied to the event generator This feedback is given by the impulse response $c(t)$, which starts after the end of τ_{abs}

$$c(t) = -Re^{-(\frac{t-\tau_{abs}}{\tau_R})}\Theta(t-\tau_{abs}) \tag{9}$$

The refractory mechanism is illustrated in Figs 1G and 1K, with $\tau_{abs} = 1$ ms and $\tau_R = 2$ ms In a simulation with binwidth Δt the function $g(w)$ is constant within a single bin When $\Delta t < \tau_{abs}$ at most one event can be generated in a single bin and we have

$$P[\Delta N(t) = 1] + P[\Delta N(t) = 0] = 1 \tag{10}$$

Here $\Delta N(t) = N(t+\Delta t) - N(t)$ Suppose we divide the bin Δt in n parts, and let n go to infinity Then the probability of zero events in the interval Δt becomes

$$P[\Delta N(t) = 0] = \lim_{n\to\infty}(1-\tfrac{g(w)\Delta t}{n})^n = e^{-g(w)\Delta t} \tag{11}$$

Combining Eqs 10 and 11 we get

$$P[\Delta N(t) = 1] = 1 - e^{-g(w)\Delta t} \tag{12}$$

For the generator function $g(w)$ any non-negative function can be chosen We have used a half-linear function

$$g(w) = \nu(w-m)\Theta(w-m) \tag{13}$$

For w less than m, the threshold parameter $g(u)$ is zero As a consequence, when m is positive, spontaneous activity can only be generated with a positive generator potential Parameter ν determines the slope of $g(w)$ In Figs 1J and 1M the probability of event generation according to Eqs 12 and 13 is drawn for two different values of ν

2.1.6 Convergence of inputs

We assume that there is a convergence of many NVIII fibres upon a single DMN neuron Based upon Rall's model (1977) of neuronal cable properties, convergence of inputs is modelled as linear summation of the input point processes, which are then low-pass filtered to arrive at compound EPSP's In formula (Johannesma and Van den Boogaard, 1985)

$$y(t) = \sum_{i=1}^{n}\int ds\ e_i(s)x_i(t-s) \tag{14}$$

$$\text{with } e_i(t) = We^{-\frac{t}{\tau_d}}(1-e^{-\frac{t}{\tau_u}})\Theta(t) \tag{15}$$

Here $x_i(t) = \sum_{j=1}^{N_i}\delta(t-t_{i,j})$ represents the events at times $t_{i,j}$ of NVIII fibre i In Fig 1L two different EPSP shapes $e_i(t)$ are drawn In our simulations we have chosen an EPSP with rise and decay time-constants of, respectively, 0 and 1 ms

2.2 Implementation of the model

The model was programmed in Fortran 77 on a VAX 11/785 computer Stimuli which were used for single unit recording from auditory neurons were sampled and provided the input to the model The sample interval usually was 0 1 ms, but for lengthy stimuli it was 0 2 or 0 25 ms A summary of the parameters used in the main simulations of this paper is given in Table I The degrees of freedom are the amount of nonlinearity in the transduction, the tuning characteristics, the short-term adaptation and recovery time-constants, and, most important, the parameters

Table I Model parameters

Parameters	Eq	related to	value
γ, ω_1	1	middle ear filter	1 297 $(ms)^{-1}, 2\pi$ 0 876 kHz †
ρ	2	transduction asymmetry	4 §
q°, r°	2,4	transduction saturation	1
ω_t, β_t	3	tuning characteristics	variable
u_o	5	spontaneous activity	0
λ^{-1}, μ^{-1}	6	short-term adaptation	5 ms, 1000 ms
ω_2	7	dendritic low-pass filter	1 $(ms)^{-1}$ ‡
τ_{abs}, R, τ_R	9	refractory properties	NVIII 4-5 ms, 0 05, 2 ms
			DMN 6 ms, 1 2, 2 ms
m, ν	13	event generation	NVIII 0 0003-0 003, 250 $(ms)^{-1}$
			DMN 0 45, 10 $(ms)^{-1}$
n	14	amount of convergence	16
W	15	EPSP height	0 1
τ_d, τ_u	15	EPSP shape	1 ms, 0 ms
		time delay	NVIII—DMN 2 ms

†) derived from Aertsen et al (1986) p 21 25
§) Crawford and Fettiplace (1981b), p 326
‡) Crawford and Fettiplace (1980), p 91

which determine the event generation and refractory properties

Outputs of the model are the generator potentials w and y, and the time-series x and z, which mimic the occurrences of action potentials in, respectively, a NVIII fibre or a DMN neuron The generator potentials help to understand the action of the several nonlinearities incorporated in the model The time-series x and z, or averages thereof in the form of histograms, are directly compared to experimental data obtained in the NVIII and the DMN, described in the literature or obtained in our lab

3 Results

3.1 Frequency tuning

The frequency tuning of the model will be illustrated with plots of isopotential contours of the generator potential w These are comparable to frequency tuning-curves as measured in the NVIII In Fig 2 filter properties and tuning characteristics are illustrated Column one and two show, respectively, the impulse response and powerspectrum of filters with centre frequencies of 1 25, 0 625 and 0 2 kHz and of the middle ear filter In the third column isopotential contours are shown The carrier frequency of the tonepips varies horizontally, the intensity vertically, both on a logarithmic scale The intensity varies from −40 to +20 dB relative to the half-saturation point q°, respectively r° (see Eqs 2 and 4) From top to bottom tuning is visible with the centre frequency approximately equal to that of the filter The main parameter responsible for the tuning quality is β A larger β means a longer impulse response and a sharper tuning

3.2 Two-tone suppression

The consequences of the different order of bandpass filter and nonlinearity in Figs 1B,C and 1D,E are demonstrated with a two-tone stimulus A second tonepip with an intensity of −20 dB relative to q° or r° and a carrier frequency equal to the F_c of the filter was added to the tonepip stimulus The isopotential contours are shown in the fourth column of Fig 2 Suppression of the response to the second tonepip is visible for both amphibian papilla filters In particular, the area indicated by the minus sign in the F_c = 0 2 kHz box is comparable to a suppression tuning curve as shown in Fig 11 of Capranica and Moffat (1980) The suppression can be understood as follows a high intensity tone away from F_c drives the nonlinearity (Eq 2, Fig 1B) in the saturation range which results in a signal compression Thus the second tone at F_c is compressed by the nonlinearity, re-

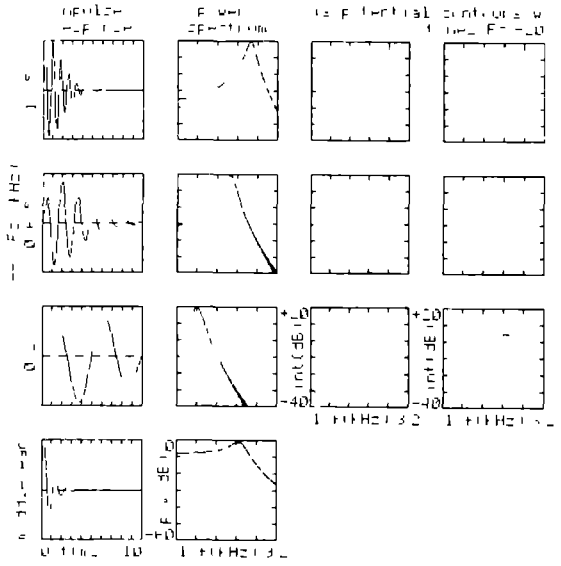

Fig. 2. Characteristics of the filters and of the generator potential w for three sets of parameters.
Column one: first 10 ms of impulse response of filter.
Column two: power spectrum on a logarithmic scale from 0.1 to 3.2 kHz.
Column three: isopotential contours of the generator potential w obtained with tonepip stimuli. The carrier frequency varied logarithmically between 0.1 and 3.2 kHz, the intensity between −40 and +20 dB relative to q° or r°. Adaptation was left out of the model. The difference between two isopotential contours is a factor two.
Column four: isopotential contours of w obtained with two-tone stimuli. A second tonepip at the centre frequency of the filter and at an intensity of −20 dB relative to q° or r° was added to the stimulus of column three. The shading represents values higher than the maximum divided by 16. The minus sign in row three represents values below the maximum divided by 32.
Row one: Basilar papilla haircell, $F_c = 1.25$ kHz, $\beta = 0.8$ ms, see Eq. 3.
Row two: Amphibian papilla haircell, $F_c = 0.625$ kHz, $\beta = 1.5$ ms.
Row three. Amphibian papilla haircell, $F_c = 0.2$ kHz, $\beta = 4.0$ ms.
Row four: middle ear, see Eq. 1.

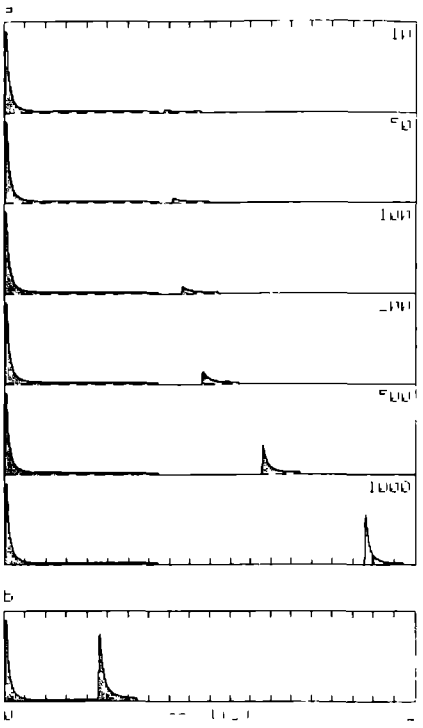

Fig. 3.
Simulation of forward and simultaneous masking.
(a) In the forward masking paradigm of Megela and Capranica (1982) a masking tone of 750 ms is followed after an interval by a test tone of 200 ms. The intervals are indicated at the right. The generator potential w is plotted on a timebase of 2 s.
(b) In the simultaneous masking paradigm the test tone was started 450 ms after the onset of the masking tone.

sulting in a suppression of the haircell potential u and generator potential w. In the basilar papilla branch of the model a high intensity tone away from F_c will simply be filtered out (Fig. 1D).

3.3 Adaptation and masking

According to Eggermont (1985) short-term adaptation and forward masking are interrelated phenomena. In his model (see also Eqs. 5 and 6) the short-term adaptation and the forward masking time-constants are, respectively, $(\mu+\lambda)^{-1}$ and μ^{-1} The relative steady state firing rate is $\frac{\mu}{\mu+\lambda}$ This interrelation is supported by the experiments of Megela and Capranica (1982), who found that masking was strongest (μ^{-1} large) for fast-adapting amphibian papilla fibres (λ large, $\frac{\mu}{\mu+\lambda}$ small).

A forward masking experiment following the protocol of Megela and Capranica was simulated. In their experiments a masking tone of 750 ms was followed by a test tone of 200 ms, after an interval which varied between 10 and 1000 ms. Fig. 3a shows the generator potential w as a function of time. First there is adaptation to the 750 ms masking tone. The peak of the response to the test tone is negligible just after the offset of the masker, but almost recovers within 1 s, in accordance with the recovery time-constant μ^{-1}, which is 1 s in this simulation. As an extension simultaneous

masking is illustrated in Fig. 3b, where a test tone was presented during the masking tone, starting at 450 ms after the onset of the masker. The increment response is similar to the onset response to the masker. Note that after the end of the test tone the response to the masker is totally suppressed.

3.4 Response to temporally structured stimuli

In the NVIII Rose and Capranica (1985) found no selectivity for amplitude modulation frequency (AMF) with respect to firing rate. However, with respect to synchronization to the envelope, they found low-pass characteristics for fibres innervating the amphibian papilla. Basilar papilla fibres showed increased synchronization to AMF's between 100 and 150 Hz. This is in accordance with the findings of Hillery (1984), who reported a larger AP with these AMF's, using a carrier frequency of 2 kHz. The AP presumably results from synchronized activity of NVIII fibres.

Schneider-Lowitz (1983) studied the responses to trains of 10 ms pulses, with a duration of 500 ms and a pulse repetition rate varying between 5 and 100 Hz, in the NVIII and in the DMN. With respect to firing rate all NVIII fibres increased their response with increasing PRR, until they reached a saturation level at PRRs between 35 and 100 Hz. In the DMN only 28% showed the same behaviour, the other neurons showed a decline of the rate response above a PRR between 10 and 60 Hz.

DMN units showing a strong preference for fast intensity changes were reported by Van Stokkum (1987). This is illustrated by the responses of unit 297,0,6 in Fig. 4, a unit which was already described elaborately in Van Stokkum (1987). The frequency selectivity parameters of the unit are: threshold just below 80 dB peak SPL, CF 0.63 kHz. In Figs. 4a and 4b the response to pulse shape variations, at stimulus intensities of, respectively, 80 and 90 dB peak SPL, is shown in the form of a reordered eventdisplay along with a spike rate histogram. In this paper spike rate is defined as the average number of action potentials per stimulus presentation. The action potentials in response to the 20 presentations of a pulse shape are drawn one underneath the other as dots. From top to bottom the stimulus consists of a click (c), a pulse from the mating call (*), a time-reversed pulse from the mating call (r*), tonepips (p) with a duration of 5, 10, 20 and 50 ms, and tonepips of 10, 20 and 50 ms with a gamma-envelope (Γ) (Aertsen and Johannesma, 1980), alternated by their time-reversed versions (rΓ). Rise and fall times of the different pulse shapes are: 0.1 ms (c), 2 and 10 ms (*), 10 and 2 ms (r*), 1 ms (p), 20% and 80% of the duration (Γ), and 80% and 20% of the duration (rΓ). The carrier frequency for the tonepips is 0.63 kHz. A remarkable finding is that this unit has a lower threshold for pulse shapes with a fast rise time and a slow fall time (* and Γ) than for their time-reversed versions. Unit 297,0,6 does not respond to rΓ50 at either intensity. The response to r* changes both in rate and latency. In response to rΓ20 only two action potentials are seen at 90 dB.

The second stimulus (Figs. 4c and 4d) consists of amplitude-modulated tone bursts (Epping and Eggermont, 1986) of 500 ms, with overall rise and fall times of 100 ms, a carrier frequency of 0.63 kHz, and stimulus intensities of, respectively, 80 and 90 dB peak SPL. At the bottom line responses to an unmodulated tone burst are depicted. The AMF of the other tone bursts varied logarithmically between 7.8 and 250 Hz (top). Unit 297,0,6 responds to AMF's between 62 and 125 Hz during the rise time of the tone burst. The response is about twice as strong at 90 dB. To click trains with a pulse repetition rate varying from 7.8 to 250 Hz (Fig. 4e) the unit responds in a time-locked fashion to each click up to a PRR of 62 Hz. With higher PRR the response deteriorates, until at 250 Hz only one action potential is left at the onset. This low-pass character of the rate response corresponds well with the findings of Schneider-Lowitz (1983) mentioned above.

The mating call of the grassfrog consists of a series of pulses with a PRR of about 36 Hz and a slowly increasing pulse amplitude. The energy in a pulse is concentrated at frequencies near 0.55 kHz. The stimulus of Fig. 4f consists of mating calls (*), and time-reversed mating calls (r*), against an increasing background of pink noise. The response to the mating calls decreases with decreasing signal-to-noise ratio (SNR) whereas there is practically no response to the time-reversed mating calls. The SNR is defined here as the peak ratio between the vocalizations and the noise. There is no response to the pink noise, which is indicated by the empty lines between r* and * in Fig. 4f. Other units with similar response characteristics were also found, see Table I in Van Stokkum (1987).

There are several possible ways to model the

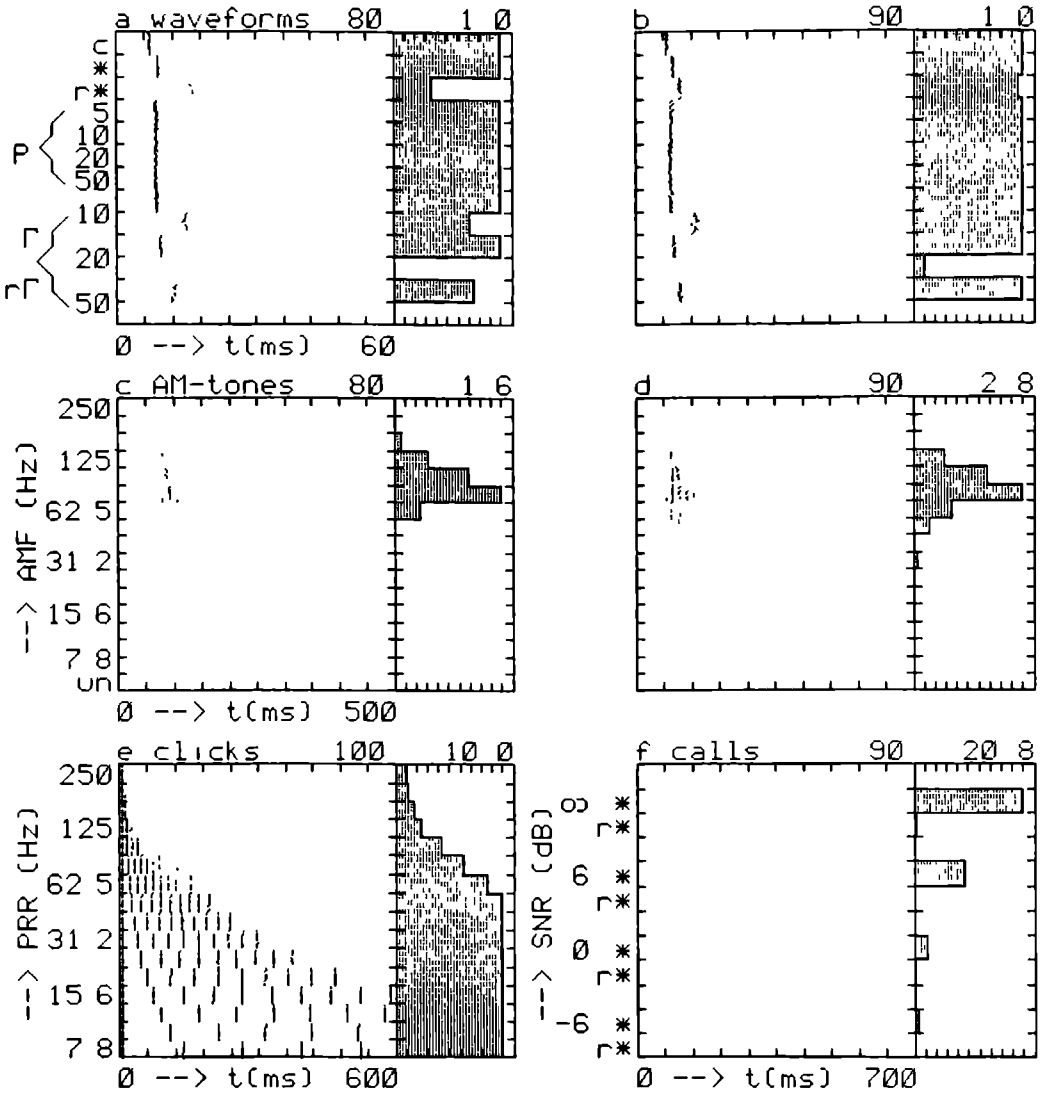

Fig. 4. Reordered eventdisplays together with rate histograms of responses of DMN unit 297,0,6 to six different stimuli. At the left the stimulus parameter variation is indicated. All stimuli were presented ipsilaterally. The intensities, in dB peak SPL, are indicated above each eventdisplay. Carrier frequency in Figs. a-d 0.63 kHz. Above each histogram the maximum value is written. Note the different timebases, which are indicated under the eventdisplays.

The different stimulus waveforms in Figs. a and b were: click (c), pulse from the mating call (∗), tonepip (p), gammatone (Γ), and time-reversed versions (r∗ and rΓ). The durations of the tonepips and of the gammatones are indicated. The AMF of the tone bursts (Figs. c and d) varied between 7.8 and 250 Hz, in addition an unmodulated tone burst (un) was presented. The equidistant click trains of Fig. e consisted of 10 clicks with PRR varying between 7.8 and 250 Hz. The mating call (∗) and time-reversed mating call (r∗) (Fig. f) were first presented in silence (SNR ∞). Next an increasing pink noise background was added (SNR decreasing from 6 to −6 dB). Further explanation in text.

preference for fast intensity changes. To model the transient response to the AM tone bursts (Figs. 4c and 4d) we take brief short-term adaptation in combination with slow recovery, to achieve strong adaptation.

In Figs. 5a-c and 6a-c the effect of this strong adaptation on the generator potential w is shown The generator potential shown in Figs. 5a and 6a is calculated excluding the negative feedback provided by the refractory mechanism (Fig. 1G). Each row shows w as a function of the time indicated at the bottom and belonging to the stimulus

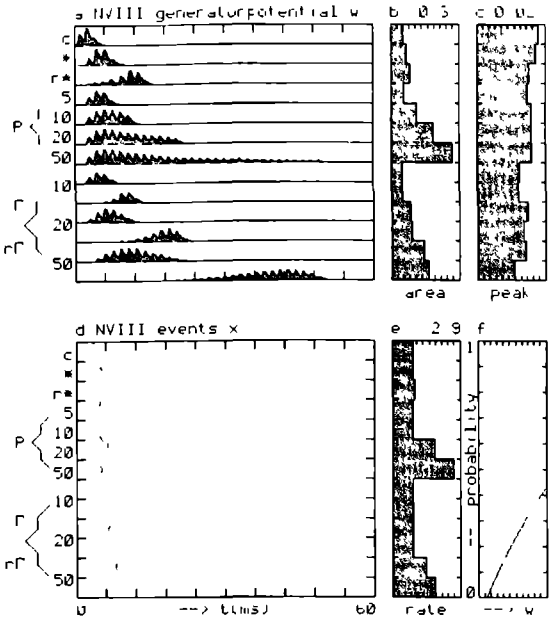

Fig. 5. Output of a model simulation of a NVIII fibre showing the timecourse of the generator potential w (a), its area (b) and its peak (c) as a function of pulse shape. Stimulus parameters: intensity −20 dB relative to q°, carrier frequency 0.625 kHz. Tuning: F_c 0.625 kHz, β 1.0 ms, amphibian papilla. The reordered eventdisplay (d) and rate histogram (e) of the NVIII events x are produced with help of the probability of event generation shown in Fig. 5f. Parameters for the event generation: m 0.003, binwidth 0.1 ms. A delay of 2 ms was incorporated. Refractory parameter: r_{abs} 5 ms. Other parameters in Table I.

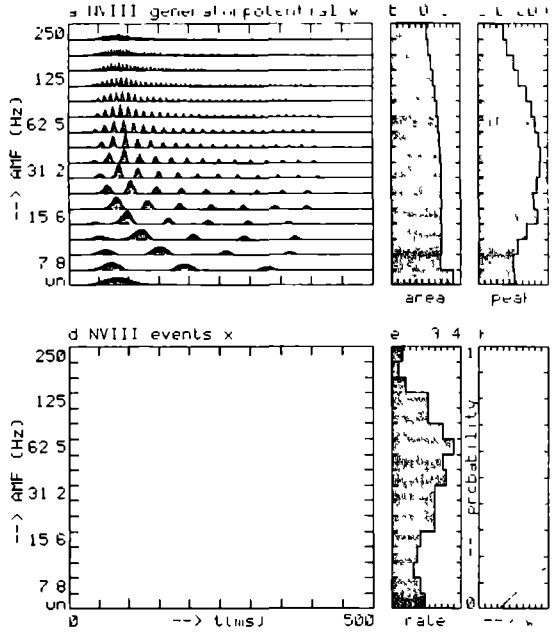

Fig. 6. Simulation of a NVIII fibre. Outputs w, the generator potential, and x, the events, as a function of AMF. Format and parameters as in Fig. 5.

indicated at the left. The histograms of Figs. 5b and 5c depict the area under and the peak of the generator potential, belonging to a row in Fig. 5a. With the pulse shape variations the generator potential shows a greater peak and a smaller area for the normal versus the time-reversed shapes (Figs. 5 a-c). With the AM tone bursts (Fig. 6a) a transient response character is visible: the peak of w is reached between 50 and 100 ms after the onset, thereafter the response declines. The peak of the generator potential (Fig. 6c) shows a broad maximum for intermediate AMF's.

The next step is to consider the generation of action potentials. In this model the event generator plays a central role, and it is important to visualize the probability of event generation, according to Eq. 12. Figs. 5f and 6f show this probability as function of the generator potential w, drawn for the potential range of, respectively, Figs. 5c and 6c. The rate response of the NVIII model-neuron is non-selective with regard to pulse shape (Figs. 5d and 5e) and shows a weakly band-pass character with regard to AMF (Figs. 6d and 6e). Furthermore, the response to the AM tone bursts, Fig. 6d, shows the desired transient character.

Now we model the convergence of NVIII fibres upon a DMN neuron. We slightly vary the thresholds of 16 NVIII fibres and their absolute refractory periods, to achieve a range of response patterns (see legend Fig. 7). These NVIII fibres will demonstrate a large amount of synchrony in their responses to fast intensity changes, but will respond more asynchronously to slow intensity changes. Convergence of these fibres upon a DMN unit will result in a peaked generator potential for the DMN unit in case of synchronous inputs, and in a smaller but more prolonged generator potential in case of asynchronous inputs. The threshold of the DMN unit is adjusted to the height of several EPSP's. So the second mechanism (the first being adaptation) to favour the fast intensity changes is to take a number of NVIII units with slightly different characteristics, and model the DMN unit as a coincidence detector. The effect of the coincidence detection is expected to grow along with the number of different inputs.

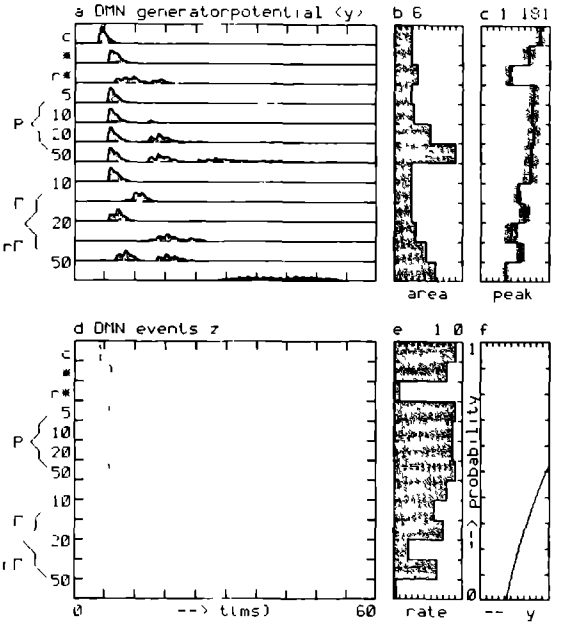

Fig. 7. Simulation of a DMN neuron. Outputs y, the generator potential, and z, the events, as a function of pulse shape In contrast with Fig. 5 the timecourse of the ensemble averaged generator potential $< y(t) >$ (a), its area (b) and the average and standard deviation of the peak of $y(t)$ (c) are depicted Inputs are 16 units, with m varying linearly between 0.0003 and 0.003, and τ_{abs} between 4 and 5 ms The values of 0.003 for m and 5 ms for τ_{abs} where used in Figs 5 and 6.

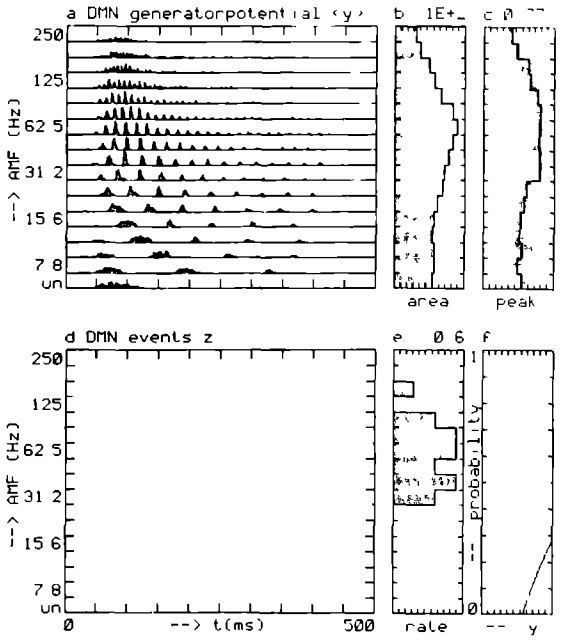

Fig. 8. Simulation of a DMN neuron. Outputs y, the generator potential, and z, the events, as a function of AMF. Format and parameters as in Fig. 7

The characteristics of the DMN generator potential y are illustrated in Figs. 7a-c and 8a-c, where as before refractory effects have been excluded. In Fig. 7a we have averaged $y(t)$ over the 20 presentations of the stimulus, resulting in an ensemble average $< y(t) >$. In Fig. 7c the average peak of $y(t)$ is drawn, which is not equal to the peak of $< y(t) >$. The deviations from the solid line in Fig. 7c indicate the standard deviation of the peak of $y(t)$.

Comparing Figs. 5a and 7a we note the following differences: the periodicity in Fig. 5a, which was the result of phase-locking, has almost disappeared in Fig. 7a. This is due to the smoothing by the EPSP, the convergence of the 16 inputs, and to the ensemble averaging. The average peak of y is higher for all normal versus time-reversed shapes (Fig. 7c). This difference is still larger for the peak of $< y(t) >$ in Fig. 7a. Figs. 8a and 8c show a larger peak for AMF's around 50 Hz, the difference again being larger in Fig. 8a. Using the probabilities of event generation shown in Figs. 7f and 8f we now obtain selective responses, which resemble those of Figs. 4a and 4c qualitatively The rate histogram in Fig 7e shows a decreased response to the time-reversed stimuli r∗, rΓ20 and rΓ50. Furthermore, the response to the stimuli with short rise times is very precisely timed (Fig. 7d). The response to the AM tone bursts (Figs. 8d and 8e) shows a band-pass character with respect to AMF.

The responses of this DMN modelneuron to all of the stimuli of Fig. 4 are shown in Fig. 9. The parameters were adjusted in order to achieve a qualitative resemblance to the responses to all six different stimuli of Fig. 4. Comparing Figs. 4 and 9 we note the following deviations: the response in Fig. 4b is restricted to the onset, in Fig. 4d the response is more transient, and the rate response to the click trains (Fig. 4e) is larger. The time-reversed mating calls (r∗) and the noise evoke practically no response (Fig. 4f). Enhancement of the transient character of the model's response by means of stronger adaptation will decrease the response to the click trains, which already suffers from the adaptation. Nevertheless the response of this model (Fig. 9) qualitatively resembles the real data in Fig. 4. We have found other DMN neurons which showed responses more like Figs. 9b and 9d, see e.g. Fig. 6b in Van Stokkum (1987).

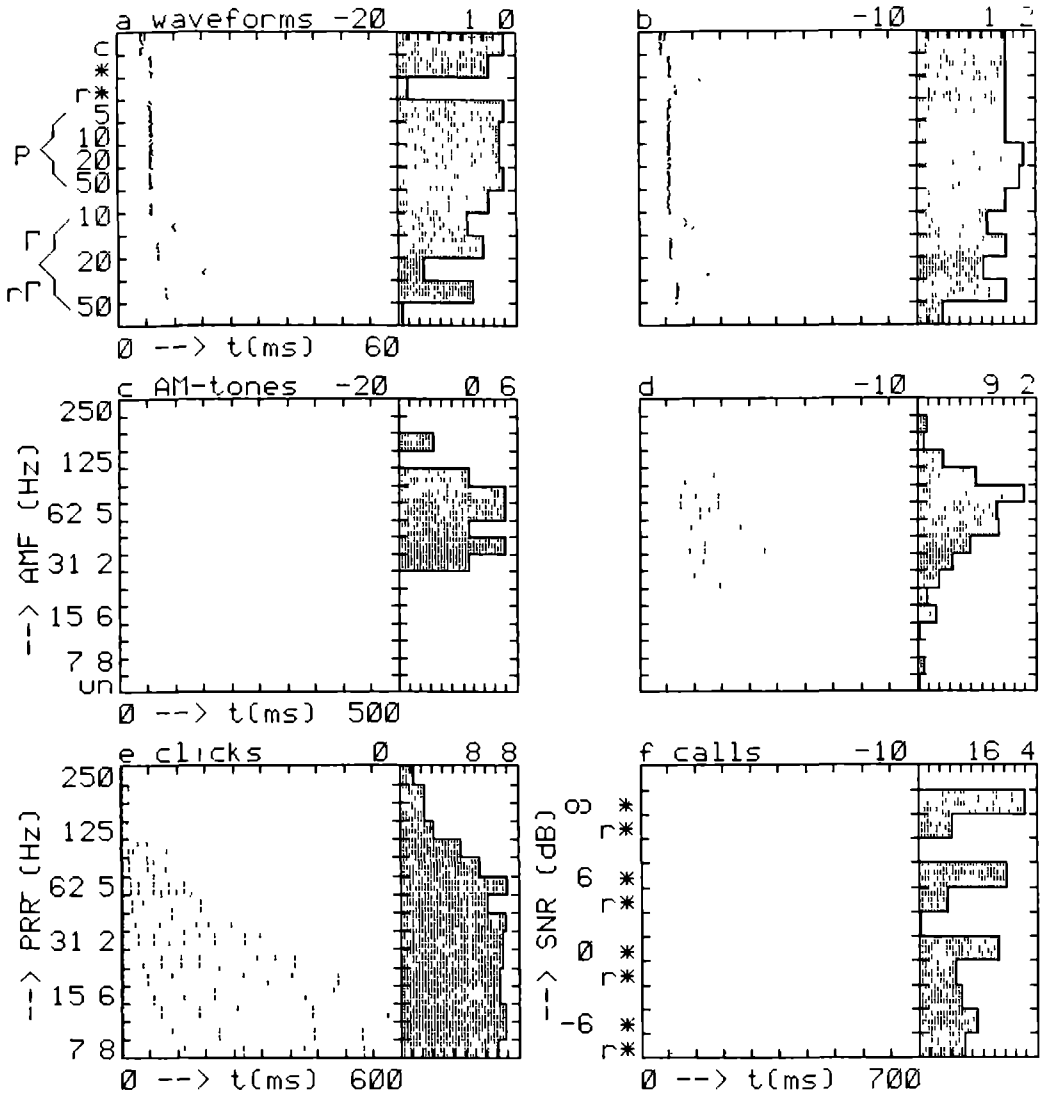

Fig. 9. Reordered eventdisplays together with rate histograms of the model DMN neuron of Figs. 7 and 8 in response to the six stimuli of Fig. 4. Figs. 9a and 9c are equal to, respectively, Figs. 7d-e and 8d-e. All stimuli are presented at the relative intensities of Fig. 4. The intensities in dB relative to q° are indicated above each eventdisplay.

Not shown here are the responses to tonepips with varying carrier frequency. The model generates onset events between 0.4 and 0.8 kHz at −20 dB relative to q° and between 0.2 and 1.0 kHz at −10 dB. This deviates only slightly from the onset response of unit 297,0,6 to tonepips with carrier frequencies between 0.5 and 0.8 kHz at 80 dB and between 0.4 and 1.1 kHz at 90 dB.

Recently, Hall and Feng (1988a) investigated phasic neurons in the DMN of the leopard frog (*Rana p. pipiens*). In accordance with the findings of Van Stokkum (1987) in the grassfrog (*Rana temporaria*), they also found a preference for rapid rise times. Their stimulus consisted of tonepips at CF with a duration of 300 ms and a linear rise time varying between 1 and 100 ms. At 10 dB above threshold most phasic neurons did not respond to tonepips with rise times larger than 25 ms, just like our unit 297,0,6 did not respond to rΓ50 (Figs. 4a and 4b) which has a rise time of 40 ms. Hall and Feng systematically investigated the rate and latency as a function of rise time, at several intensities. We presented their stimuli to our model with the same parameters as in Figs. 5-9. The simulated NVIII fibre (Figs. 10a and 10b) responds only to rise times shorter than 25 ms at an inten-

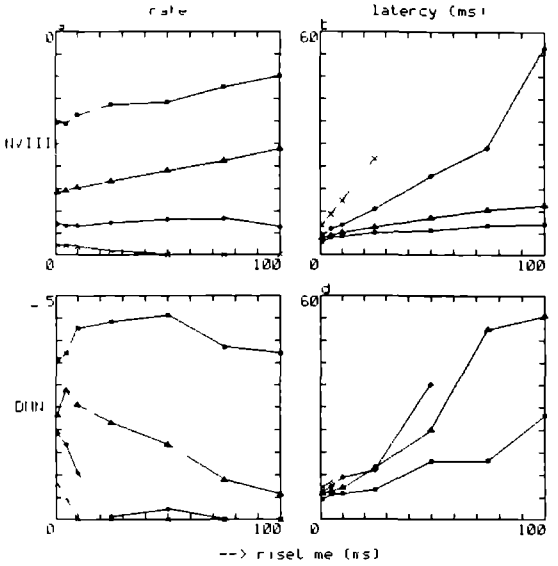

Fig 10 Response of the NVIII (a,b) and of the DMN neuron (c,d) simulated in Figs 5-9 to tonepips at CF with varying rise time, following the paradigm of Hall and Feng (1988a) The intensity, in dB relative to q°, is indicated by symbols $-30(\times)$, $-20(\diamond)$, $-10(\triangle)$, 0 ($\square$) All data points are averages over 25 stimulus presentations The rate response is measured in spikes per stimulus presentation

sity of -30 dB relative to q° ($\times$) At an intensity of -20 dB ($\diamond$) and above the rate response is non-selective, in accordance with Fig 5e The latency characteristics in Fig 10b show large slopes at the lowest intensities ($\times$ 0 75, $\diamond$ 0 35) and are nearly flat at the highest intensities ($\triangle$ 0 1, $\square$ 0 05) The simulated DMN neuron responds preferentially to the rapid rise times at intensities between -30 and -10 dB (Fig 10c) This is in accordance with the responses shown in Figs 9a and 9b, and also corresponds well with Fig 3 in Hall and Feng (1988a) The latency characteristics in Fig 10d show larger slopes than in Fig 10b In accordance with the findings of Hall and Feng, the slope decreases when the intensity is increased from -20 to 0 dB ($\diamond$ 0 6, $\square$ 0 15)

4 Discussion

The aim of our study was to model the response characteristics of NVIII fibres and DMN neurons by incorporating several data from the literature on isolated parts of the peripheral auditory system into a coherent model We conclude that the model was successful in reproducing the general behaviour of NVIII fibres and DMN neurons In particular, by varying the adaptation parameters and the amount of coincidence detection we obtained the different temporal selectivities found in the NVIII and in the DMN To arrive at a parameter set which reproduces all of the response characteristics of a single neuron in detail is a time consuming trial and error procedure In our view, the main result of this study is that the responses of different neurons in the NVIII and DMN to a wide set of stimuli can be modelled adequately with a single set of parameters for each single neuron

4.1 Model simulations

The main deviations between Figs 4 and 9 arise with spectrally broader stimuli like clicks, mating calls and noise In our model we have assumed that the NVIII units which converged upon the DMN unit all had the same spectral characteristics When we also allow the centre frequencies of the input units to vary a little, an improvement is expected of the responses to fast intensity changes Fast intensity changes are spectrally broad, and thus are expected to excite a larger number of inputs with slightly different spectral characteristics In contrast, tonal stimuli are spectrally narrow and will excite a relatively smaller number of inputs

The responses of the real neuron were more transient than those of the model neuron, compare Figs 4b,d with Figs 9b,d We expect a more transient response of the model neuron when we include adaptation in the synapses between NVIII fibres and DMN neuron This can be modelled with a long τ_R of the DMN neuron (see also Bibikov and Ivanitskii, 1985)

It was shown in Fig 10 that our model also reproduces the rate and latency characteristics of Hall and Feng (1988a) They concluded that the phasic DMN neurons behaved as low-pass temporal filters with respect to envelope rise time We prefer to interpret the selectivity for rapid rise times as a preference for fast intensity changes Our simulations show that at intensities more than 30 dB above threshold the preference for rapid rise times has vanished (Fig 10c) At these high intensities even the onset of a tonepip with a rise time of 100 ms corresponds with a large increment in absolute intensity, relative to the preceding silence The simulations of the NVIII fibre in Figs 10a and 10b predict that the phasic NVIII fibres also prefer fast intensity changes at stimulus intensities just above threshold

There remains a fundamental problem with the evaluation of the the model's output, since it is an unsolved problem how event trains with a stochastic character should be compared quantitatively (Aertsen et al., 1979). How can we measure the difference between, say, the responses shown in Figs. 4a and 9a? Qualitatively we may look for global differences, such as the presence or absence of selectivity, see e.g. the lack of response to rΓ50. In this study we have used averages of the response, such as rate or mean and standard deviation of the latency. We have presented reordered eventdisplays, which form a complete representation of the data, and rate histograms. Comparing Figs. 4d and 9d we immediately note, next to the global resemblance, the differences in the transient character of the response and in the degree of AMF selectivity.

4.2 Frequency tuning

With regard to the spectral filtering it is clear that the model is rather crude, and has some simplifying assumptions. We want to discuss the following points:

- We have assumed linearity of the middle ear, which is only justified up to 1.5 kHz (Vlaming et al., 1984).

- We have chosen the effective stimulus for the haircells to be the sound pressure displacement. Choosing the velocity, i.e. its derivative, will produce a gain of 6 dB per octave in the middle-ear transfer function at the bottom of Fig. 2. The tuning curve of the low-frequency unit of Fig. 2 will then be broadened.

- The two different parallel sequences, nonlinearity followed by band-pass filter (Figs. 1B,C) and vice-versa (Figs. 1D,E), are two extremes. In addition to the band-pass filter and the static nonlinearity the membrane of the basilar papilla haircell performs a low-pass filtering action. This is not incorporated in the model.

  The nonlinear phenomenon of two-tone suppression has only been observed in fibres with characteristic frequencies (CF's) under 0.5 kHz. Fibres innervating the amphibian papilla with CF between 0.5 and 1.0 kHz do not show two-tone suppression. This suggests two stages of filtering in the amphibian papilla: a mechanical stage which is perhaps related to the travelling wave suggested by Hillery and Narins (1984), and an active electrical tuning of the haircell membrane. The mechanical filtering in the amphibian papilla would then prevent two-tone suppression in haircells tuned to frequencies between 0.5 and 1.0 kHz.

  In summary, both papillae should be modelled with a band-pass filter followed by a nonlinear mechano-electrical transduction. In the amphibian papilla the haircell membrane probably represents a band-pass filter, whereas in the basilar papilla it performs a low-pass filtering action. In our model we have chosen the two extremes to demonstrate the sequence effect, and because of simplicity.

- We have made no attempt to model active tuning of the amphibian papilla. This is expected to improve the frequency tuning, but would require the introduction of additional nonlinearities. Lewis (1988), in discussing the fundamental problems which arise in modelling bidirectional active processes, pointed at the need of considering the amphibian papilla as a whole.

- We have disregarded the dynamical aspects of the mechano-electrical transduction. This is a simplification, since Corey and Hudspeth (1983) found that the time-constants involved are on the order of 0.1 ms, which is not instantaneous with respect to filter time-constants.

4.3 Coincidence detection

The main mechanisms which appear to contribute to temporal selectivity are short-term adaptation, event generation and coincidence detection. Coincidence detection has also been suggested by Kim et al. (1986) to explain the 'pitch-period following response' found in neurons of the posteroventral cochlear nucleus in cats. These neurons responded to the fast intensity changes in speech-like sounds. The coincidence detection is of course critically dependent upon the EPSP shape and the number of inputs. A longer EPSP duration results in more temporal integration, and favours the stimuli which produce more events in NVIII. This deteriorates the selectivity for fast intensity changes, as developed with this model. It has been shown by Bibikov and Kalinkina (1983) that DMN neurons integrate the stimulus energy over a range of 2 to

5 ms This supports our choice of 1 ms for the EPSP decay time-constant.

With regard to the number of inputs, we also tried convergence of two, four and eight NVIII fibres upon a DMN unit. The preference for fast intensity changes was already present with four inputs, albeit weaker. Thus far we have not allowed for intranuclear inhibition, because this has not yet been demonstrated in the anuran DMN.

4.4 Parameter variation

Finally we summarize the significance of the parameters of Table I. A first group of parameters $(\gamma, \omega_1, \rho, q^o, r^o, \omega_t, \beta_t, u_0, \lambda, \mu, \omega_2)$ is responsible for the NVIII generator potential w. Variation of ω_t and β_t produces different spectral selectivities (Fig. 2). Variation of the adaptation parameters λ and μ produces the different types of short-term adaptation found in the NVIII by Megela and Capranica (1981, 1982) (Fig. 3).

The neuronal refractory (τ_{abs}, R, τ_R) and event generation (ν, m) properties have to be adjusted to produce realistic response properties. Thereby τ_{abs} is chosen equal to the neuron's smallest interspike interval. Presumably the pauser neurons recently reported by Hall and Feng (1988b) can be modelled with an appropriate choice of the refractory parameters. The threshold m was responsible for the response selectivity derived from the generator potential.

The amount of spatiotemporal integration is responsible for the developed selectivity for temporal characteristics of sound. The response with one NVIII input will resemble that input.
Thereby temporal integration may decrease the phase-locking ability. The response to a larger number of NVIII inputs may show coincidence detection as discussed above. The degree of coincidence detection grows with increasing m and n, and with decreasing τ_d and τ_u.

We conclude that detailed neural modelling contributes to the appreciation of neural data. In particular the use of one set of parameters to reproduce the response characteristics of a single neuron to a broad ensemble of stimuli results in a functional description of the neuron.

Acknowledgements
This investigation was supported by the Netherlands Organization for Scientific Research (NWO). The authors thank Willem Epping and Peter Johannesma for insisting on systematic modelling of the auditory periphery and Willem Melssen for software assistance. Furthermore all three are thanked for helpful discussions and critical reading of the text.

Chapter VI

A model for the auditory midbrain of the grassfrog for monaural stimuli

Ivo van Stokkum

Abstract

In a foregoing paper (Van Stokkum and Gielen, 1989) a model was presented to describe the processing of monaural stimuli by the auditory periphery of the grassfrog The main components of this model were a middle ear filter, transduction and tuning of the haircell, short-term adaptation, event generation with refractory properties, and spatiotemporal integration of converging inputs The model is now extended to model auditory midbrain neurons as third order neurons The mechanisms that generate selectivity for temporal characteristics of sound are adaptation, coincidence detection of second order neurons, temporal integration of third order neurons and, most important, event generation of the first, second and third order model neurons Variation of the parameters of the model successfully reproduces the range of response patterns which have been obtained from eighth nerve fibres, dorsal medullary nucleus neurons, and torus semicircularis neurons With a single set of parameters the output of the model in response to a set of spectrally and temporally structured stimuli qualitatively resembles the responses of a single neuron to all these stimuli In this way the responses to the different stimuli are synthesized into a framework, which functionally describes the neuron

1 Introduction

Since the pioneering work of Potter (1965b) the auditory midbrain of anurans has been the subject of auditory research (for reviews see Fritzsch et al , 1988) Anurans use stereotyped, species-specific calls for intraspecific communication In the grassfrog, *Rana temporaria*, these calls have a periodic pulsatile character (Fig 1f) The pulses have a duration of 12 ms and a pulse repetition rate which, depending on temperature (Van Gelder et al , 1977, Walkowiak and Brzoska, 1982) varies between 20 and 40 Hz The distinct temporal character of the natural calls has led many investigators into a study of the coding of fine temporal characteristics of sound (for review see Walkowiak, 1988)

The auditory midbrain contains temporally selective neurons In *Rana ridibunda* Bibikov (1971 a,b) discovered that about half the midbrain units ceased to respond to an unmodulated tone within a few seconds, but fired continuously when this pure tone was replaced by a pulse train with a pulse duration of 8 ms and a PRR of 20 Hz A further investigation of such neurons in *Rana temporaria* showed that at a constant PRR of 27 Hz the optimal pulse duration varied between 6 and 12 ms (Bibikov, 1980)

The selectivity for PRR has been investigated in several stations of the auditory pathway In the grassfrog Schneider-Lowitz (1983) studied the responses to trains of 10 ms pulses, with a train duration of 500 ms and a PRR varying between 5 and 100 Hz, in the NVIII, DMN and SON With respect to firing rate all NVIII fibres increased their response with increasing PRR, until they reached a saturation level at PRR's between 35 and 100 Hz This corresponds with a non-selective response type In the DMN and SON only 30% showed the same behaviour, the other neurons displayed a low-pass response type, that is their rate response started to decline at PRR's between 10 and 60 Hz This range encompasses the PRR's of natural calls Using the same stimulus in the TS Walkowiak (1984) found in 12% of the units non-selective responses and in 56% of the units low-pass responses Furthermore, 6% of the neurons responded only to the highest PRR's (high-pass), 8% responded exclusively to a small

range of PRR's (band-pass) and 18% showed the opposite behaviour (band-stop or bimodal) From these results it becomes clear that the development of temporal selectivity starts already in the DMN and SON

Next to the rate aspect of the response also the synchronization aspect has been studied NVIII fibres synchronize their firings to the envelope of the amplitude modulator This synchronization capability is retained for AMF's above 100 Hz (Rose and Capranica, 1985) In contrast, the firings of 38% of the TS units are not significantly synchronized to the envelope (Epping and Eggermont, 1986b) In the other TS units synchronization to the envelope is a low-pass function of AMF, with lower cut-off AMF's than found in the NVIII (Rose and Capranica, 1985)

An explanation for these findings can be found in the integrative properties of neurons The cable properties of neurons, especially of their dendrites, cause temporal integration of inputs (Rall, 1977) NVIII fibres have integration times of about 1 ms (Crawford and Fettiplace, 1980) allowing them to synchronize their firings to stimulus envelopes with AMF's greater than 100 Hz Likewise, DMN neurons have integration times of 1-5 ms (Bibikov and Kalinkina, 1983), which enables them to pass on the synchrony code But in the TS Bibikov (1974, 1977, 1978) found integration times ranging from 1 to 100 ms TS units with long integration times loose their synchronization capability, but develop selectivity for PRR by temporal integration of inputs This hypothesis will be tested quantitatively with help of the model Another hypothesis is that local circuits in the TS are responsible for the development of temporal selectivity This second hypothesis will be investigated by recording simultaneously from pairs of single units and look for the presence of neural interaction

In a foregoing paper (Van Stokkum and Gielen, 1989) a model was developed for NVIII and DMN neurons This model for first and second order auditory neurons is now extended to produce the responses of third order neurons In Ranidae the main ascending auditory inputs to the TS come from the ipsilateral SON and from the ipsi- and contralateral DMN (Wilczynski, 1988) In view of this TS neurons can be regarded as third or fourth order auditory neurons The known temporal selectivities of SON neurons deviate only slightly from those of DMN neurons Therefore TS neurons are modelled as third order neurons This reduces the number of degrees of freedom for the modeler Care was taken to keep the characteristics of first and second order model neurons in line with data from the literature and with those used in the previous model (Van Stokkum and Gielen, 1989)

To characterize TS neurons a broad ensemble of stimuli was used to explore the selectivity for carrier frequency, PRR, AMF and pulse shape The main goal of this paper was to describe the selectivities of some typical TS neurons, and to compare their responses to a set of stimuli with the responses of a model neuron Matching the responses of the model neuron to the electrophysiological data enabled us to find a reliable set of parameters for the model Similarities between the selectivities of the real and model neuron indicate the plausibility of the model for the temporal processing in the TS It will be shown that spatiotemporal integration of second order inputs reproduces the new types of temporal selectivity found in the TS

2 Methods

2.1 Animal preparation and recording procedure

Adult grassfrogs (*Rana temporaria* L) from Ireland were anaesthetized with a 0 05% solution of MS-222 A hole was drilled into the parietal bones above the midbrain, leaving the dura intact The animal was allowed to recover overnight The next day it was immobilized with an intralymphatic injection of Buscopan (0 12 mg per gram bodyweight) A local anaesthetic, Xylocaine 2% was applied to the wound margins The animal was placed in a sound attenuated room (IAC type 1202A) onto a damped vibration-isolated frame Temperature was maintained around 15°C and the skin was kept moist to aid cutaneous respiration The animal's condition was monitored with help of ECG recording (Epping and Eggermont, 1987) and by examination of the blood flow in superficial vessels below the dura The preparation was usually kept intact for two days

Ultrafine or tapered tungsten microelectrodes (Micro Probe Inc), coated with Parylene-c, having a 5-25 μm exposed tip and a 1 kHz impedance of 1-5 MΩ were used for extracellular recording Using hydraulic microdrives two independent electrodes, tip distance on the roof of the midbrain between 100 and 400 μm, were lowered into the TS

and separable few-unit recordings were obtained with help of a spike separation procedure (Epping and Eggermont, 1987). Waveform features and spike epochs were stored on a PDP 11/34 with a resolution of 40 μs, and analyzed off-line with a PDP 11/44 and a VAX 11/785.

2.2 Acoustic stimulus presentation and response analysis

The acoustic stimuli were generated by a programmable stimulus generator, as described by Epping and Eggermont (1985). The stimuli were presented to the animal by two electrodynamic microphones (Sennheiser MD211N) coupled to the tympanic membrane using a closed sound system. The frog's mouth was kept open during the experiment, in order to decouple both ears (Vlaming et al., 1984). The sound pressure level was measured in situ with a half inch condenser microphone (Brüel and Kjær 4143) connected to the coupler. The frequency response of the system was flat within 5 dB for frequencies between 100 and 3000 Hz, a sufficient range for studying the auditory system of the grassfrog (Brzoska et al., 1977). The amplitude characteristics of the left and right coupler were equal within 2 dB for the range of interest. The stimuli were usually presented contralaterally with respect to the recording site, at sound pressure levels of 70 to 100 dB peak. These sound pressure levels are sufficient to evoke behavioural responses (Walkowiak and Brzoska, 1982; Brzoska, 1984).

The following stimulus ensembles have been used:

(1) *Tonepips* (Fig. 1a). To study spectral selectivity tonepips of 46 ms duration, modulated with a gamma envelope (Aertsen and Johannesma, 1980), were presented once per second. The carrier frequency was chosen pseudorandomly from 45 logarithmically equidistant values between 0.1 and 5 kHz. Also a rectangular envelope was used for the tonepips, with a duration of 100 ms and rise and fall times of 5 ms. To study two-tone suppression a second tonepip at the neuron's best frequency , attenuated by 0, 10 or 20 dB with respect to the tonepip stimulus, was presented simultaneously.

(2) *Pulse shape variations* (Fig. 1b). To study the effect of pulse shape a sequence consisting of a click, a pulse from the mating call, tonepips, gammatones, and if appropriate also their time-reversed versions, was used. The tonepips had 1 ms rise and fall times and durations of 5, 10, 20 and 50 ms. The gammatones had rise and fall times of, respectively, 20% and 80% of 10, 20 and 50 ms. The peak amplitude of the click was ten times that of the other pulse shapes. The neuron's best frequency was chosen as carrier frequency for the tonepips and gammatones. Onset interval of the pulse shapes was 1 s.

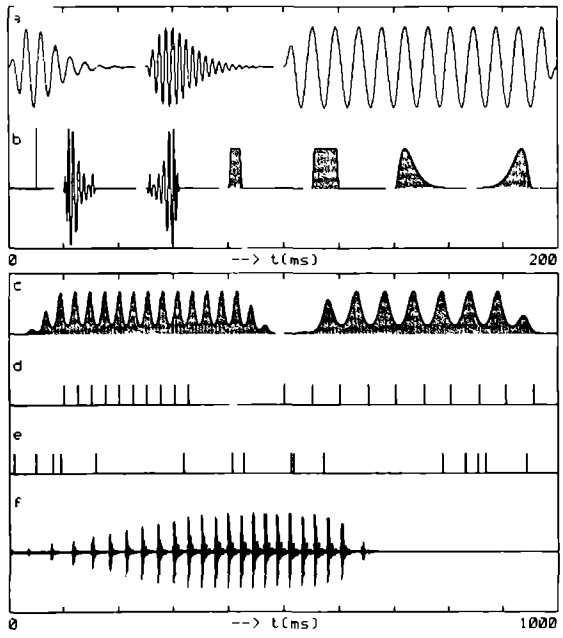

Fig. 1. Stimulus waveforms and envelopes. (a) two gammatones of 46 ms duration and a 100 ms tonepip. (b) click, normal and time-reversed pulse from the mating call, envelopes of tonepips of 5 and 10 ms duration, normal and time-reversed gammatones of 20 ms duration. (c) envelope of two AM tone bursts. (d) two periodic click trains. (e) segment from random click ensemble. f) mating call, recorded at 15°C.

(3) *Sinusoidally amplitude modulated tone bursts* (Fig. 1c). Tone bursts of 500 ms duration with 100 ms overall rise and fall times were presented every 3 s. The neuron's best frequency was chosen as carrier. The modulation depth was 16 dB, corresponding to 84%. The AMF's were varied pseudorandomly between 7.8 and 250 Hz. In addition an unmodulated tone burst was presented (Epping and Eggermont, 1986b).

(4) *Spectrotemporal stimulus.* Amplitude modulated sound bursts with different carriers were used to study the interdependency of spectral and temporal selectivity. Onset interval of the 500 ms duration sound burst was 2 s. One spectrotemporal stimulus consisted of combinations of four carriers with three modulators (100% modulation depth), another stimulus contained combinations

of six carriers with five modulators (84% modulation depth, Fig 1c)

(5) *Periodic click trains* (Fig 1d) Trains of 10 equidistantly spaced clicks, with onset intervals of 3 s The interclick intervals of the trains were varied pseudorandomly between 128 and 4 ms, corresponding with logarithmically equidistant PRR's of 7 8 to 250 Hz The duration of the condensation click was 0 7 ms, and its amplitude spectrum was flat within 5 dB for the range of interest (Epping and Eggermont, 1986a)

(6) *Random clicks* (Fig 1e) Stimulus ensemble consisting of clicks with an average rate of 16/s The interclick intervals are drawn independently from a negative exponential distribution with a minimum interval of 1 ms The interval distribution corresponds to a Poisson process with a deadtime of 1 ms (Epping and Eggermont 1986a)

(7) *Mating call ensemble* The basic sequence consisted of 10 s silence, followed by three original mating calls (Fig 1f) After this the envelope of the original mating call served as amplitude modulator for carrier frequencies of 201, 557, 1067 and 1542 Hz Then the interpulse intervals of the original mating call were multiplied by 0 5, 1, 2 and 4, corresponding with PRR's of 72, 36, 18 and 9 Hz Finally the original mating call was presented again followed by its time-reversed version Intervals between the calls were about 2 5 s This basic sequence, which had a duration of 50 s, was first presented in silence Thereafter a pink noise background, whose amplitude was increased stepwise, was added to the basic sequence The peak ratios between vocalizations and noise (SNR) were consecutively 6, 0 and −6 dB After the basic sequence with the highest noise level a 50 s period of silence was added (Eggermont and Epping, 1986)

To check the reproducibility of the responses and to collect adequate data all stimuli were repeated at least three times The response to the random clicks was analyzed by crosscorrelating the stimulus clicks (z_1) with the neural response (z_2), resulting in a crosscoincidence histogram (CCH) In formula

$$CCH_{12}(m) = \frac{1}{T\Delta} \int_0^T dt \int_{(m-\frac{1}{2})\Delta}^{(m+\frac{1}{2})\Delta} d\tau \, z_1(t) z_2(t+\tau) \quad (1)$$

Here $z_i(t) = \sum_{j=1}^{N_i} \delta(t - t_{i,j})$ represents the events at times $t_{i,j}$ of point process z_i, T is the duration of the experiment and Δ is the binwidth of the crosscoincidence histogram

The responses to the other stimuli are presented in the figures as reordered eventdisplays along with spike rate histograms Thereby the actual response is reordered systematically according to a stimulus parameter In this paper spike rate is defined as the average number of action potentials per stimulus presentation

The presence of neural interaction was investigated by crosscorrelation of simultaneously recorded spike trains (Epping and Eggermont, 1987, Melssen and Epping, 1987) Neural synchrony resulted in a peak or trough in the simultaneous crosscoincidence histogram (Eq 1, with z_1 and z_2 the responses of the two neurons) The contribution of a common stimulus influence to this synchrony was estimated by the nonsimultaneous crosscoincidence histogram (NCH) also called shift predictor (Perkel et al 1967) The nonsimultaneous crosscoincidence histogram results from crosscorrelation of one unit's spike train with the spike train of the other unit shifted circularly over the length L of a stimulus sequence (Eq 2) Hereby it was verified that the responses of the neurons were periodically stationary, i e that the response probability remained identical for subsequent stimulus sequences

$$NCH_{12}(m) = CCH_{12}(m + \frac{L}{\Delta}) \quad (2)$$

A difference between the simultaneous and nonsimultaneous crosscoincidence histogram indicates that the neural synchrony is not merely caused by stimulus influences, but that neural interaction also contributes

2.3 The model

As starting point a simplified version of the model for the peripheral auditory system (Van Stokkum and Gielen, 1989) is taken The model's components are shortly described below and are shown in Fig 2 A cascade consisting of a linear middle ear filter (Fig 2A, impulse response in Eq 3), a linear band-pass filter (Fig 2B, impulse response in Eq 4), and a static nonlinearity (Fig 2C, Eq 5) produces a haircell potential u The middle ear filter is described by the resonance frequency ω_1 and decay rate γ

$$h(t) = 2\gamma e^{-\gamma t} \sin(\omega_1 t)\Theta(t) \quad (3)$$

with $\Theta(t) = 1$ if $t > 0$, and $\Theta(t) = 0$ if $t \leq 0$ The band-pass filter is characterized by a centre frequency ω_i and by a time constant β_i which determines the sharpness of the filter

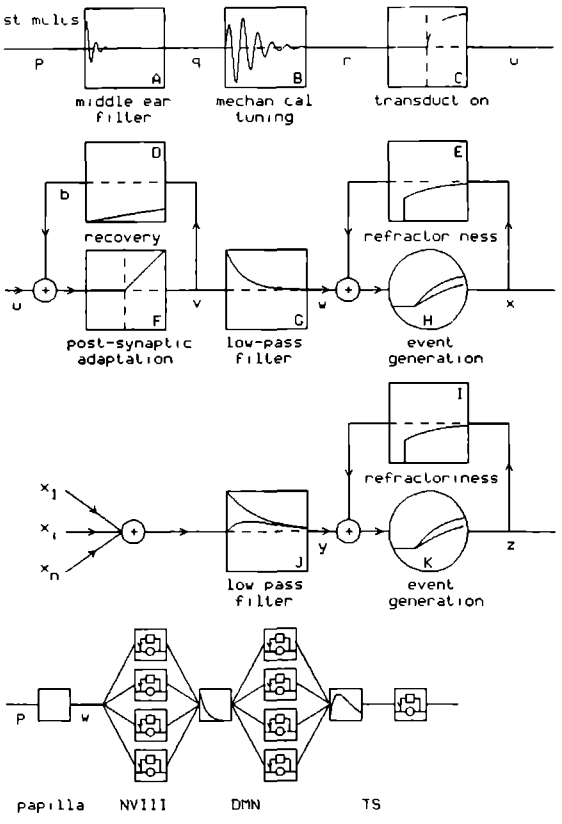

Fig 2 Model for the processing of sound by the papilla, NVIII, DMN and TS of the grassfrog The stimulus waveform is band-pass filtered by the middle ear (Fig 2A), and filtered and transduced into a hair-cell potential (Figs 2B,C) The synapse between the haircell and the dendrite of the NVIII fibre comprises of a short-term adaptation mechanism (Figs 2D,F) and a low-pass filter (Fig 2G) From the generator potential w of the NVIII fibre action potentials are generated (Fig 2H), which form the point process x Absolute and relative refractory mechanisms are incorporated in the negative feedback loop (Fig 2E) Outputs from lower order neurons ($x_1, \quad , x_i, \quad , x_n$) converge upon a higher order neuron, where they add linearly and are convoluted with an EPSP shape (Fig 2J) From the generator potential y of the higher order neuron action potentials are generated in the same way as explained above
In Figs 2A,B,D,E,G,I and J impulse responses are drawn on a timebase of 5 ms Figs 2C and F represent the instantaneous nonlinearities of, respectively, Eqs 5 and 6 Figs 2H,K show probabilities of event generation (Eqs 9,11) as function of the generator potentials w, y
The lower flow diagram symbolizes the connections used in the simulations of this paper The generator potential w is used to generate events in four NVIII units Four DMN units receive input from these four NVIII units Finally the four DMN units converge upon the third order model neuron, which represents a TS neuron One EPSP shape is used between NVIII and DMN, and another EPSP shape is used between DMN and TS Further explanation in text

$$f_i(t) = 2\beta_i^{-2} t e^{-\frac{t}{\beta_i}} \sin(\omega_i t)\Theta(t) \tag{4}$$

Parameter r^0 of the transduction non-linearity (Eq 5) is related to the half-saturation sound pressure level (Crawford and Fettiplace, 1981b)

$$u(r) = \frac{r}{r + r^0}\Theta(r) \tag{5}$$

The potential u provides the input to an adaptation component which was adopted from Eggermont (1985), and which is described by an inactivation rate λ and a recovery rate μ

$$v = (u + b)\Theta(u + b) \tag{6}$$

$$\frac{db}{dt} = -\lambda v - \mu b \tag{7}$$

The differential equation for b corresponds to that describing a first-order low-pass filter Note that omission of the rectifier (Fig 2F) would leave us with a high-pass filter Low-pass filtering by the dendrites of the NVIII neuron (Fig 2G, impulse response in Eq 8) produces the generator potential w of the first order model neuron

$$l(t) = \omega_2 e^{-\omega_2 t}\Theta(t) \tag{8}$$

Action potentials (events) are generated stochastically with help of a generator function $g(w)$, known in point process literature (e g Cox and Isham, 1980) as the intensity function The probability of event generation in a bin with width Δt is (see Van Stokkum and Gielen, 1989)

$$P[\Delta N(t) = 1] = 1 - e^{-g(w)\Delta t} \tag{9}$$

Here $N(t)$ is the counting process, which represents the number of events up to time t, and $\Delta N(t) = N(t + \Delta t) - N(t)$ The argument of the generator function depends in two ways on the events generated in the past Firstly, after an event has been generated the probability per unit of time to generate an event, $g(w)$, is zero for an absolute refractory period τ_{abs} Secondly, to model relative refractoriness a negative feedback is supplied to the event generator This feedback is given by the impulse response $c(t)$, which starts after the end of τ_{abs}

$$c(t) = -Re^{-(\frac{t-\tau_{abs}}{\tau_R})}\Theta(t-\tau_{abs}) \quad (10)$$

The refractory mechanism is illustrated in Figs 2E and 2I with $\tau_{abs} = 1$ ms and $\tau_R = 2$ ms When τ_R is much larger than τ_{abs} the negative feedback produces adaptation of the model neuron (see also Bibikov and Ivanitskii, 1985) For the generator function $g(w)$ a half-linear function is chosen

$$g(w) = \nu(w-m)\Theta(w-m) \quad (11)$$

For w less than m, the threshold parameter, $g(w)$ is zero Parameter ν determines the slope of $g(w)$ In Figs 2H,K the probability of event generation according to Eqs 9 and 11 is drawn for two different values of ν

2.3.1 Spatiotemporal integration of inputs

It is assumed that lower order neurons converge upon a higher order neuron This convergence of inputs is modelled as a linear summation of the input point processes, which are then low-pass filtered to arrive at compound EPSPs In formula (Johannesma and Van den Boogaard, 1985)

$$y(t) = \sum_{i=1}^{n} \int ds\ e_i(s)x_i(t-s) \quad (12)$$

$$\text{with } e_i(t) = We^{-\frac{t}{\tau_d}}(1-e^{-\frac{t}{\tau_u}})\Theta(t) \quad (13)$$

Here $x_i(t) = \sum_{j=1}^{N_i} \delta(t-t_{i,j})$ represents the events at times $t_{i,j}$ of lower order neuron i In Fig 2J different EPSP shapes $e_i(t)$ are drawn In the lower part of Fig 2 a schematic diagram for a third order neuron is illustrated The generator potential w provides input to four NVIII neurons, which differ in threshold and absolute refractory period Spatiotemporal integration of these four NVIII inputs produces a generator potential y for four DMN neurons with different thresholds Finally spatiotemporal integration of these four DMN inputs produces a generator potential y for a TS neuron Each model neuron box consists of an event generator and a negative feedback provided by the refractory mechanisms

2.3.2 Implementation of the model

The model was programmed in Fortran 77 on a VAX 11/785 computer The seven stimuli were sampled and provided the input to the model The sample interval was 0 1 ms for stimuli 1-3, and 0 2 ms for stimuli 4-7 The number of stimulus presentations usually differs between real and model neuron Because of limited computer capacity the duration of the mating call stimulus (250 s) was shortened to 68 s by reducing the intervals between the calls to 400 ms This results in forward masking of consecutive responses to the mating call variations

A summary of the parameters used in the simulations of this paper is given in Table I The degrees of freedom are the tuning characteristics, the stimulus amplitude relative to r^0, the degree of spatiotemporal integration (EPSP shape) and most important, the parameters which determine the event generation and refractory properties

Outputs of the model are the generator potentials w and y of, respectively, the first and higher order neuron, and the time-series x and z, which mimic the occurrences of action potentials in, respectively, a first or higher order neuron The generator potentials help to understand the action of the several nonlinearities incorporated in the model The time-series z, or averages thereof in the form of histograms, can directly be compared to experimental data obtained in higher order neurons

3 Results

3.1 Data base

Recordings were made from 161 auditory midbrain neurons in 30 grassfrogs Stimuli 1, 2 and 3 were presented to almost all units At least five different stimuli were presented to 54 units Fifteen units were fully characterized A full characterization requires the presentation of all seven stimulus ensembles and comprises investigation of the different kinds of selectivities at several intensities

In Table II a summary of the rate responses to the click train, pulse shape and mating call stimuli is given The different response types as determined with the click trains have already been explained in the introduction A response was classified as selective if the response decreased by at least 50% relative to the maximum response The PRR evoking a 50% response was termed the cut-off PRR

Some units responded only to pulse shapes exceeding a minimum duration, an example is shown in Figs 5a,b Usually this implied a larger response to the time-reversed versus the normal pulse shapes This type of response to pulse shapes is interpreted as evidence for the presence

Table I Model parameters.

Parameters	Eq.	related to	value
γ, ω_1	3	middle ear filter	1.297 $(\text{ms})^{-1}$, $2\pi \cdot 0.876$ kHz †
ω_t, β_t	4	tuning characteristics	variable, 1 ms
r°	5	transduction saturation	1
λ^{-1}, μ^{-1}	7	short-term adaptation	10 ms, 1000 ms
ω_2	8	dendritic low-pass filter	1 $(\text{ms})^{-1}$‡
τ_{abs}, R, τ_R	10	refractory properties	NVIII: 3-6 ms, 2, 1 ms
			DMN: 6 ms, 0.015, 400 ms
			TS: variable
m, ν	11	event generation	NVIII: 0.0001-0.001, 100 $(\text{ms})^{-1}$
			DMN: variable, 40 $(\text{ms})^{-1}$
			TS: variable
n	12	amount of convergence	4
W	13	EPSP height	0.2
τ_d, τ_u	13	EPSP shape	NVIII→DMN:variable, 0 ms
			DMN→TS :variable
		time delay	NVIII→DMN:2 ms
			DMN→TS :variable

†) derived from Aertsen et al. (1986), p. 21,25.
‡) Crawford and Fettiplace (1980), p. 91.

of temporal integration. Twenty-five units did not, and twenty-four units did show a temporal integration effect. Out of the neurons without a visible integration effect three showed a preference for pulse shapes of short duration and one for short rise times.

Eight of the 11 units which did not respond to the click trains were strongly inhibited by frequencies around 600 Hz. The two units which showed a bimodal response both showed an inhibition followed by excitation response type as determined with the random clicks (type III of Epping and Eggermont, 1986a). The distribution of the response types with the click trains agreed with the findings of Epping and Eggermont (1986a). Neurons which showed clear signs of integration effects (column two in Table II) showed a high-pass, band-pass or no response to the click trains. However, nearly all units without visible integration effects (column one) showed a non-selective or low-pass response to the click trains. Units which did not respond to the pulse shapes (column three) showed a band-pass or no response to the click trains. The neurons which preferred the higher PRR variations of the mating call (indicated by +) are all contained in columns two and three.

Table II. Summary of rate responses to pulse shapes (horizontal) and click trains (vertical).

Fourteen units with a particular rate response type with respect to PRR in the mating call ensemble are indicated between parentheses. +: high-pass, −: non-selective.

	integration effect			
	no	yes	no response	total
non-selective	9(− − −)			9
low-pass	10(−)			10
high-pass	2	9(+)		11
band-pass		8(+−)	5(+ + +)	13
bimodal	1	1(+)		2
no response	3	6(++)	2(+)	11
total	25	24	7	56

Rows one and two have been lumped and also rows three, four and five in order to perform a χ^2 statistical test. The selectivities for pulse shapes and for click trains were not independent ($\chi^2 = 36.5, \text{df} = 4, P < 0.05\%$). This strengthens the hypothesis that temporal integration effects are responsible for the band-pass and high-pass response characteristics, which appear for the first time in the TS.

About 40% of the data were obtained while simultaneously recording from two or three units. Table III summarizes the inferences made from crosscorrelations of 32 pairs of units. The great majority of these, 29 pairs, showed signs of neural

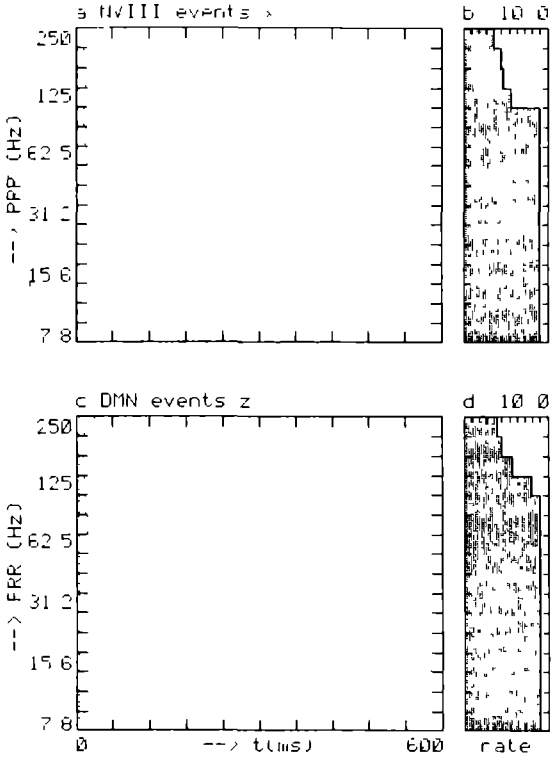

Fig. 3. Reordered eventdisplays together with rate histograms of responses of first and second order model neurons to the periodic click trains Stimulus intensity 22 dB relative to r° Model parameters: tuning centre frequency 0.4 kHz; first order event generation m 0 001, τ_{abs} 6 ms. The second order unit receives input from four units as in (a), with m varying linearly between 0.0001 and 0.001 and τ_{abs} varying linearly between 3 and 6 ms. Further model parameters: EPSP shape: τ_d 3 ms; second order event generation: m 0.33. A delay of 2 ms was incorporated.

Table III. Summary of unit pair analysis.

	recorded on		
	1 electrode	2 electrodes	total
no synchrony	1	2	3
synchrony	11	18	29
common input	3	2	5

synchrony, visible as a peak or trough in the simultaneous crosscoincidence histogram. A clear difference between the simultaneous and nonsimultaneous crosscoincidence histogram was seen in only five of these 29 pairs. Most probably the differences have to be ascribed to neural common input. No clear differences were observed between unit pair recordings made from one or two electrodes. Thus in agreement with a larger study

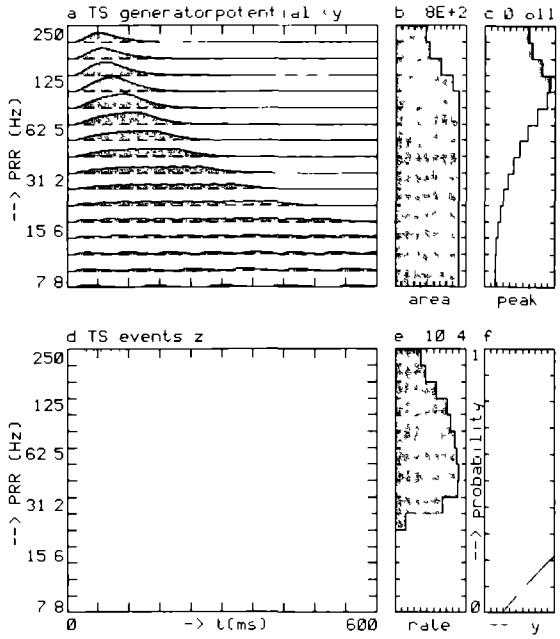

Fig. 4 Simulation of a TS neuron, which receives input from four DMN neurons as in Figs 3c,d. Outputs y, the generator potential, and z, the events, as a function of PRR. The timecourse of the ensemble averaged generator potential $< y(t) >$ (a), its area (b) and the average and standard deviation of the peak of $y(t)$ (c) are depicted Inputs are four units, with m varying linearly between 0 27 and 0 33. The m-value of 0 33 was used in Figs 3c,d EPSP parameters. τ_u 60 ms, τ_d 30 ms Parameters for the TS event generation ν 2 $(\text{ms})^{-1}$, m 0 21. Refractory parameters: τ_{abs} 10 ms, R 0.6, τ_R 2 ms. A delay of 10 ms was incorporated in order to fit the latency.

by Epping and Eggermont (1987) neural interaction seems to play a minor role in the auditory midbrain of immobilized anurans. Therefore the hypothesis that local circuits are responsible for temporal selectivity seems not likely. This result justifies the model to predict responses of TS units from convergent input from lower order neurons, disregarding interactions between TS units.

3.2 Modelling two typical TS units

It will be shown how the model produces a high-pass response to the click train stimulus by means of temporal integration. Then the complex of selectivities found for a TS unit showing temporal integration and a high-pass response to the click trains will be compared with the model neuron's selectivities.

In Fig. 3 the response to the click trains of the

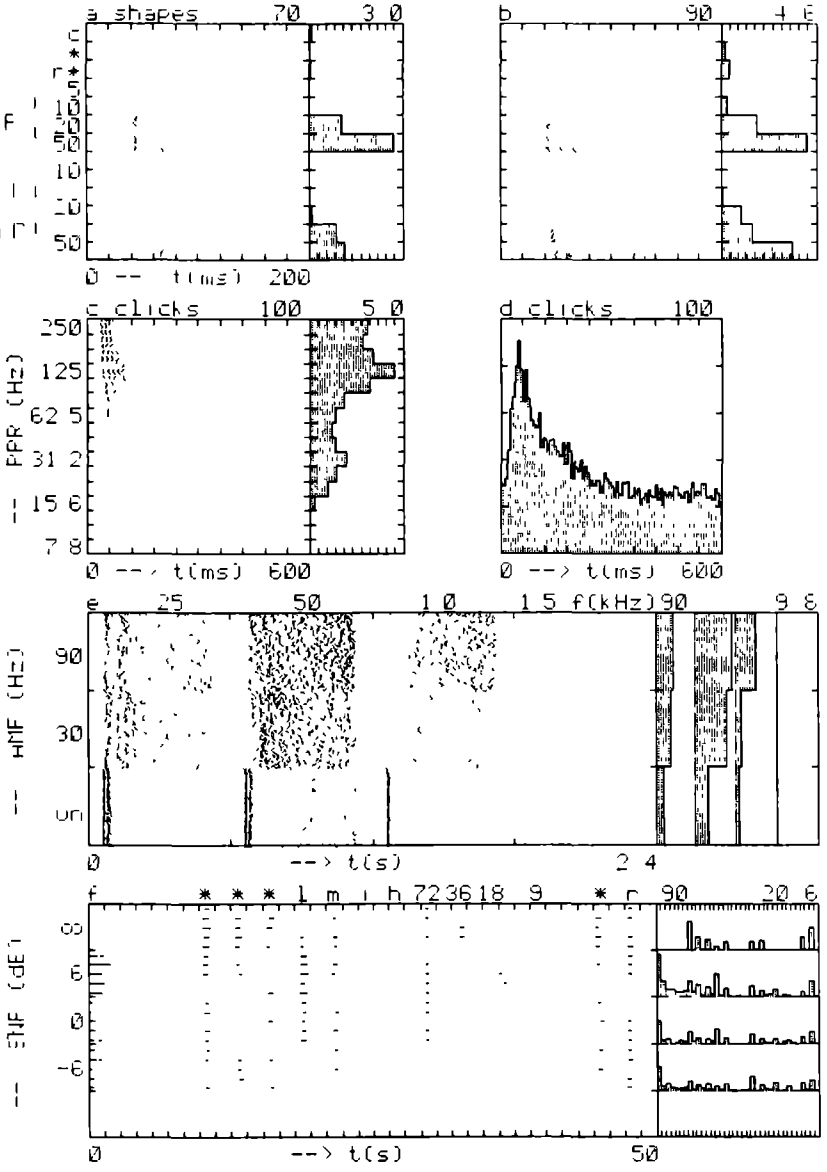

Fig. 5. Reordered eventdisplays together with rate histograms of responses of TS unit 322,3,0 to six different stimuli. At the left the stimulus parameter variation is indicated. All stimuli were presented contralaterally. The intensities, in dB peak SPL, are indicated above each eventdisplay. Carrier frequency in Figs. a and b was 0.5 kHz. Above each rate histogram the maximum value is written. Note the different timebases, which are indicated under the eventdisplays. In Fig. d the crosscoincidence histogram between the random click stimulus and the events is drawn.

The different pulse shapes in Figs. a and b were: click (c), pulse from the mating call (*), tonepip (p), gammatone (Γ), and time-reversed versions (r* and rΓ). The durations (in ms) of the tonepips and of the gammatones are indicated. The click trains of Fig. c consisted of 10 clicks with PRR varying between 7.8 and 250 Hz. With the spectrotemporal stimulus (Fig. e) carrier frequency varies horizontally, whereas AMF varies vertically. In addition to tone bursts with AMF's of 30 and 90 Hz an unmodulated tone burst (un) was presented. The mating call ensemble (Fig. f) was first presented in silence (SNR ∞). Next a stepwise increasing pink noise background was added (SNR decreasing from 6 to −6 dB). Further explanation in text.

first and second order model neuron is visible. The second order model neuron receives four inputs (Fig. 2). The absolute refractory periods of the NVIII inputs vary linearly between 3 and 6 ms, and their thresholds vary linearly between 0.001 and 0.0001. The NVIII input with the highest threshold and the longest τ_{abs} is illustrated in Figs. 3a,b. The first and second order neuron both show rate responses of a low-pass type with a cut-off PRR of 200 Hz (Figs. 3b,d). This is caused mainly by the absolute refractory period of 6 ms which interferes with the highest PRR's. Note that there is a one to one correspondence between stimulus and response up to a PRR of 100 Hz.

As a next step an EPSP (Eq. 13) with a rise time τ_u of 60 ms and a fall time τ_d of 30 ms is chosen to model the temporal integration. These time constants were chosen in order to fit the response of neuron 322,3,0 (Fig. 5). In Fig. 4a the spatiotemporal integration performed by the third order model neuron is visible in the generator potential, averaged over the ensemble of five stimulus presentations. The negative feedback provided by the refractory mechanisms has been excluded from Figs. 4a-c. Fig. 4b shows the average area of the generator potential as a function of PRR. The

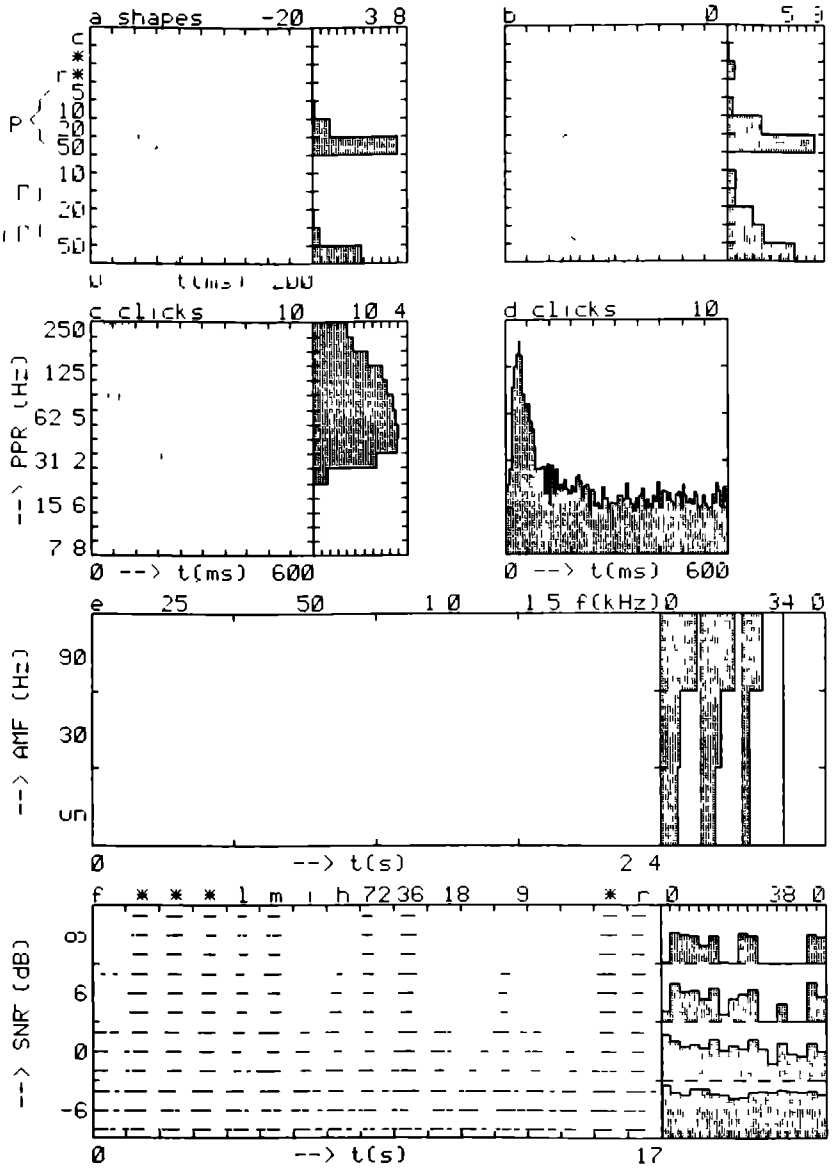

Fig 6 Reordered event-displays together with rate histograms of the model TS neuron of Fig 4 in response to the stimuli of Fig 5 Fig 6c is equal to Figs 4d-e All stimuli were presented at the relative intensities of Fig 5

solid line in Fig. 4c corresponds with the average peak of the generator potential, and the deviations from the solid line correspond with the standard deviation of this peak. A high-pass character is clearly visible in Fig. 4c. The probability of event generation function (Eqs 9,11) in Fig. 4f, which for comparison is drawn to the scale of Fig. 4c, is now used to generate the response shown in Figs 4d and 4e. Because of the high threshold a single click produces no response, and temporal integration is necessary to reach threshold Note that in contrast to Fig 3 the synchronization to the individual stimulus clicks is lost

The responses of unit 322,3,0 and of the model neuron to six stimuli are compared in Figs. 5 and 6. Because unit 322,3,0 responds to carrier frequencies up to 1.0 kHz (Fig. 5e) it receives excitatory input originating from the amphibian papilla. This is modelled with a band-pass filter (Eq. 2) tuned to 0 4 kHz, the unit's best frequency. Threshold of this unit was 50 dB peak SPL. At intensities of 70 and 90 dB the unit showed practically no response to pulse shapes with a duration shorter than 20 ms (Figs 5a,b) This is very well reproduced by the model neuron (Figs. 6a,b) The responses to the click trains, Figs. 5c and 6c,

show a high-pass character and a decline of latency with increasing PRR Quantitatively however the model neuron's response is stronger for PRR's between 40 and 100 Hz The crossco-incidence histograms between the clicks and the events (Figs 5d and 6d) both show a broad peak, whose width is somewhat smaller for the model neuron The greatest deviation between data and simulation is found with the spectrotemporal stimulus (Figs 5e and 6e) Unit 322,3,0 responds well to the onset of unmodulated tones, and this onset response is followed by a rebound in case of the 0 5 kHz carrier This pause response pattern might be caused by inhibition, which was not included in the model Furthermore the rate response of Fig 5e shows a high-pass character with respect to AMF This is modelled with a modest degree of coincidence detection at the DMN level In a foregoing paper (Van Stokkum and Gielen, 1989) it was demonstrated that part of the DMN units respond selectively to fast intensity changes These fast intensity changes synchronize the NVIII inputs, and convergence of these inputs upon a DMN unit using a short integration time, produces a peaked generator potential In contrast, an unmodulated tone produces a flatter generator potential, because the input firings will gradually become distributed in time, due to their refractory properties The thresholds of the DMN units of this model produced a modest high-pass response with respect to AMF (not shown) This modest high-pass response is preserved at the TS level (Fig 6e) Finally in Figs 5f and 6f the response to the mating call ensemble is depicted Without noise (SNR ∞) both unit 322,3,0 and the model neuron show no response to the carrier frequency variations of 1067 and 1542 Hz (i and h), because of their frequency selectivity Both units also do not respond to the 9 and 18 Hz PRR variation, which implies a high-pass response with respect to PRR Unit 322,3,0 adapts to the noise, which is visible in the first 10 s of Fig 5f Thereafter the response to the mating calls remains distinct up to the highest noise level In contrast the model neuron's response to the calls is masked by the response to the noise for the highest noise levels

Now the same model is applied to a unit which did not respond to the pulse shape stimulus and which showed a band-pass response to both the click trains and the AM tone bursts To model a band-pass response to the AM tone bursts the degree of coincidence detection on the DMN level is increased by shortening the EPSP and slightly increasing the thresholds The effect of this is pictured in Fig 7 The rate response of the NVIII unit shows a non-selective character (Fig 7b) Note that the responses to the five presentations of each AM tone burst are aligned very well for AMF's around 62 5 Hz (Fig 7a) Recall that the absolute refractory periods of the NVIII inputs varied between 3 and 6 ms, and their thresholds varied between 0 001 and 0 0001 These differences desynchronize the responses to the lowest and highest AMF's This results in a DMN generator potential peak histogram with a band-pass character (not shown) Because of its high threshold the DMN unit produces a band-pass response with respect to AMF (Figs 7c,d) Temporal integration of the four DMN inputs produces the generator potential characteristics of Figs 8a-c Both the averaged area and the averaged peak (Figs 8b and c) show a band-pass character The probability of event generation (Fig 8f) utilizes this by means of a high threshold and produces a distinct band-pass response (Figs 8d and e)

Now the response of unit 314,1,0 to six stimuli (Fig 9) is compared with a model simulation (Fig 10) Unit 314,1,0 did not respond to unmodulated tone bursts (Fig 9e) Like unit 322,3,0 it received excitatory input derived from the amphibian papilla, which can be concluded from the response to carrier frequencies below 1 1 kHz in Fig 9e Its threshold was 50 dB peak SPL The frequency selectivity is modelled with a band-pass filter tuned to 0 625 kHz In contrast to the band-pass response with AM tone bursts, the response to AM noisebursts (rightmost carrier) shows a weaker selectivity (Fig 9e) This is reproduced well by the model (Fig 10e) A more detailed investigation of the AMF selectivity, using a carrier frequency of 0 55 kHz, is shown in Figs 9a,b and 10a,b At intensities differing by 20 dB a clear selectivity for AMF's between 31 and 125 Hz is visible Note that the rate response to the AM tone burst with a carrier frequency of 0 55 kHz and an AMF of 60 Hz (Fig 9e) is twice as large as the maximum response in Fig 9b This points to a habituation effect caused by the repeated presentation of 0 55 kHz AM tone bursts, despite the onset interval of 3 s At the highest intensity the model's response deviates in that the AMF selectivity is no longer absolute, some response is visible to the lower and higher AMF's The response to the click trains in both cases shows a band-pass character (Figs 9c and 10c) Unit 314,1,0 adapted totally

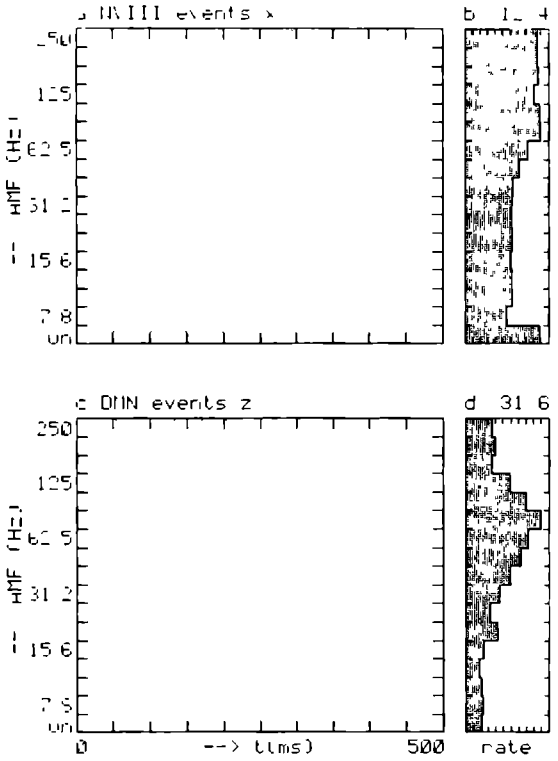

Fig 7. Reordered eventdisplays together with rate histograms of responses of first and second order model neurons to AM tone bursts. Stimulus parameters: intensity: 12 dB relative to r°, carrier frequency 0.55 kHz. Model parameters: tuning: centre frequency 0.625 kHz. All other parameters as in Fig. 3 except: EPSP shape: τ_d 1 ms; second order event generation: m 0.38.

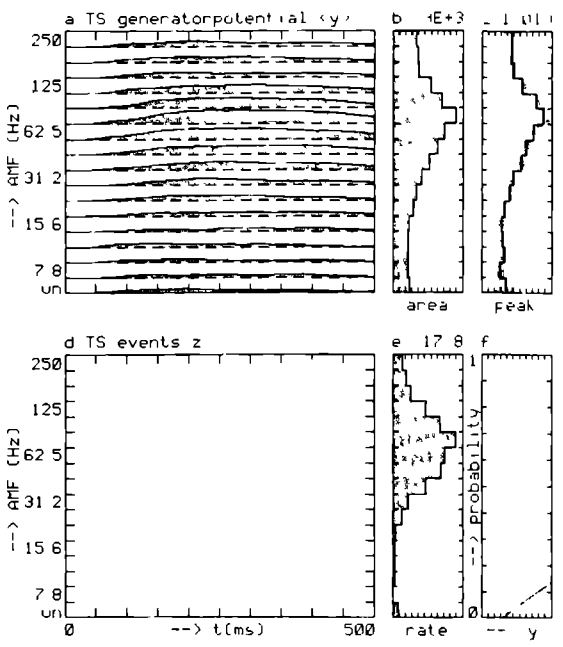

Fig. 8 Simulation of a TS neuron, which receives input from four DMN neurons as in Figs. 7c,d. Outputs y, the generator potential, and z, the events, as a function of AMF. Inputs are four units, with m varying linearly between 0.35 and 0.38. The m-value of 0.38 was used in Figs. 7c,d. Model parameters for the third order neuron: EPSP shape: τ_u 100 ms, τ_d 70 ms. Parameters for the TS event generation: ν 1 $(\text{ms})^{-1}$, m 0.3. A delay of 2 ms was incorporated. Refractory parameters: τ_{abs} 15 ms, R 0.5, τ_R 5 ms.

after 90 s of the random click stimulus, which the model neuron did not (not shown). The cross-coincidence histograms (Figs. 9d and 10d) both show a broad peak, which is somewhat broader for the model neuron. Finally the responses to the mating call ensemble (Figs 9f and 10f) agree with respect to the PRR variations in that no response is visible to the 9 Hz PRR variation. The frequency selectivity of the model agreed well at 90 dB peak SPL (compare Figs. 9e and 10e), but differed for the mating calls at 70 dB peak SPL, where unit 314,1,0 responded weakly to the carrier frequency variations of 201 and 1067 Hz (l and i). Both unit 314,1,0 and the model neuron practically do not respond to the noise, which is visible in the first second of the reordered eventdisplays. The response of unit 314,1,0 is completely masked by the noise, except for the 72 Hz PRR variation. In contrast the response of the model neuron persists up to the highest noise level, which reminds of the response of unit 322,3,0 in Fig. 6f.

Thus from Figs. 3 to 10 it is concluded that a change of only a few parameters, notably the EPSP shapes between first and second, and between second and third order neurons, in concordance with the adjustment of the pulse generating properties, produces two model neurons which reflect the properties of two qualitatively different auditory midbrain units.

4 Discussion

4.1 Modelling

The model of the anuran auditory periphery (Van Stokkum and Gielen, 1989) has been extended to model the monaural properties of auditory midbrain neurons. Using a single parameterset the response of the model to a set of spectrally and temporally structured stimuli corresponded with the response characteristics of some typical TS neu-

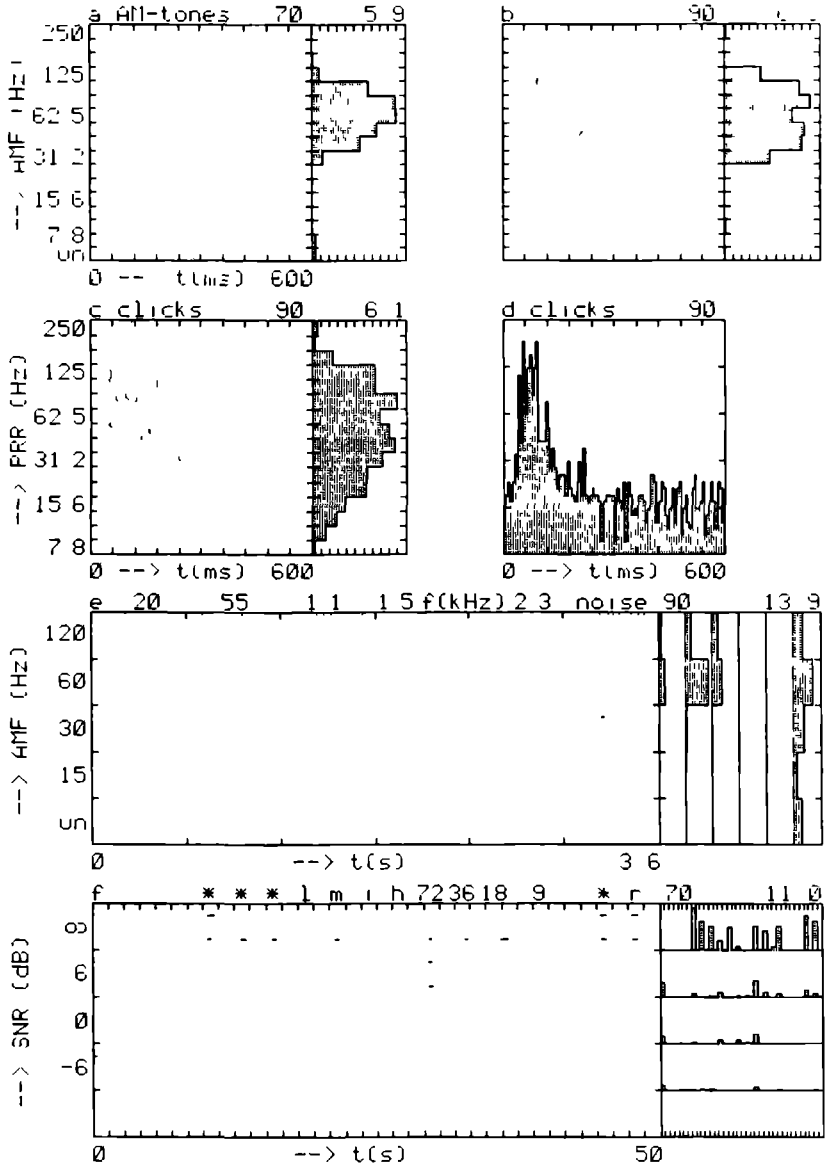

Fig. 9. Reordered event-displays together with rate histograms of responses of TS unit 314,1,0 to six different stimuli The AMF of the tone bursts (Figs. a and b) varied between 7.8 and 250 Hz, in addition an unmodulated tone burst (un) was presented. Carrier frequency in Figs. a and b was 0 55 kHz. With the spectrotemporal stimulus (Fig. e) carrier frequency varies horizontally between 0 2 and 2 3 kHz. In addition a white noise burst was used as carrier. AMF varies vertically between 15 and 120 Hz, in addition an unmodulated sound burst was presented. Rest of legend as in Fig. 5.

rons. Variation of only a few parameters, notably the EPSP shapes, produced response characteristics corresponding with those of another TS neuron whose responses were qualitatively different. Together with the results of the previous paper it is concluded that variation of the parameters of this monaural model reproduces most of the response characteristics found with NVIII fibres, DMN neurons and TS neurons.

4.2 Mechanisms

The different model stages, which correspond with different stations along the auditory pathway, perform different operations on the stimulus envelope To begin with, in the NVIII a variety of short-term adaptation patterns exists (Megela and Capranica, 1981) In the DMN a group of units is selective for fast intensity changes, like the onsets of the mating call pulses (Hall and Feng, 1988; Van Stokkum, 1987). This was modelled with a coincidence detection mechanism, which detected synchrony of converging fast adapting NVIII inputs. In the TS a group of units possesses long integration times, which enables them to develop selectivity for pulse duration and PRR (this study). Using tonepips Bibikov (1977) found that 45% of the TS neurons have integration times in the range between 10 and 100 ms This sample of 45% corresponds well with column two of Table II, which

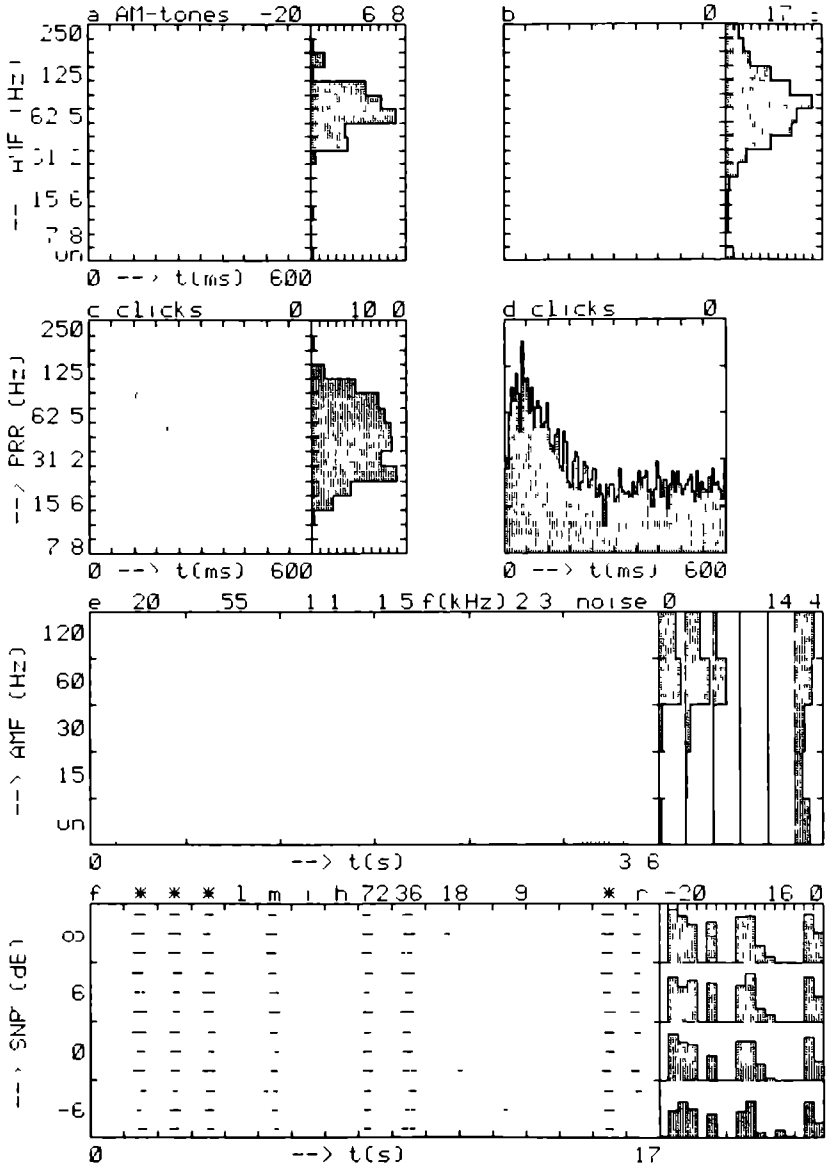

Fig 10 Reordered event-displays together with rate histograms of the model TS neuron of Fig 8 in response to the stimuli of Fig 9 Fig 10b is equal to Figs 8d-e. All stimuli are presented at the relative intensities of Fig 9

comprises the group of TS neurons that showed an integration effect with the pulse shape stimulus Adding to this group the neurons which do not respond to pure tones (column three of table II, unit 314,1,0) it is found that over half of the TS units possess integration times larger than 10 ms.

Feng (1983) observed dendritic lengths up to 350 μm in the TS. Inputs arriving at such dendrites give rise to a long duration EPSP at the event generation site of the neuron (Rall, 1977). Intracellular recordings from neurons in the optic tectum of the grassfrog (Matsumoto et al 1986) have shown that EPSP time constants of more than 10 ms are present All this evidence supports the hypothesis that temporal integration is responsible for the temporal selectivities that appear for the first time in the TS. Next to the adaptation and spatiotemporal integration of inputs the event generation is crucial A nonlinearity, the threshold mechanism of Eq. 11, was necessary to produce the temporal selectivities at the DMN and TS level.

4.3 Parameter variation

The significance of the parameters of Table I will be discussed in connection with the various responses in Table II. A first group of parameters $(\gamma, \omega_1, \beta_i, \omega_i, r^o, \lambda, \mu, \omega_2)$ is responsible for the NVIII generator potential w. Variation of ω_i and β_i produces different spectral selectivities. Variation of the adaptation parameters λ and μ produces the different types of short-term adaptation found in the NVIII by Megela and Capranica (1981). The neuronal refractory (τ_{abs}, R, τ_R) and event generation (ν, m) properties have to be adjusted to produce realistic response properties. Thereby τ_{abs} was chosen equal to the neuron's smallest interspike interval. The threshold m was responsible for the response selectivity derived from the generator potential.

Desynchronization of NVIII inputs is a prerequisite for coincidence detection on the DMN level. This desynchronization is caused by the different m, τ_{abs} and the large R of the NVIII inputs. The second prerequisite for the coincidence detection is spatiotemporal integration. At least two inputs are necessary. The effect of reducing the decay time τ_d from 3 to 1 ms was demonstrated in this paper (Fig. 7, compare Figs. 6 and 10).

The larger τ_d and τ_u of the third order neuron, the more temporal integration. A neuron with small τ_d and τ_u will show a non-selective or low-pass response pattern with respect to PRR (rows 1 and 2 of Table II). These responses will be comparable to those shown in Figs. 3c,d. It was shown in Figs. 3-6 that the combination of moderate coincidence detection on the DMN level (τ_d = 3 ms) with temporal integration on the TS level produced a high-pass response with respect to PRR (row 3 in Table II). Increasement of the coincidence detection on the DMN level (τ_d = 1 ms) in combination with temporal integration produced a band-pass response with respect to PRR (row 4 in Table II, Figs. 7-10). The majority of the units with a bimodal or no response to the click trains showed signs of inhibition (see the discussion below).

4.4 Adaptation

Next to the adaptation in the NVIII it was assumed that there is also adaptation in the higher order neurons of the model. To model this a negative feedback was supplied to the DMN neuron, with a time constant of 400 ms. This improved the correspondence between data and model simulations. Because of methodological problems, especially with stimulus 7, the time constants have been limited to 1000 ms. Non-stationarities involving longer time constants were found with the complete adaptation of unit 314,1,0 to the random click stimulus in 90 s and the adaptation to the noise of unit 322,3,0 in the first 10 s of Fig. 5f. These non-stationarities may be related to long-term adaptation or to habituation. Megela and Capranica (1983) found that NVIII fibres do not habituate to repeated stimuli, whereas in the TS habituation was observed with stimulus repetition rates larger than one per second. Presumably habituation is related to inhibitory processes, which were not included in the model.

4.5 Neural interaction

Epping and Eggermont (1987) investigated neural interaction in the grassfrog's TS. In a sample of 264 unit pairs they found that 60% of the pairs showed neural synchrony, which in 77% of the cases was caused by stimulus influences. The remaining 23% showed signs of two sorts of neural interaction: excitation (4%) and common input (19%). In the smaller sample of this paper 90% of the unit pairs showed neural synchrony, which in 83% of the cases was caused by the stimulus. This confirms the suggestion of Epping and Eggermont that their 60% neural synchrony was a lowerbound, because part of the unit pairs had not been tested with the more effective temporally structured stimuli. From these numbers it is concluded that in immobilized anurans local circuits in the TS are of minor importance for the processing of temporal characteristics of sound.

4.6 Inhibition

In this paper inhibition was not included in the model. Using random clicks inhibition has been demonstrated in the temporal domain by Bibikov (1981) who described a group of units receiving inhibitory followed by excitatory input (type III of Epping and Eggermont, 1986a).

In the spectral domain Fuzessery and Feng (1982) demonstrated abundant two-tone inhibition. To model two-tone inhibition the model was extended with an inhibitory branch which started with a band-pass filter tuned to the best inhibitory frequency. This model showed two-tone inhibition.

A problem with modelling inhibition is to derive the temporal properties of the inhibitory branch. Experiments using temporally structured two-tone

stimuli are necessary to enable more systematic modelling

4.7 Temperature dependence

Brenowitz et al (1985) have shown that the AMF selectivity of auditory midbrain units is temperature dependent For one unit they found that the preferred AMF shifted from 15 to 25 Hz when the temperature was increased by 8°C The model offers an explanation for this when the temperature dependence of the EPSP is taken into account A higher temperature will shorten the EPSP A shorter EPSP between NVIII and DMN increases the preference for fast intensity changes, which are found with higher AMF's A shorter EPSP between DMN and TS leads to less temporal integration, and causes a preference for stimuli with a shorter periodicity, corresponding with higher PRR's and AMF's

4.8 Identification and localization

Thus far only the processing of monaural stimuli was regarded Experiments using temporally structured binaural stimuli (Melssen and Van Stokkum, 1988) suggested that identification and localization of sound are coupled processes which make use of common mechanisms So it would be worthwhile to extend the model to binaural stimuli in order to achieve a more complete picture of the information processing in the anuran auditory brainstem

Acknowledgements
This investigation was supported by the Netherlands Organization for Scientific Research (NWO) Koos Braks skilfully prepared the animals The experiments were conducted in close cooperation with Willem Melssen, who is also thanked for software assistance Willem Epping, Stan Gielen, Peter Johannesma, Willem Melssen and Henk van den Boogaard are thanked for helpful discussions and critical reading of the text

Chapter VII

Summary

The natural calls of the grassfrog (*Rana temporaria* L) consist of trains of identical pulses The spectral content of the pulses and the pulse repetition rate (PRR) are important cues for the recognition of species-specific calls (Section I 1) In this thesis the role of auditory brainstem neurons in the identification of natural calls was investigated Thereby special attention was paid to the selectivity for temporal characteristics of sound in auditory neurons in two different brainstem nuclei A thorough analysis of these neurons required the presentation of a broad ensemble of spectrally and temporally structured stimuli In these stimuli, which were inspired by the natural calls, parameters like PRR and carrier frequency were varied, in order to investigate the neuronal basis for the behavioural responses To understand the function of these neurons composite pictures were made, in which the responses to a variety of stimuli were related (Figs III 5, V 4, VI 5 and VI 9) While analysing and relating the responses a possible underlying model was imagined In Chapters V and VI a structural model was proposed which reproduced the monaural response properties of most of the auditory brainstem neurons in the grassfrog For a more complete understanding of the function of these neurons the binaural response properties should be included To reproduce the binaural response properties, and the monaural response properties discussed in Section VI 4 6, the model should be extended with inhibitory processes

When analysing correlations between stimulus and neural events, or between events from different neurons, stationarity is usually assumed However, in general neuronal responses are non-stationary Ascending from eighth nerve (NVIII) to torus semicircularis (TS) adaptation and habituation become more prominent (Section I 3 2, Megela and Capranica, 1983) The technique of time averaging, which is performed to obtain a clear picture of the neuronal responses, becomes questionable with non-stationary point processes In Chapter II time-dependent correlation functions have been introduced, which have been applied in Chapters III and IV to analyse non-stationary point processes

The model contains components which reproduce short-term adaptation (Fig VI 2D,F,E and I) It remains an open question whether long-term non-stationarities (e g Figs II 4 and III 5c) can be accommodated by the present model, because they probably originate higher in the nervous system

In the past Epping and Eggermont (1986a,b, 1986) investigated the responses of TS neurons to spectrally and temporally structured stimuli These same stimuli and some new ones were used to characterize dorsal medullary nucleus (DMN) and TS neurons Thereby special attention was paid to possible underlying mechanisms It was hypothesized that neurons develop their selectivity by means of spatiotemporal integration of inputs from lower level neurons Based upon simultaneous recordings of TS neurons the alternative hypothesis that local circuits are involved was rejected (Chapter VI)

Spectral information processing starts with the band-pass filtering characteristics of NVIII fibres which innervate the papillae (Figs VI 2A and B) In the brainstem convergence of different frequency channels in an excitatory or inhibitory manner is found (Sections I 3 1 and VI 4 6)

This thesis has focused on temporal information processing in the auditory brain stem In the DMN a group of neurons functions as coincidence detectors which detect synchronous firings of converging NVIII fibres In this way they develop a preference for fast intensity changes, like the pulses of natural calls (Chapters III and V) The TS contains a diversity of neurons An important criterion to distinguish among them is their temporal integration (Section I 3 2 and Chapter VI) About half of the TS neurons possesses integration times longer than 10 ms These neurons loose

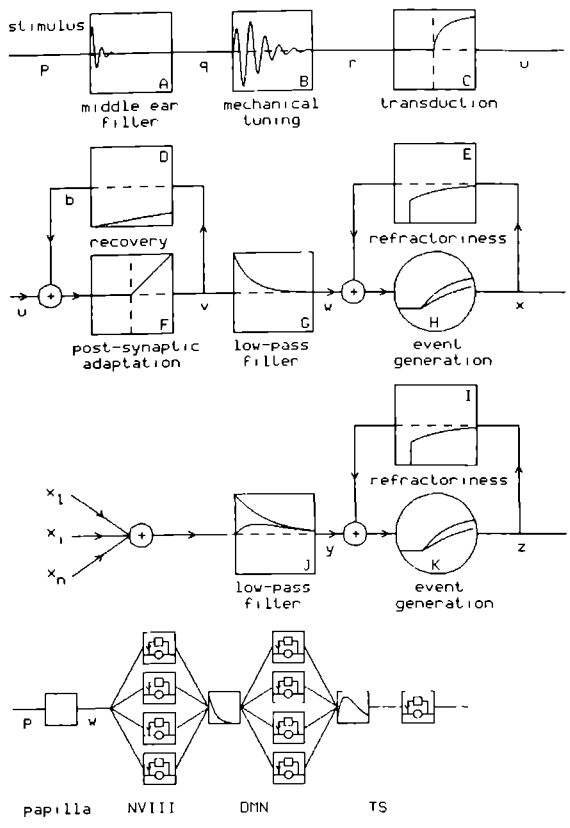

Fig. VI.2 Model for the processing of sound by the papilla, NVIII, DMN and TS of the grassfrog. The stimulus waveform is band-pass filtered by the middle ear (Fig. A), and filtered and transduced into a haircell potential (Figs. B,C). The synapse between the haircell and the dendrite of the NVIII fibre comprises of a short-term adaptation mechanism (Figs. D,F) and a low-pass filter (Fig. G). From the generator potential w of the NVIII fibre action potentials are generated (Fig. H), which form the point process x. Absolute and relative refractory mechanisms are incorporated in the negative feedback loop (Fig. E). Outputs from lower order neurons $(x_1, \ldots, x_i, \ldots, x_n)$ converge upon a higher order neuron, where they add linearly and are convoluted with an EPSP shape (Fig. J). From the generator potential y of the higher order neuron action potentials are generated in the same way as explained above.
In Figs. A,B,D,E,G,I and J impulse responses are drawn on a timebase of 5 ms. Figs. C and F represent the instantaneous nonlinearities of, respectively, Eqs. VI.5 and VI.6. Figs. H,K show probabilities of event generation (Eqs. VI.9,11) as a function of the generator potentials w, y.
The lower flow diagram symbolizes the connections used in the simulations of this paper. The generator potential w is used to generate events in four NVIII units. Four DMN units receive input from these four NVIII units. Finally the four DMN units converge upon the third order model neuron, which represents a TS neuron. One EPSP shape is used between NVIII and DMN, and another EPSP shape is used between DMN and TS.

their time-locking ability. But temporal integration enables them to develop high-pass characteristics with respect to PRR, which is an important cue for the recognition of natural calls (Sections I.1 and I.4).

1 Discussion

1.1 Characterization

An important issue in the characterization of sensory neurons is the notion of receptive field. The receptive field consists of those stimuli to which a neuron responds with a change in the generation of action potentials. Aertsen (1981) investigated the stimulus (in)dependence of the spectro-temporal receptive field. In Fig. III.2 (see page 76) examples of spectro-temporal receptive fields are shown for two DMN neurons. In this figure the responses are shown to tonepips with a varying carrier frequency and to a noise stimulus. Based upon their characteristic frequency (CF) units are classified as low frequency (CF < 0.4 kHz), mid frequency (0.4 < CF < 1 kIlz) and high frequency (CF > 1 kHz). Low-frequency unit 297,0,1 can be well modelled with the first part of the model, Figs. VI.2A-H. It responds to frequencies between 0.1 and 0.2 kHz in a phase-locked manner (Fig. III.2a). Because of its phase-locking ability the reverse correlation function between noise stimulus and action potentials resembles a reversed impulse response of a band-pass filter (cf. Fig. VI.2.B). High-frequency unit 284,0,2 responds to frequencies between 0.2 and 2 kHz, but without phase-lock (Fig. III.2b). The loss of phase-lock is probably caused by dendritic low-pass filtering (Figs. VI.2G,J). A second order analysis of the noise preceding a spike by means of a CoSTID (Johannesma et al., 1981) reveals the high-frequency selectivity (Fig. III.2.d), but now the response is restricted to frequencies between 0.8 and 1.6 kHz. The response to a broader range of carrier frequencies in Fig. III.2b can be explained by short-term adaptation (Figs. VI.2D,F) which produces different degrees of postsynaptic

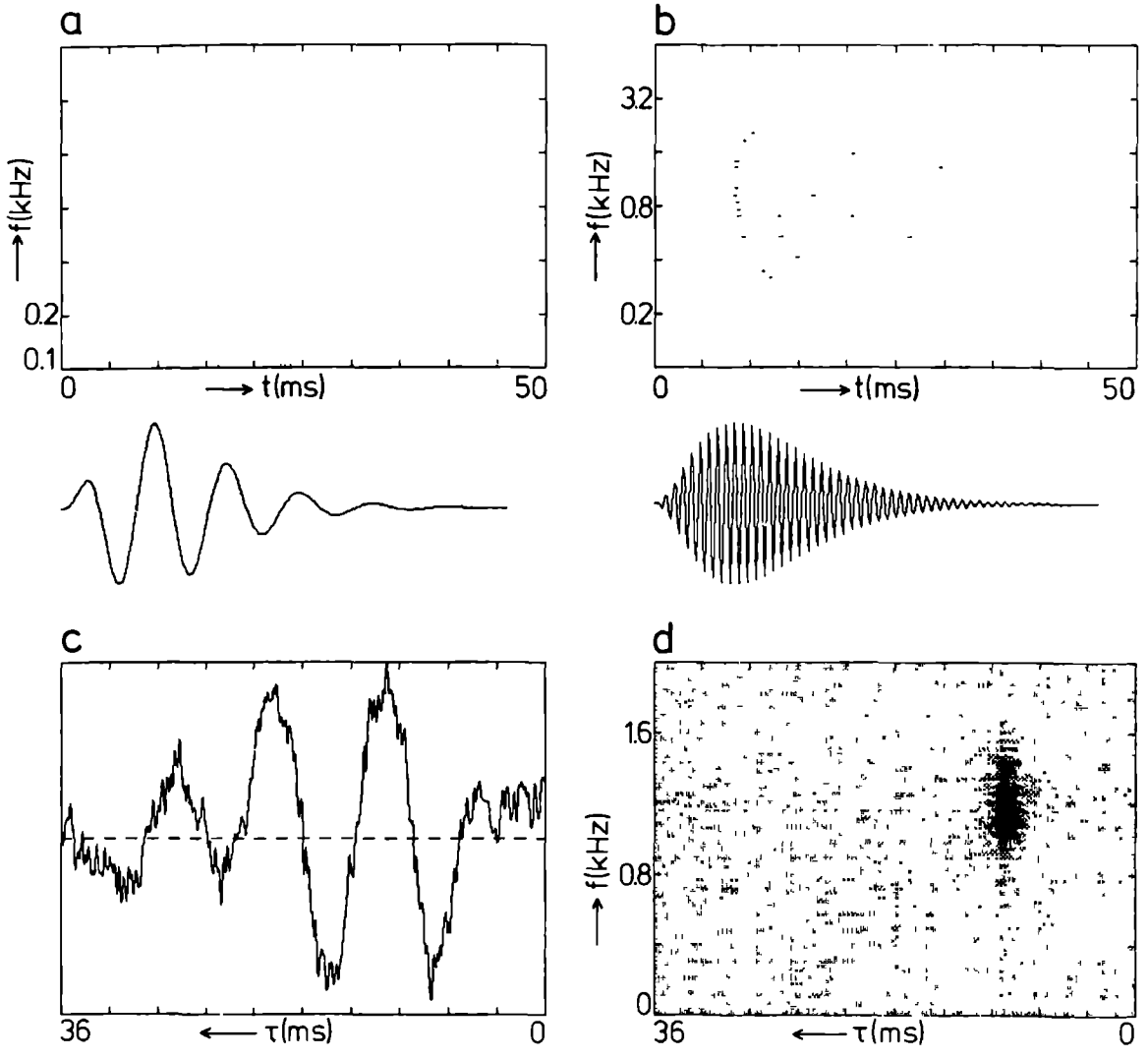

Fig. III.2. Spectral sensitivities of DMN units 297,0,1 (a,c) and 284,0,2 (b,d) as determined with gammatones and noise. (a) Unit 297,0,1. Reordered eventdisplay of response to tonepip stimulus, 34 events. Underneath gammatone with carrier frequency of 131 Hz on the above time scale. (b) Unit 284,0,2. Reordered eventdisplay of response to tonepip stimulus, 507 events. Underneath gammatone with carrier frequency of 1111 Hz. (c) Unit 297,0,1. Reverse correlation function of 129 events during 335 s of pink noise stimulus. (d) Unit 284,0,2. Average PESE-CoSTID of 1570 events during 84 s of white noise stimulus. All stimuli were presented ipsilaterally at intensities of 90 dB peak SPL.

inactivation for tonepips presented in silence and for continuous noise. Thus even with the most elementary stimuli, tonepips and noise, different spectro-temporal receptive fields appear. A model which includes short-term adaptation is necessary to reconcile the different characteristics.

A group of mid-frequency DMN neurons showed a more complex response, they preferred fast intensity changes. An example is unit 297,0,6 (Figs. III.5 and V 4). This neuron responded phasically to the tonepips (Fig. III.5e) and did not respond to a noise stimulus. The spectro-temporal receptive field determined with gammatones is of limited value to characterize the unit. A coincidence detection mechanism was proposed in Chapter III, and described in detail in Chapter V, to model the preference for fast intensity changes.

As mentioned above TS neurons can be distinguished by their integration time. TS units possessing short integration times show time-locking,

i.e. their responses are synchronized to the stimulus envelope. These neurons possess spectro-temporal characteristics comparable to those shown in Figs. III.2b,d. TS units possessing integration times longer than 10 ms reveal no time-locking. These neurons show response characteristics which appear for the first time in the TS (Chapter VI). For instance unit 322,3,0 responds only to tonepips exceeding a minimum duration (Figs. VI.5a,b). The response to the click stimuli also shows evidence of temporal integration (Figs. VI.5 c,d). This unit's temporal integration was modelled with an EPSP with a decay time-constant of 30 ms (Fig. VI.2J and bottom right).

TS unit 314,1,0 did not respond to unmodulated tonepips or continuous noise. Thus, unlike the DMN units in Fig. III.2., this unit could not be characterized with these stimuli. Instead it was characterized with amplitude modulated tones and noise (Fig. VI.9e). This spectro-temporal stimulus, which has three parameters, sound pressure level, carrier and amplitude modulation frequency, appeared suited to characterize complex TS neurons. Again the response to the click stimuli (Figs. VI.9c,d) pointed at temporal integration. This unit was modelled with a combination of coincidence detection on the DMN level, which caused a preference for fast intensity changes, and temporal integration on the TS level, which caused the high-pass character of the response to click and pulse trains (Figs. VI.9c,f).

From this overview it is clear that a stimulus invariant spectro-temporal receptive field does not exist (see also Aertsen, 1981). The fact that part of the TS neurons does not respond to unmodulated tonepips or noise jusitifies the use of temporally structured stimuli. Characterization of auditory brainstem neurons should be based upon a structural model, and not upon mere stimulus-response correlation. This model then contains the spectro-temporal receptive field determined with any stimulus.

1.2 Interpretation

Tightly related to the concept of spectro-temporal receptive field is the sensory interpretation of neural activity (Johannesma, 1981). Primitive neurons can adequately be described with a Revcor function or CoSTID. For these neurons a reverse mapping of neural activity to stimulus space can be constructed (Hesselmans, 1988). Each neural event signals the presence of a sound element like the Revcor function of Fig. III.2c or the CoSTID of Fig. III.2d.

But how can the activity of more complex neurons like DMN unit 297,0,6 (Chapters III and V) and TS units 314,1,0 and 322,3,0 (Chapter VI) be interpreted? Is it possible to use the functional model description in a reverse manner? Which stimulus aspects can be reconstructed from the selective responses of these neurons? A first step will be to estimate a generator function $g(y)$ from the generated action potentials z (Figs. VI.2I,K and bottom right). The second step will be to deconvolute the generator potential y with the EPSP function $e_t(t)$ and thereby recover the input point processes (Eq. VI.12). When such a procedure is feasible, a generator potential w of NVIII fibres can be recovered. The final step is then to estimate a stimulus p which produces w through the cascade of linear filters and nonlinearities (Figs. VI.2A-D,F,G). As a check the output of the reverse estimation procedure can be calculated forwardly at any stage.

What could be the outcome of such a reverse procedure for the three aforementioned neurons? Phase information of the stimulus surely is lost as a result of the dendritic low-pass filtering (Figs. VI.2.G,J). DMN unit 297,0,6 signals fast intensity changes with a spectral content encompassing its CF of 0.63 kHz.

The two TS units discussed above signal the presence of sounds with a spectral content in the range of 0.2 to 1.0 kHz. Furthermore TS unit 322,3,0 signals a sound duration of at least 20 ms, and by means of its latency also some information about the onset of the sound. But from this unit no information considering the timing of the individual pulses of a mating call can be recovered. Instead the presence of at least two pulses with a PRR higher than 18 Hz is signaled. The loss of time-locking ability is even stronger in TS unit 314,1,0. Action potentials of this unit signal the presence of a number of fast intensity changes with sufficient PRR. Thus we arrive at a more abstract description of sound stimuli, where different neurons code several aspects of the stimulus at the same time, and the stimulus information is distributed over an ensemble of neurons.

Addition of the spatial dimension to the interpretation of neural activity (Melssen and Van Stokkum, 1988; manuscript in preparation) will at first complicate matters, but may ultimately simplify them.

1.3 Neuroethology

This thesis has been concerned with auditory brainstem neurons. Having understood more about their functional properties, what can be said about their behavioural role? In Section I.1 the importance of carrier frequency and PRR for the recognition of conspecific calls was recapitulated (Walkowiak and Brzoska, 1982). It was already remarked in Chapter I that the diversity of spectral and temporal selectivities of brainstem neurons seemed suitable for call recognition. But the quest for neurons that function as mating call detectors has been fruitless (e.g. Eggermont and Epping, 1986). The three representative neurons which were discussed in Chapters III, V and VI responded well but not exclusively to mating calls. DMN neurons like unit 297,0,6 seem well suited to detect the pulses of natural calls against a noisy background (Fig. III.5d and Section III.4.5). Furthermore these neurons showed a low-pass rate response with respect to PRR, with cut-off frequencies above the natural PRR.

Gerhardt and Doherty (1988) showed that pulse shape was an important cue for mating call phonotaxis in *Hyla versicolor*. Probably pulse shape is also important in *Rana temporaria*, and in that case the class of DMN neurons that prefer fast intensity changes might be involved.

The two TS neurons presented in Chapter VI both showed a high-pass response with the PRR variations of the mating call, with cut-off frequencies below the natural PRR. These neurons can signal the presence of a train of pulses with a minimum PRR. The model simulations resulted in EPSP decay time-constants of 30 and 70 ms, which are well suited to integrate the neural activity resulting from a call with a natural PRR of about 30 Hz. It was already suggested in Section VI.4.7 that the temperature-dependence of call PRR might be compensated by the temperature-dependence of EPSP time-constants.

Investigation of neuronal responses in behaving animals would allow testing the conjectures made in the present study, which were based upon recordings in immobilized animals.

Aertsen, A.M.H.J. (1981) Spectro-temporal characterization of auditory neurons. Ph.D. Thesis, Catholic University of Nijmegen.

Aertsen, A.M.H.J. and Johannesma, P.I.M. (1980) Spectro-temporal receptive fields of auditory neurons in the grassfrog. I. Characterization of tonal and natural stimuli. Biol. Cybern. 38, 223-234.

Aertsen, A.M.H.J., Smolders, J.W.T. and Johannesma, P.I.M. (1979) Neural representation of the acoustic biotope: On the existence of stimulus-event relations for sensory neurons. Biol. Cybern. 32, 175-185.

Aertsen, A.M.H.J., Vlaming, M.S.M.G., Eggermont, J.J. and Johannesma, P.I.M. (1986) Directional hearing in the grassfrog (*Rana temporaria* L.): II. Acoustics and modelling of the auditory periphery. Hear. Res. 21, 17-40.

Bibikov, N.G. (1971a) The reaction of single neurons in the auditory system of the frog *Rana ridibunda* to pulsed tonal stimuli. J. Evol. Biochem. Physiol. 7, 178-185.

Bibikov, N.G. (1971b) Responses of auditory neurons in the midbrain of the frog. Proc. VIIth Int. Congr. Acoust., Budapest, pp.549-552.

Bibikov, N.G. (1973) Unit responses of the torus semicircularis of frogs to acoustic stimuli of different duration. Neurophysiol. 5, 9-14.

Bibikov, N.G. (1974) Encoding of stimulus envelope in peripheral and central regions of the acoustic system of the frog. Acustica 31, 301-305.

Bibikov, N.G. (1975) Evaluation of the dynamics of synaptic potentials from the evoked impulse activity of the neurones. Biophysics 20, 901-906.

Bibikov, N.G. (1977) The classification of the neurons in the auditory system on the basis of the function of the expected rate probability. Akust. Zh. 23, 346-355.

Bibikov, N.G. (1978) Dynamics of the expected rate probability in auditory system neurons for different intensities of tonal stimuli. Akust. Zh. 24, 816-825.

Bibikov, N.G. (1980) The reaction of the torus semicircularis units of *Rana temporaria* to the signals simulating the mating call temporal characteristics. Zool. Zh. 59, 577-586.

Bibikov, N.G. (1981) Cross-correlation analysis of the activity of the auditory neurones on exposure to sound clicks. Biophysics 26, 346-352.

Bibikov, N.G. and Gorodetskaya O.N. (1981) Single unit responses in the midbrain auditory center of the frog mesencephalon to amplitude modulated tones. Neurophysiol. 12, 185-191.

Bibikov, N.G. and Kalinkina, T.V. (1983) Properties of the acoustic neurons of the dorsal medullary nucleus in *Rana ridibunda*. J. Evol. Biochem. Physiol. 18, 346-352.

Bibikov, N.G. and Ivanitskii, G.A. (1985) Modelling spontaneous pulsation and short-term adaptation in the fibres of the auditory nerve. Biophysics 30, 152-156.

Brenowitz, E.A., Rose, G. and Capranica, R.R. (1985) Neural correlates of temperature coupling in the vocal communication system of the gray treefrog (*Hyla versicolor*). Brain Res. 359, 364-367.

Brzoska, J. (1984) The electrodermal response and other behavioural responses of the grass frog to natural and synthetic calls. Zool. Jb. Physiol. 88, 179-192.

Brzoska, J. and Obert, H.-J. (1980) Acoustic signals influence the hormone production of the testes in the grass frog. J. Comp. Physiol. 140, 25-29.

Brzoska, J., Walkowiak, W. and Schneider, H. (1977) Acoustic communication in the grass frog (*Rana t. temporaria* L.): Calls, auditory thresholds and behavioural responses. J. Comp. Physiol. 118, 173-186.

Capranica, R.R. (1976) Morphology and physiology of the auditory system. In: R. Llinas, W. Precht (Eds.), Frog Neurobiology, Springer, Berlin, pp. 551-575.

Capranica, R.R. and Moffat, A.J.M. (1980) Nonlinear properties of the peripheral auditory system of anurans. In: A. Popper and R. Fay (Eds.), Comparative studies of hearing in vertebrates, Springer, New York, pp. 139-165.

Corey, D.P. and Hudspeth, A.J. (1983) Kinetics of the receptor current in bullfrog saccular hair cells. J. Neurosci. 5, 962-976.

Cox, D.R. and Isham, V. (1980) Point processes. Chapman and Hall, London.

Crawford, A.C. and Fettiplace, R. (1980) The frequency selectivity of auditory nerve fibres and hair cells in the cochlea of the turtle. J. Physiol. 306, 79-125.

Crawford, A.C. and Fettiplace, R. (1981a) An electrical tuning mechanism in turtle cochlear hair cells. J. Physiol. 312, 377-412.

Crawford, A.C. and Fettiplace, R. (1981b) Nonlinearities in the responses of turtle hair cells. J. Physiol. 315, 317-338.

De Boer, E. and Kuyper, P. (1968) Triggered correlation. IEEE Trans. Biomed. Eng. 15, 169-179.

De Valk J.P.J., Epping W.J.M. and Heringa A. (1985) Colour representation of biomedical data. Med. & Biol. Eng. & Comput. 23, 343-351.

Eggermont, J.J. (1985) Peripheral auditory adaptation and fatique: A model oriented review. Hear. Res. 18, 57-71.

Eggermont, J.J. and Epping, W.J.M. (1986) Sensitivity of neurons in the auditory midbrain of the grassfrog to temporal characteristics of sound. III. Stimulation with natural and synthetic mating calls. Hear. Res. 24, 255-268.

Eggermont, J.J. and Epping, W.J.M. (1987) Coincidence detection in auditory neurons: A possible mechanism to enhance stimulus specificity in the grassfrog. Hear. Res. 30, 219-230.

Eggermont, J.J., Epping, W.J M. and Aertsen, A.M.H.J. (1983a) Stimulus dependent neural correlations in the auditory midbrain of the grassfrog (*Rana temporaria* L.). Biol. Cybern. 47, 103-117.

Eggermont J.J., Johannesma P.I.M. and Aertsen A.M.H.J. (1983b) Reverse correlation methods in auditory research. Quart. Rev. Biophys. 16, 341-414.

Epping, W.J.M. (1985) Auditory information processing in the midbrain of the grassfrog. Ph.D. Thesis, Catholic University of Nijmegen.

Epping, W.J.M. and Eggermont, J.J. (1985a) Single unit characteristics in the auditory midbrain of the immobilized grassfrog. Hear. Res. 18, 223-243.

Epping, W.J.M. and Eggermont, J.J. (1985b) Relation of binaural interaction and spectro-temporal characteristics in the auditory midbrain of the grassfrog. Hear. Res. 19, 15-28.

Epping, W.J.M. and Eggermont, J.J. (1986a) Sensitivity of neurons in the auditory midbrain of the grassfrog to temporal characteristics of sound. I. Stimulation with acoustic clicks. Hear. Res. 24, 37-54.

Epping, W.J.M. and Eggermont, J.J. (1986b) Sensitivity of neurons in the auditory midbrain of the grassfrog to temporal characteristics of sound. II. Stimulation with amplitude modulated sound. Hear. Res. 24, 55-72.

Epping, W.J.M. and Eggermont, J.J. (1987) Coherent neural activity in the auditory midbrain of the grassfrog. J. Neurophysiol. 57, 1464-1483.

Feng, A.S. (1982) Quantitative analysis of intensity-rate and intensity-latency functions in peripheral auditory nerve fibers of northern leopard frogs (*Rana p. pipiens*). Hear. Res. 6, 241-246.

Feng, A.S. (1983) Morphology of neurons in the torus semicircularis of the northern leopard frog, *Rana pipiens pipiens*. J. Morphol. 175, 253-269.

Feng, A.S. (1986) Afferent and efferent innervation patterns of the cochlear nucleus (dorsal medullary nucleus) of the leopard frog. Brain Res. 367, 183-191.

Feng, A.S. and Capranica, R.R. (1976) Sound localization in anurans. I. Evidence of Binaural interaction in dorsal medullary nucleus of bullfrogs (*Rana catesbeiana*). J. Neurophysiol. 39, 871-881.

Feng, A.S., Narins, P.M. and Capranica, R.R. (1975) Three populations of primary auditory fibers in the bullfrog (*Rana catesbeiana*): Their peripheral origins and frequency sensitivities. J. Comp. Physiol. 100, 221-229.

Frishkopf, L.S. and Capranica, R.R. (1966) Auditory responses in the medulla of the bullfrog: Comparison with eighth nerve responses. J. Acoust. Soc. Am. 40, 1262-1263.

Frishkopf, L.S. and Goldstein, M.H. (1963) Responses to acoustic stimuli from single units in the eighth nerve of the bullfrog. J. Acoust. Soc. Am. 35, 1219-1228.

Fritzsch, B., Ryan, M.J., Wilczynski, W., Hetherington, T.E. and Walkowiak, W. (Eds.) (1988) The Evolution of the Amphibian Auditory System. Wiley, New York.

Fuzessery, Z.M. and Feng, A.S. (1981) Frequency representation in the dorsal medullary nucleus of the leopard frog, *Rana p. pipiens*. J. Comp. Physiol. 143, 339-347.

Fuzessery, Z.M. and Feng, A.S. (1982) Frequency selectivity in the anuran auditory midbrain: Single unit responses to single and multiple tone stimulation. J. Comp. Physiol. 146, 471-484.

Fuzessery, Z.M. and Feng, A.S. (1983) Frequency selectivity in the anuran medulla: Excitatory and inhibitory tuning properties of single neurons in the dorsal medullary and superior olivary nuclei. J. Comp. Physiol. 150, 107-119.

Gerhardt, H.C. and Doherty, J.A. (1988) Acoustic communication in the green treefrog, *Hyla versicolor*: Evolutionary and neurobiological implications. J. Comp. Physiol. A 162, 261-278.

Gerstein G.L. and Perkel D.H. (1972) Mutual temporal relationships among neuronal spike trains. Statistical techniques for display and analysis. Biophys. J. 12, 453-473.

Goldberg, J.M. and Brown, P.B. (1969) Response of binaural neurons of dog superior olivary complex to dichotic tonal stimuli: Some physiological mechanisms of sound localization. J. Neurophysiol. 32, 613-636.

Gorodetskaya, O.N. and Bibikov, N.G. (1985) Responses of auditory medullary units of the frog to temporally amplitude-modulated tones. Neurophysiol. 17, 287-292.

Hall, J.C. and Feng, A.S. (1988a) Influence of envelope rise time on neural responses in the auditory system of anurans. Hear. Res. 36, 261-276.

Hall, J.C. and Feng, A.S. (1988b) Response properties of single auditory neurons in the dorsal medullary nucleus of the frog. Soc. Neurosci. Abstr. 14, 649.

Hermes, D.J. (1982) Spectro-temporal characterisation of auditory neurons in the torus semicircularis of the grass frog, *Rana temporaria* L. Ph.D. Thesis, Catholic University of Nijmegen.

Hermes, D.J., Aertsen, A.M.H.J., Johannesma, P.I.M. and Eggermont, J.J. (1981) Spectro temporal characteristics of single units in the auditory midbrain of the lightly anaesthetised grass frog (*Rana temporaria* L.) investigated with noise stimuli. Hear. Res. 5, 147-178.

Hermes, D.J., Eggermont, J.J., Aertsen, A.M.H.J. and Johannesma, P.I.M. (1982) Spectro-temporal characteristics of single units in the auditory midbrain of the lightly anaesthetised grass frog (*Rana temporaria* L.) investigated with tonal stimuli. Hear. Res. 6, 103-126.

Hesselmans, G.H.F.M. (1988) Sensory interpretation of neural events. Ph.D. Thesis, Catholic University of Nijmegen.

Hillery, C.M. (1984) Detection of amplitude modulated tones by frogs: Implications for temporal processing mechanisms. Hear. Res. 14, 129-143.

Hillery, C.M. and Narins, P.M. (1984) Neurophysiological evidence for a traveling wave in the amphibian inner ear. Science 225, 1037-1039.

Hillery, C.M. and Narins, P.M. (1987) Frequency and time domain comparison of low-frequency auditory nerve fiber responses in two anuran amphibians. Hear. Res. 25, 233-248.

Hudspeth, A.J. (1983) Transduction and tuning by vertebrate hair cells. Trends Neurosci. 6, 366-369.

Johannesma, P.I.M. (1971) Dynamical aspects of the transmission of stochastic neural signals. In: E. Broda, A. Locker, H. Springer-Lederer (Eds.), First European Biophysics Congress, Verlag der Wiener Medizinischen Akademie, Vienna, pp. 329-333.

Johannesma, P.I.M. (1980) Functional identification of auditory neurons based on stimulus-event correlation. In: G. Van den Brink and F.A. Bilsen (Eds.), Psychophysical, Physiological and Behavioural Studies in Hearing, Delft University Press, pp. 77-84.

Johannesma, P.I.M. (1981) Neural representation of sensory stimuli and sensory interpretation of neural activity. In: Gy. Székely, E. Lábos, S. Damjanovich (Eds.) Neural communication and control, Adv. Physiol. Sci. Vol. 30 , 103-125.

Johannesma, P.I.M., Aertsen, A.M.H.J., Cranen, L. and Van Erning, L. (1981) The phonochrome: A coherent spectro-temporal representation of sound. Hear. Res. 5, 123-145.

Johannesma, P.I.M. and Van den Boogaard, H.F.P. (1985) Stochastic formulation of neural interaction. Acta Applic. Math. 4, 201-224.

Kim, D.O., Rhode, W.S. and Greenberg, S.R. (1986) Responses of cochlear nucleus neurons to speech signals: Neural encoding of pitch, intensity and other parameters. In: B.C.J. Moore and R.D. Patterson (Eds.), Auditory Frequency Selectivity, Plenum, New York, pp. 39-48.

Lewis, E.R. (1988) Tuning in the bullfrog ear. Biophys. J. 53, 441-447.

Lewis, E.R., Leverenz, E.L. and Koyama, H. (1980) Mapping functionally identified auditory afferents from the peripheral origins to their central terminations. Brain Res. 197, 223-229.

Lewis, E.R., Leverenz, E.L. and Koyama, H. (1982) The tonotopic organization of the bullfrog amphibian papilla, an auditory organ lacking a basilar membrane. J. Comp. Physiol. 145, 437-445.

Matsumoto, N., Schwippert, W.W. and Ewert, J.-P. (1986) Intracellular activity of morphologically identified neurons of the grass frog's optic tectum in response to moving configurational stimuli. J. Comp. Physiol. A 159, 721-739.

Meddis, R. (1986) Simulation of mechanical to neural transduction in the auditory receptor. J. Acoust. Soc. Am. 79, 702-711.

Megela, A.L. (1984) Diversity of adaptation patterns in responses of eighth nerve fibers in the bullfrog, *Rana catesbeiana*. J. Acoust. Soc. Am. 75, 1155-1162.

Megela, A.L. and Capranica, R.R. (1981) Response patterns to tone bursts in peripheral auditory system of anurans. J. Neurophysiol. 46, 465-478.

Megela, A.L. and Capranica, R.R. (1982) Differential patterns of physiological masking in the anuran auditory nerve. J. Acoust. Soc. Am. 71, 641-645.

Megela, A.L. and Capranica, R.R. (1983) A neural and behavioral study of auditory habituation in the bullfrog, *Rana catesbeiana*. J. Comp. Physiol. 151, 423-434.

Melssen, W.J. and Epping, W.J.M. (1987) Detection and estimation of neural connectivity based on crosscorrelation analysis. Biol. Cybern. 57, 403-414.

Melssen, W.J. and Van Stokkum, I.H.M. (1988) Selectivity for interaural time-difference and amplitude modulation frequency in the auditory midbrain of the grassfrog. In: H. Duifhuis, J.W. Horst and H.P. Wit (Eds.) Basic Issues in Hearing, Academic Press, London, pp. 279-284.

Narins, P.M. and Zelick, R. (1988) The effects of noise on auditory processing and behavior in amphibians. In: B. Fritzsch et al. (Eds.), The Evolution of the Amphibian Auditory System, Wiley, New York, pp. 511-536.

Opdam, P., Kemali, M. and Nieuwenhuys, R. (1976) Topological analysis of the brainstem of the frogs *Rana esculanta* and *Rana catesbeiana*. J. Comp. Neurol. 165, 307-332.

Palmer, A.R. and Russell, I.J. (1986) Phase-locking in the cochlear nerve of the guinea-pig and its relation to the receptor potential of inner hair-cells. Hear. Res. 24, 1-15.

Perkel D.H. (1970) Spike trains as carriers of information. In: Schmitt, F.O. (Ed.) Neurosci. Second Study Program, Rockefeller University Press, New York, pp. 587-596.

Perkel D.H., Gerstein G.L. and Moore G.P. (1967) Neuronal spike trains and stochastic point processes. II. Simultaneous spike trains. Biophys. J. 7, 419-440.

Pitchford, S. and Ashmore, J.F. (1987) An electrical resonance in hair cells of the amphibian papilla of the frog *Rana temporaria*. Hear. Res. 27, 75-83.

Potter, H.D. (1965a) Mesencephalic auditory region of the bullfrog. J. Neurophysiol. 28, 1132-1154.

Potter, H.D. (1965b) Patterns of acoustically evoked discharges of neurons in the mesencephalon of the bullfrog. J. Neurophysiol. 28, 1155-1184.

Rall, W. (1964) Theoretical significance of dendritic trees for neuronal input-output relations. In: R.F. Reiss (Ed.) Neural theory and modelling. Stanford Univ. Press, Stanford, CA, pp. 73-97.

Rall, W. (1977) Core conductor theory and cable properties of neurones. In: Handbook of Physiology, Sect. 1: The nervous system, Vol. I: Cellular biology of neurons, Part 1, American Physiological Society, Bethesda ML, pp. 39-97.

Rose, G.J. and Capranica, R.R. (1985) Sensitivity to amplitude modulated sounds in the anuran auditory nervous system. J. Neurophysiol. 53, 446-465.

Rose, G.J. and Wilczynski, W. (1984) The anuran superficial reticular nucleus: Evidence for homology with nuclei of the lateral lemniscus. Brain Res. 304, 170-172.

Russell C.J., Myers J.P. and Bell C.C. (1974) The echo response in *Gnathonemus petersii* (Mormyridae). J. Comp. Physiol. 92, 181-199.

Schneider J., Eckhorn R. and Reitböck H. (1983) Evaluation of neuronal coupling dynamics. Biol. Cybern. 46, 129-134.

Schneider-Lowitz, B. (1983) Neuronaler Verarbeitung einfacher und komplexer Schallsignale in der Peripherie und den unteren Stationen der Hörbahn des Grasfrosches (*Rana t. temporaria* L.). Ph.D. Thesis, Rheinischen Friedrich-Wilhelms-Universität zu Bonn, F.R.G.

Van den Boogaard, H.F.P. (1988) System identification based on point processes and correlation densities. II. The refractory neuron model. Math. Biosci. 91, 35-65.

Van Gelder J.J., Evers P.M.G. and Maagnus G.J.M. (1978) Calling and associated behaviour of the common frog, *Rana temporaria*, during breeding activity. J. Anim. Ecol. 47, 667-676.

Van Gisbergen, J.A.M., Grashuis, J.L., Johannesma, P.I.M. and Vendrik, A.J.H. (1975) Neurons in the cochlear nucleus investigated with tone and noise stimuli. Exp. Brain Res. 23, 387-406.

Van Stokkum, I.H.M. (1987) Sensitivity of neurons in the dorsal medullary nucleus of the grassfrog to spectral and temporal characteristics of sound. Hear. Res. 29, 223-235.

Van Stokkum, I.H.M. (1989) A model for the auditory midbrain of the grassfrog for monaural stimuli. Hear. Res. (submitted)

Van Stokkum, I.H.M. and Epping, W.J.M. (1989) Responses of auditory brainstem neurons in the grassfrog to clicks. Acta Biolog. Hung. (in press)

Van Stokkum, I.H.M. and Gielen, C.C.A.M. (1989) A model for the peripheral auditory system of the grassfrog. Hear. Res. (in press)

Van Stokkum, I.H.M., Johannesma, P.I.M. and Eggermont, J.J. (1986) Representation of time-dependent correlation and recurrence time functions. A new method to analyse non-stationary point processes. Biol. Cybern. 55, 17-24.

Vlaming, M.S.M.G., Aertsen, A.M.H.J. and Epping, W.J.M. (1984) Directional hearing in the grassfrog (*Rana temporaria* L.): I. Mechanical vibrations of the tympanic membrane. Hear. Res. 14, 191-201.

Walkowiak, W. (1980) The coding of auditory signals in the torus semicircularis of the fire-bellied toad and the grass frog: Responses to simple stimuli and to conspecific calls. J. Comp. Physiol. 138, 131-148.

Walkowiak, W. (1984) Neuronal correlates of the recognition of pulsed sound signals in the grass frog. J. Comp. Physiol. A 155, 57-66.

Walkowiak, W. (1988) Central temporal encoding. In: B. Fritzsch et al. (Eds.), The Evolution of the Amphibian Auditory System, Wiley, New York, pp. 275-294.

Walkowiak, W. and Brzoska, J. (1982) Significance of spectral and temporal call parameters in the auditory communication of male grass frogs. Behav. Ecol. Sociobiol. 11, 247-252.

Whitehead, M.L., Wilson, J.P. and Baker, R.J. (1986) The effects of temperature on otoacoustic emission tuning properties. In: B.C.J. Moore and R.D. Patterson (Eds.), Auditory Frequency Selectivity, Plenum, New York, pp. 39-48.

Wilczynski, W. (1988) Brainstem auditory pathways in anuran amphibians. In: B. Fritzsch et al. (Eds.), The Evolution of the Amphibian Auditory System, Wiley, New York, pp. 209-231.

Wilczynski, W. and Capranica, R.R. (1984) The auditory system of anuran amphibians. Progr. Neurobiol. 22, 1-38.

Zakon, H.H. and Wilczynski, W. (1988) The physiology of the anuran eighth nerve. In: B. Fritzsch et al. (Eds.), The Evolution of the Amphibian Auditory System, Wiley, New York, pp. 125-155.

Zelick, R. and Narins, P.M. (1985) Temporary threshold shift, adaptation and recovery characteristics of frog auditory nerve fibers. Hear. Res. 17, 161-176.

1 Inleiding

De bruine kikker behoort tot de orde der anura, de staartloze amfibieën. Elke anura soort bezit een klein repertoire van stereotype roepen. De belangrijkste daarvan is de paarroep. In het paarseizoen roepen de mannetjes kikkers en padden om vrouwtjes vol eitjes aan te trekken. Om een mannelijke soortgenoot te vinden moet het vrouwtje de paarroep identificeren, en de zender ervan localiseren.

Anura vormen een goed model om auditieve communicatie te onderzoeken omdat men te maken heeft met een beperkte groep stereotype stimuli, die na juiste identificatie en localisatie aanleiding geven tot specifieke gedragingen. Daarom vormt dit auditief systeem al enkele tientallen jaren een favoriet onderzoeksonderwerp.

2 Kort overzicht van het auditief systeem

De paarroep van de bruine kikker bestaat uit een serie kortdurende ($\approx$ 12 ms) pulsjes, met een herhalingsfrequentie van ongeveer 30 Hz (Fig. I.1). De frequentie-inhoud van de pulsjes en de pulsherhalingsfrequentie vormen belangrijke kenmerken voor de herkenning van de soortspecifieke roep (Fig. I.2).

In de hersenstam van de kikker bevinden zich een aantal kernen met auditieve neuronen (Fig. I.3). In de amfibische en basilaire papil wordt het geluid omgezet in actiepotentialen van achtste zenuw vezels. Deze vezels projecteren naar de dorsale medullaire nucleus (DMN). Neuronen in de DMN verwerken de binnenkomende actiepotentialen en sturen op hun beurt weer actiepotentialen naar andere kernen. Neuronen in de torus semicircularis (TS) ontvangen actiepotentialen afkomstig van de DMN en van de superior olijf kern. Ook in de TS vindt verwerking van de binnenkomende actiepotentialen plaats. In dit proefschrift worden de responseigenschappen van DMN en TS neuronen geanalyseerd op aanbieding van geluid aan één oor.

3 Neuronale selectiviteit

Opklimmend van de achtste zenuw, via DMN naar TS veranderen de responseigenschappen van neuronen. Achtste zenuwvezels worden gekarakteriseerd door hun frequentieselectiviteit (Fig. I.4) en door hun vuurpatroon. Deze vezels genereren actiepotentialen wanneer de stimulus voldoende energie bevat in een frequentieband waarvoor de vezel gevoelig is. Bij een aanhoudende toon worden verschillende vuurpatronen gevonden, variërend van voortdurend (tonisch) tot alleen aan het begin (fasisch) (Fig. I.5).

In de DMN komen complexere neuronen voor, die een voorkeur bezitten voor snelle intensiteitsveranderingen in het geluid, zoals de pulsjes van natuurlijke roepen. In Hoofdstuk III en V staat een voorbeeld hiervan, neuron 297,0,6, beschreven.

In de TS komen neuronen voor met nog complexere eigenschappen. Een voorbeeld is neuron 322,3,0 (Fig. VI.5) dat vuurt wanneer het geluid minstens 20 ms duurt, of wanneer de pulsherhalingsfrequentie groter is dan 18 Hz. Een ander voorbeeld is neuron 314,1,0 dat niet respondeert op ongemoduleerd geluid (Fig. VI.9). Het neuron vuurt echter wel op een amplitude gemoduleerde toon (Fig. VI.1c) met een amplitude modulatiefrequentie tussen 30 en 125 Hz. Ook respondeert dit neuron op natuurlijke roepen met een pulsherhalingsfrequentie groter dan 9 Hz.

Achtste zenuwvezels signaleren dus de aanwezigheid van bepaalde frequenties in het geluid. Een groep DMN neuronen signaleert snelle intensiteitsveranderingen, zoals pulsjes uit de paarroep. Een groep TS neuronen signaleert de duur van het geluid en de pulsherhalingsfrequentie.

4 Modellering

In Hoofstuk V en VI wordt voor het eerst een model voorgesteld dat de zojuist beschreven neuronale selectiviteiten reproduceert. Het model, dat wordt geschetst in Fig. VI.2, begint met twee banddoorlaatfilters die verantwoordelijk zijn voor de frequentieselectiviteit van de achtste zenuwvezels.

De impulsresponsies van deze lineaire filters staan getekend in Fig. VI.2A,B. Na mechano-electrische transductie (Fig. VI.2C), korte termijn adaptatie (Fig. I.5 en VI 2D,F), en laagdoorlaatfiltering (Fig. VI.2G) ontstaat een generatorpotentiaal w. Als functie van de grootte van w ontstaan op stochastische wijze actiepotentialen in de achtste zenuw (Formule VI.9,11).

De voorkeur van DMN neuronen voor snelle intensiteitsveranderingen wordt gemodelleerd met een coincidentiedetectie mechanisme. Dit houdt in dat wanneer de achtste zenuw vezels die convergeren op een DMN neuron gelijktijdig vuren, hun excitatoire postsynaptische potentialen (EPSP's, Fig. VI.2J) optellen. Dan overschrijdt de generatorpotentiaal y van het DMN neuron de drempel en worden actiepotentialen gegenereerd. Langzame intensiteitsveranderingen geven geen aanleiding tot synchronie van actiepotentialen in inkomende vezels en de generatorpotentiaal y blijft beneden de drempel (Fig. V.7,8).

De duurgevoeligheid van TS neuron 322,3,0 werd gemodelleerd door een lange duur van de EPSP aan te nemen. Daardoor tellen op elkaar volgende EPSP's op. Geluid dat aanleiding geeft tot snel op elkaar volgende vuringen van inkomende neuronen veroorzaakt een generatorpotentiaal y die de drempel overschrijdt. Geluiden die te weinig inkomende actiepotentialen genereren, of geluidspulsjes die niet snel genoeg op elkaar volgen, veroorzaken een onderdrempelige generatorpotentiaal (Fig. VI.4).

De selectiviteit van TS neuron 314,1,0 voor amplitude gemoduleerd geluid wordt gemodelleerd door een combinatie van de zojuist beschreven mechanismes. De DMN neuronen die convergeren op het TS neuron zijn selectief voor snelle intensiteitsveranderingen (Fig. VI.7). De door hen veroorzaakte langdurende EPSP's worden geintegreerd, zodat het TS neuron pas vuurt na een aantal snel opeenvolgende intensiteitsveranderingen (Fig. VI.8).

5 Conclusies

De analyse van auditieve hersenstamneuronen in de bruine kikker vereist het aanbieden van een breed scala van spectraal en temporeel gestructureerde stimuli. Om een relatie te leggen met auditieve communicatie dienen de stimuli gebaseerd te zijn op natuurlijke roepen. Om de functie van neuronen te begrijpen dient een samenhangend overzicht gemaakt te worden, waarin de responsies op de verschillende stimuli met elkaar in verband gebracht worden (Fig. III.5, V.4, VI.5 en VI.9). Bij het analyseren en relateren van de responsies dient een onderliggend model bedacht te worden. Het structureel model voorgesteld in Hoofstuk V en VI beschrijft op functionele wijze de responseigenschappen van de meeste auditieve hersenstamneuronen. Met één groep parameters reproduceert het model de responsies van een neuron op een breed scala van stimuli, aangeboden aan één oor. Door variatie van deze parameters worden de responseigenschappen van andere neuronen gereproduceerd.

Voor een vollediger begrip van de functie van auditieve hersenstamneuronen is een uitbreiding naar de responsies op geluid aangeboden aan twee oren noodzakelijk. Geluid kan in neuronen niet alleen actiepotentialen veroorzaken, maar ze ook tegenhouden (inhibitie). Het model dient uitgebreid te worden om ook verschijnselen van inhibitie door geluid te beschrijven.

De interpretatie van actiepotentialen van DMN en TS neuronen is zeer complex. De hierboven beschreven neuronen signaleren op een verstrengelde wijze temporele eigenschappen van het geluid, zoals intensiteitsveranderingen, pulsherhalingsfrequentie en geluidsduur. Deze neuronen responderen alle goed, maar niet uitsluitend, op natuurlijke roepen. De DMN neuronen met een voorkeur voor snelle intensiteitsveranderingen zijn geschikt om de pulsjes van natuurlijke roepen te detecteren tegen een ruisachtergrond (Fig. III.5d en §III.4.5). De laag- en hoogdoorlaat eigenschappen met betrekking tot pulsherhalingsfrequentie omvatten de natuurlijke pulsherhalingsfrequenties. Bij de modellering van de beide TS neuronen in Hoofdstuk VI werden EPSP afval tijdconstantes gevonden van 30 en 70 ms. Deze tijdconstantes zijn geschikt om de neurale activiteit te integreren afkomstig van een natuurlijke roep met een pulsherhalingsfrequentie van 30 Hz. Onderzoek van neuronale responsies in zich gedragende dieren zou de mogelijkheid bieden om de conclusies uit deze studie, die gebaseerd zijn op experimenten in verlamde dieren, te testen.

Curriculum vitae

Op 11 februari 1962 werd ik geboren te Boxmeer, als eerste kind van Ank Biemans en Emile van Stokkum. Twintig maanden later volgde mijn zusje Milian en was het ideale gezin af. Van 1968 tot 1973 volgde ik de lagere school Sint Jan de Doper in Sambeek. Daar sloeg ik een klas over, en werd sindsdien uitgescholden voor *professor*. Van 1973 tot 1979 bezocht ik het Elzendaalcollege in Boxmeer. Toen ik in 4 Gym β zat werd ik getest in het kader van de keuzebegeleiding. Zelf had ik als mogelijke studie biologie opgegeven, de keuzebegeleiders adviseerden politicologie, sociologie of een talenstudie. Daar zag ik geen brood in, en om lotingsproblemen te voorkomen, besloot ik natuurkunde met tweede hoofdvak scheikunde en bijvak wiskunde te gaan studeren. Dat heb ik geweten. Vier jaar pendelde ik tussen Sambeek en Nijmegen, vijf dagen colleges, werkcolleges en practica, in het weekend de sommetjes en de verslagen.

Al die jaren zweefde mij het interdisciplinaire onderzoeksgebied *Hersenen en Gedrag* voor ogen. Toen ik eindelijk een afdeling mocht kiezen, schrok ik: Peter Johannesma zei dat er eigenlijk geen plaats was bij Biofysica, het zat propvol studenten. Gelukkig zag hij nog een gaatje, het onderzoek naar de electrische activiteit en het motorisch gedrag van de olifantsvis. Samen met de bioloog en natuurkundige Rob van Son ging ik te water, en op 13 september 1984 studeerde ik cum laude af. Inmiddels had Jos Eggermont mij gevraagd voor een promotie onderzoek getiteld *De rol van neurale wisselwerking bij de detectie van signalen in ruis.* Mijn langgekoesterde wens, onderzoek naar *Hersenen en Gedrag*, werd vervuld: ik ging het auditief systeem van de bruine kikker onderzoeken. Na een goed jaar indoctrinatie van Jos en de kunst afkijken bij Willem Epping stond ik er na beider vertrek alleen voor. Niet helemaal, want Willem Melssen was net als tweede promovendus aangesteld, op de titel *Centrale mechanismen van geluidslocalisatie bij anura.* Gezamenlijk probeerden wij enkele neuronen zo volledig mogelijk te karakteriseren. We zochten naar de mechanismen verantwoordelijk voor identificatie en localisatie van pseudo-natuurlijke geluiden. Ten slotte sloeg ik na lang aandringen van Peter Johannesma en de teruggekeerde Willem Epping aan het modelleren. Daarbij was de nieuwe professor, Stan Gielen, een gedegen steun in de rug.

Na tien jaar studie en onderzoek, ben ik een stuk bescheidener geworden wat betreft de mogelijkheden van de natuurwetenschap. Maar nog steeds brandt de vraag naar het hoe en waarom, hoe ik dit denk, en daarna opschrijf.

Dankwoord

Graag wil ik hier de rol van enkele labgenoten bij de totstandkoming van dit boekje voor het voetlicht brengen. Allereerst Koos *ik mag niet klagen* Braks die, ondanks de steeds hoger wordende bezuinigingsgolven, de moed er in hield: *Problemen? Ik maak ze groter.* Als eenzame promovendus was ik wellicht koppie onder gegaan, gelukkig was er Willem Melssen om het leed, of de vreugde bij een geslaagd experiment, te delen. Het electronica driemanschap was, naast het afleveren van nieuwe apparaten, altijd bereid te helpen als er weer eens iets niet werkte. De computerboys, een tiental zag ik komen en gaan, de Gould verdwijnt maar de laser blijft staan. Peter van Mier, zelfstandig onderzoeker, die zich mijn lief en leed aantrok. Jan van Gisbergen, voor zijn vasthoudende vragen: *Je zult wel denken, waar doet te nou zo moeilijk over.* Peter Johannesma, metafysicus, wiens wijze raad ik vaak in de wind sloeg. Jos Eggermont, pragmaticus: The brain *is een grijze massa in een pot, maar* het brein *zal ik nooit begrijpen.* De promovendi, een bijzonder levendig en behulpzaam zootje ongeregeld.
Ten slotte: het is een bijzonder lab, en dat is het!

Stellingen

behorende bij het proefschrift

Analysis of auditory brainstem neurons in the grassfrog

1. Bij de karakterisatie van auditieve neuronen dient een breed scala van stimuli gebruikt te worden, die spectrale, temporele en spatiële selectiviteit gecombineerd onderzoeken.

   Hoofdstukken III, V, VI en Melssen, W.J. & Van Stokkum, I.H.M. (1988) Selectivity for interaural time-difference and amplitude modulation frequency in the auditory midbrain of the grassfrog. In: H. Duifhuis, J.W. Horst and H.P. Wit (Eds.) Basic Issues in Hearing, Academic Press, London, pp. 279-284.

2. Karakterisering met behulp van een structureel model is een noodzakelijke stap voor verder onderzoek naar auditieve neuronen.

   Hoofdstukken V en VI.

3. Zoals de on-line data analyse gemeengoed wordt, zo zal het on-line modelleren van neuronen bijdragen tot efficiënter experimenteren.

4. Onderzoek naar neurale mechanismen in het auditief systeem van anura dient te geschieden met open mond.

   Vlaming, M.S.M.G., Aertsen, A.M.H.J. & Epping, W.J.M. (1984) Directional hearing in the grassfrog (*Rana temporaria* L.): I. Mechanical vibrations of the tympanic membrane. Hear. Res. 14, 191-201.

5. Het onderzoek naar responsies op twee-toon stimuli is in bepaalde gevallen onderzoek met amplitudegemoduleerd geluid.

   Hoofdstuk I en Fuzessery, Z.M. & Feng, A.S. (1982) Frequency selectivity in the anuran auditory midbrain: Single unit responses to single and multiple tone stimulation. J. Comp. Physiol. 146, 471-484.

6. Bij al het irrationele dat in de wereld plaatsvindt, is het geen wonder dat de meerderheid in paranormale verschijnselen gelooft.

7. Stelling zeven gaat over de liefde.

Nijmegen, 13 september 1989, Ivo van Stokkum.